AN INVESTIGATION INTO DYNAMIC MODULUS OF HOT-MIX ASPHALT AND ITS CONTRIBUTING FACTORS

Except where reference is made to the work of others, the work described in this thesis is my own or was done in collaboration with my advisory committee. This thesis does not include proprietary or classified information.

_____
Mary Marjorie Robbins

Certificate of Approval:

_____	_____
Rod E. Turochy Associate Professor Civil Engineering	David H. Timm, Chair Associate Professor Civil Engineering
_____	_____
Randy C. West Director National Center for Asphalt Technology	George T. Flowers Dean Graduate School

AN INVESTIGATION INTO DYNAMIC MODULUS OF HOT-MIX ASPHALT AND ITS CONTRIBUTING FACTORS

Mary Marjorie Robbins

A Thesis

Submitted to

the Graduate Faculty of

Auburn University

in Partial Fulfillment of the

Requirements for the

Degree of

Masters of Science

Auburn, Alabama
May 9, 2009

AN INVESTIGATION INTO DYNAMIC MODULUS OF HOT-MIX ASPHALT AND

ITS CONTRIBUTING FACTORS

Mary Marjorie Robbins

_____
Mary Marjorie Robbins

_____
Date of Graduation

VITA

Mary Marjorie Robbins, daughter of Gail and Nancy (McClure) Robbins, was born January 31, 1983 in Kettering, Ohio. She graduated from Centerville High School in June, 2001. She attended the University of Toledo from where she graduated magna cum laude in December, 2005 with a Bachelor's of Science in Civil Engineering. As an undergraduate student she participated in the Co-operative Education Program, working for Lewandowski Engineers, and Wright Patterson Air Force Base. She also participated in the Undergraduate Summer Internship in Transportation held at the University of Texas during the summer of 2004. After graduation she worked for the Ohio Department of Transportation as a Transportation Engineer for one year and eight months prior to starting her graduate studies at Auburn University in August, 2007.

THESIS ABSTRACT

AN INVESTIGATION INTO DYNAMIC MODULUS OF HOT-MIX ASPHALT AND IT'S CONTRIBUTING FACTORS

Mary Marjorie Robbins

Master of Science, May 9, 2009
(B.S.C.E., University of Toledo, 2005)

174 Typed Pages

Directed by David H. Timm

One of the key elements of mechanistic-empirical (M-E) flexible pavement design is the characterization of material properties. One material property in particular, the dynamic modulus of HMA, E*, influences tensile strain levels, therefore it is necessary to investigate this property to successfully predict fatigue cracking.

E* can be determined directly by laboratory testing or it can be estimated using predictive equations as a function of mixture properties. The more recently developed M-E design program, the Mechanistic-Empirical Pavement Design Guide (MEPDG), offers both methods to characterize E*.

An investigation into the Witczak 1-37A and the Witczak 1-40D E* predictive equations, both utilized by the MEPDG and another recently developed predictive

equation, the Hirsch model, was completed. Comparisons were drawn with E* laboratory results for mixtures constructed as part of the National Center for Asphalt Technology's (NCAT) 2006 Test Track structural study. The investigation revealed that the Hirsch E* model most accurately predicted measured E* values, while the Witczak 1-40D overpredicted values and the Witczak 1-37A varied inconsistently.

To validate and optimize M-E designs it is necessary to link pavement performance to material properties. The field parameters that influence E*, load duration and temperature, and the field parameter that is most affected by E*, tensile strain, were measured under varying speeds and temperatures at the NCAT Test Track. These measurements enabled comparisons with the MEPDG analysis procedure. In comparing load durations, it was found that those determined by the MEPDG were nearly 70% greater than those measured in the field. These load durations enabled the computation of E* of each HMA layer, and the prediction of strain in a layered elastic program. Strains estimated from both load duration methods (MEPDG and measured) closely replicated each other; however they poorly replicated those strains found in the field, indicating the inaccuracy of the time-frequency relationship currently used in the MEPDG.

It is suggested that State DOT's wishing to supplement laboratory E* testing while utilizing the MEPDG for design, substitute laboratory results required for a level one design with predictions from the Hirsch model. It is not recommended that the MEPDG be used as a primary design method until further refinement of the time-frequency relationship, and further investigation into the accuracy of the pavement distresses can be completed.

ACKNOWLEDGEMENTS

I would like to thank my family and friends who have always supported me in my endeavors with patience and love, and for being a voice of reason throughout this journey. I would also like to express my deep appreciation to my advisor, Dr. David Timm for granting me this opportunity and for his guidance, wisdom and patience. I am also grateful for the guidance and support offered by my advisory committee, Dr. Randy West and Dr. Rod Turochy. I would like to thank the National Center for Asphalt Technology for the use of their facilities and support for this research. I would like to acknowledge the Alabama Department of Transportation, the Federal Highway Administration, and the Oklahoma Department of Transportation for their financial support and their commitment to development through research.

Style used: Publication Manual of the American Psychological Association, Fifth Edition

Computer software used: Microsoft Word, Microsoft Excel, WESLEA, Mechanistic-Empirical Pavement Design Guide Version 1.0

TABLE OF CONTENTS

LIST OF TABLES

LIST OF FIGURES

CHAPTER ONE

INTRODUCTION

1.1 BACKGROUND

In a mechanistic-empirical (M-E) framework for pavement design, four major inputs are utilized to predict pavement responses and ultimately pavement performance enabling the selection of a cross-section meeting the specified requirements. M-E design enables the mechanical properties of the selected materials to be used in conjunction with empirical performance information and site conditions (traffic and climate), as shown in Figure 1.1. Inputs include an initial pavement structure, climatic data, traffic volume and weight distributions, and material properties of the hot mix asphalt (HMA), base and subgrade materials. These inputs are used to predict the pavement's responses, stress (σ) and strain (ε), at critical locations through mechanical analysis. Such predictions may be made with the aid of layered elastic analysis (LEA) or finite element models. Historical performance data help create accurate transfer functions used to estimate the number of loads to failure given the predicted pavement responses for comparison to failure criteria. Recently, one specific M-E design program, the Mechanistic-Empirical Pavement Design Guide (MEPDG) has come to the forefront of design, sparking interest among state Departments of Transportation (DOTs) for implementation as their primary design method. Such a program should be validated under field conditions to determine its benefits and suitability to state DOTs.

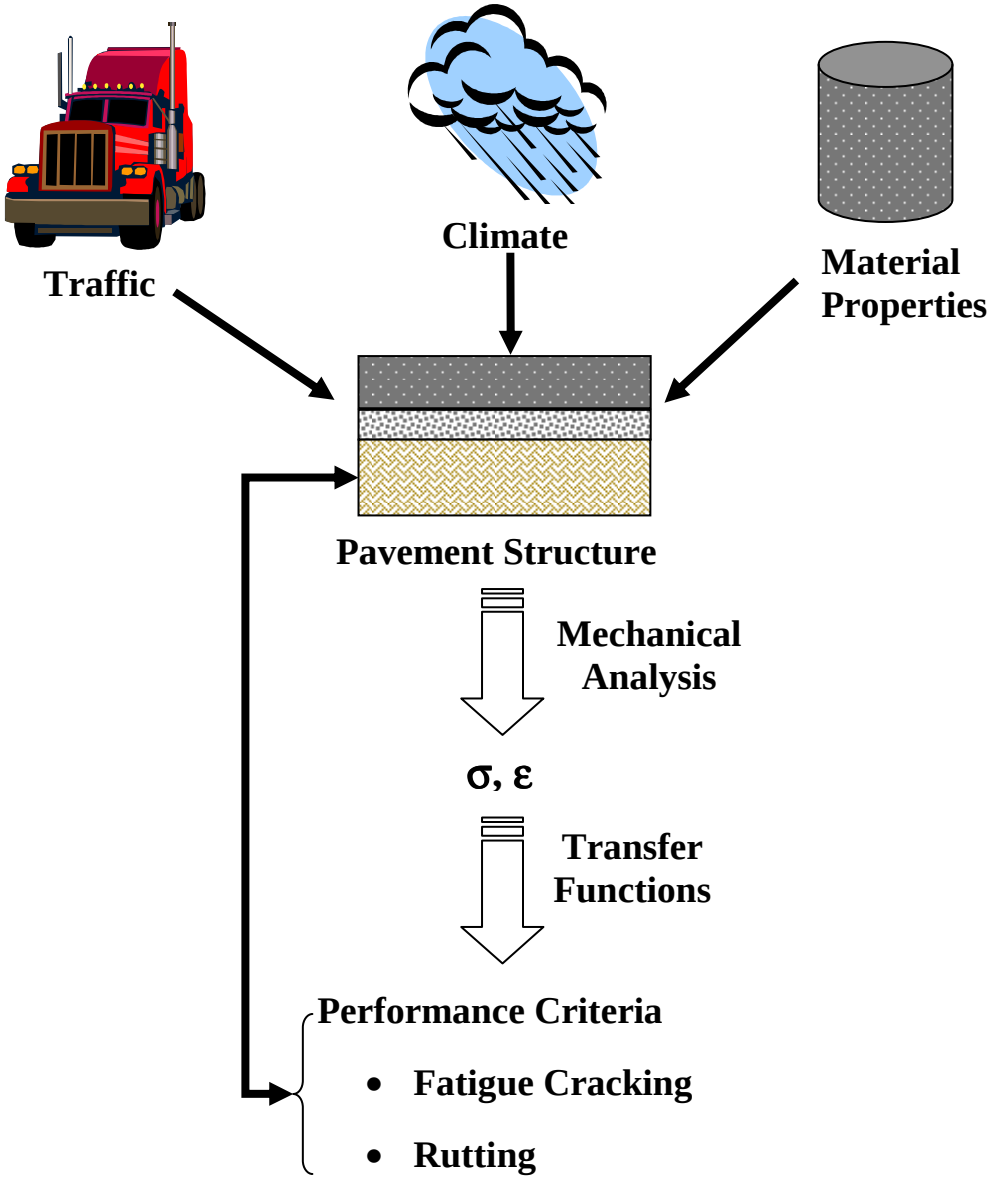

FIGURE 1.1 M-E Pavement Design Framework.

In M-E pavement design, accurate representation of material characteristics is imperative to a successful and reliable design. One in particular is the HMA dynamic modulus, E*. E* helps to define the viscoelastic nature of HMA by quantifying the effects of temperature and frequency on stiffness under dynamic loading. This is necessary to accurately predict the in-situ pavement responses to varying speeds, and

temperatures throughout the pavement's cross-section. E* can be determined in the laboratory through the AASHTO TP-62 procedure or it can be predicted by one of many E* predictive models, the three most recent including: Hirsch, Witczak 1-37A, and Witczak 1-40D (Bari and Witczak, 2006) (Christensen et al., 2003). To predict E* from one of these three models, no laboratory testing is required beyond viscosity testing, determination of gradation information and rudimentary volumetric testing. At the highest degree of complexity for design, the MEPDG utilizes E* laboratory test results, and for lower levels of design, it utilizes one of the Witczak equations (Eres, 1999). Equipment to run E* testing is costly ($75,000-$90,000) (FHWA, 2009) and many state DOTs do not currently have such equipment. For example, the Alabama DOT (ALDOT) currently operates without such equipment since it is not needed for their current design framework. However, a pooled fund study, "Implementation of the Asphalt Mixture Performance Tester (AMPT) for Superpave Validation," (Study No. TPF-5(178)) launched by the FHWA in 2008 makes this technology more economical for state transportation agencies (FHWA, 2009). As states contemplate implementing the MEPDG, it is necessary to assess the accuracy of the revised Witczak model, as well as the original Witczak and Hirsch models in estimating E* in comparison to laboratory E* test results for a range of mix types.

Although E* can be measured directly in the laboratory, it is very difficult to accurately measure it in the field. However, knowledge of E* is imperative in developing relationships between pavement response and material properties. Given the difficulty of direct measurements, focus should be placed on the factors that influence changes in E*. Due to the viscoelastic nature of HMA, the dynamic modulus is heavily

influenced by three factors: rate of loading, temperature, and depth within the pavement structure (Eres, 2003). Temperature and pavement depth are relatively easy parameters to measure in the field. Rate of loading on the other hand is much more difficult to quantify in the field. In the laboratory, rate of loading can be correlated to the applied testing frequency. During lab testing, controlling and measuring rate of loading is a simple task, but in the field it is much more arduous due to the shape of the loading waveforms transmitted throughout the pavement. Because of the complexity in measuring frequency, some design procedures simply use a fixed value such as the Asphalt Institute which assumes a value of 10Hz regardless of the conditions (Asphalt Institute, 1999). The MEPDG however, uses an iterative process to compute the time of loading that relies on E* of each HMA layer, temperature, depth in pavement and modulus of subgrade (Eres, 2003). From this computation, frequency is then computed (Eres, 2003). It should be noted that as a result of this iterative process, E* is ultimately computed for each HMA layer. Although frequency is not a measurable parameter, load duration is. It is therefore necessary that the MEPDG's load duration procedure be validated with field data to assess its accuracy.

Material properties significantly influence pavement responses. In particular, one such pavement response, tensile strain, is significantly dependent on E* (Eres, 2003). Tensile strain at the bottom of the HMA layers is of importance in designing a pavement that is resistant to fatigue (bottom-up) cracking. Thus, for a reliable pavement design it would be ideal to develop relationships between field measured E* and field measured tensile strain. Although E* cannot be accurately measured in the field, the factors influencing it can be directly measured. Thus, relationships can be drawn between these

factors and the field-measured tensile strain. Unfortunately, the design procedure investigated in this analysis (MEPDG) fails to output strain levels. However, tensile strain can be computed through external mechanical analysis using layered elastic analysis for a given pavement structure and known traffic loads. To assess the viability of the MEPDG as a pavement design method, it is necessary that the MEPDG be evaluated with respect to the effect of load duration and E* values on tensile strain.

1.2 OBJECTIVES

Given the onset of the MEPDG as a powerful pavement design tool that may be implemented as a primary design method for roadways among state DOTs, the following objectives were established to assess its benefits:

1. Evaluate the Witczak 1-37A, Witczak 1-40D, and Hirsch E* predictive models for general use HMA mixtures in the southeastern United States.
2. Evaluate the MEPDG's procedure for determination of time of loading for use in estimating E* values and strain levels.
3. Make recommendations for use by state DOTs pertinent to characterizing E* in design procedures.

1.3 SCOPE

To meet the above objectives, a laboratory investigation was completed on test sections from the 2006 structural study as part of the National Center for Asphalt Technology's (NCAT) Test Track. E* testing was completed on HMA mixtures included in that study, following the AASHTO TP-62 procedure for HMA dynamic modulus testing. Three models, the Witczak 1-37A, Witczak 1-40D and Hirsch models

were used to compute E* from gradation, binder and volumetric data of the same mixtures tested in the laboratory. Comparisons were drawn to assess the quality of the MEPDG's analysis and for recommendations to state DOTs.

One of the test sections in the 2006 structural study, section N9, was selected for further field investigation. For this section, regression analyses were completed on laboratory E* test results to determine the in-place dynamic modulus of the HMA layers under live traffic loading. The deep cross-section of N9 allowed for instrumentation at various depths within the HMA, thus enabling the collection of extensive data pertaining to temperature and strain with depth. Field testing was completed on this section over a one month period in the spring of 2007, in which live traffic was applied at a range of speeds. At various depths within N9's pavement structure, longitudinal tensile strains and in-situ pavement temperatures were captured. From the captured longitudinal strain traces at multiple depths, strain values and loading durations were measured. From these measurements, regression analyses were conducted to quantify tensile strain and load duration. Using the load durations computed by both the MEPDG and the model developed in this analysis, E* was computed using the regression equation based on laboratory test results. The effect of the E* estimates on tensile strain were then assessed and conclusions were drawn regarding pavement response as a function of material properties and the use of the MEPDG.

1.4 ORGANIZATION OF THESIS

A literature review in Chapter Two details aspects of HMA dynamic modulus, including the definition, procedure for laboratory testing, means to estimate, and its use in the MEPDG. Additionally, the literature review is extended to a discussion of factors

affecting load duration and strain. Both field and laboratory testing were completed for this investigation. Chapter Three discusses the details of the test facility, the NCAT Test Track, utilized to complete the field testing. Chapter Four includes the details of the laboratory testing to determine E* for the mixes constructed in 2006 and the comparison of the three E* models with laboratory results. Chapter Five describes the conditions of the field testing on section N9. Results of the field testing are discussed, as well as the analysis of the effect of vehicle speed, pavement temperature, and depth on load durations and strain levels. Chapter Six evaluates the MEPDG's use of E* in its design procedure. Contained in this chapter are comparisons with field measurements for load durations computed using the MEPDG procedure and strain levels resulting from the MEPDG's load duration computation. Chapter Seven concludes the aspects of this investigation, and provides recommendations to state DOTs for characterizing E* in an M-E design framework.

CHAPTER TWO

LITERATURE REVIEW

2.1 INTRODUCTION

In an M-E framework, accurate material characterization is vital in successfully predicting pavement responses and ultimately pavement performance. The difficulty in accurately characterizing HMA material properties lies in the viscoelastic nature of HMA. One such material property, dynamic modulus of HMA (E*), reflects the time and temperature dependency of HMA. This material property is the ratio of stress to strain of the mixture, and thus influences the response under loading. Therefore, a complete understanding of this material property and its contributing factors is necessary to accurately characterize it for use in structural design procedures. The factors affecting and the methods to determine dynamic modulus are further investigated through previous literature discussed in the following subsections. Additionally, given that dynamic modulus cannot be measured directly in the field, literature on the factors affecting dynamic modulus that are measurable are also investigated.

2.2 E* DEFINED

The viscoelastic nature of HMA can be characterized in part by its dynamic modulus. The dynamic modulus is a measure of the HMA's resistance to deformation under sinusoidal loading. It is the absolute value of the complex modulus. The complex modulus consists of two parts, the real part, which represents elastic stiffness, and the

imaginary part, representing the internal damping of the materials (Huang, 1993). The dynamic modulus is determined from the maximum applied stress and peak recoverable axial strain, described by Equation 2-1 (Huang, 1993). It should be noted that although dynamic modulus is the absolute value of complex modulus, it is denoted from this point forward in this thesis, simply by E*.

$$E^* = \sqrt{\left(\frac{\sigma_0}{\varepsilon_0}\cos\phi\right)^2 + \left(\frac{\sigma_0}{\varepsilon_0}\sin\phi\right)^2} = \frac{\sigma_0}{\varepsilon_0} \quad (2\text{-}1)$$

where:

E* = dynamic Modulus (psi)

σ_0 = stress amplitude (psi)

ε_0 = strain amplitude ($\mu\varepsilon$)

ϕ = phase angle (radians)

The phase angle describes the lag in the induced axial strain relative to the applied compressive stress, illustrated in Figure 2.1 (Huang, 1993), where the sinusoidal stress pulse is defined by angular velocity, ω, and time, t. This phase lag illustrates the time-dependency of HMA. Due to time-frequency relationships, it can further be stated that HMA is dependent on the loading frequency. This is illustrated by the equations defining the sinusoidal loading (stress) and the sinusoidal response (strain) in Figure 2.1. The stress pulse and resulting strain pulse are both defined by the angular frequency, which is in turn a function of loading frequency, illustrated by Equation 2-2.

$$\omega = 2\pi f \quad (2\text{-}2)$$

where:

ω = angular frequency (rad/sec)

f = loading frequency (Hz)

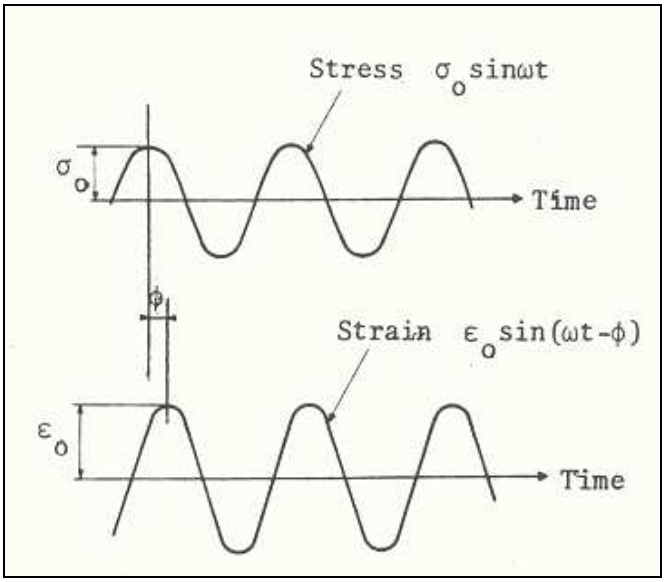

FIGURE 2.1 Phase Lag between Sinusoidal Stress and Induced Strain (Huang, 1993).

HMA is not only frequency-dependent, it is also temperature dependent. Laboratory testing of E* revealed that varying the HMA temperature results in different magnitudes of recoverable strain and thus, varied dynamic moduli (Bonnaure et al., 1977).

2.2.1 E* Defined in the Laboratory

Previous laboratory testing of E* consisted of a 2-point bending test, in which trapezoidal specimens were loaded under sinusoidal compressive stress (Bonnaure et al., 1977). From the 2-point bending test developed for Shell Laboratories, the stiffness modulus (E*) could be determined in two ways. First, E* could be determined from a simple calculation using the measured applied force and the measured displacement at the free end of the specimen. The second method utilized measured strain and the applied stress to calculate E*. By testing multiple mixes at three frequencies (4, 40, and 50Hz) and three temperatures (-15, 9, and 30ºC) Bonnaure et al. found that loading time

and temperature were “significant parameters for the bending strains of asphalt mixes since, under standard service conditions the stiffness may vary from 1,400 to 6,000,000 psi (1977).” It was reported that increasing the temperature or loading time resulted in a decrease in stiffness, defined by E* (1977). Furthermore, Bonnaure et al. discovered that an equivalency among these two factors existed, such that E* curves from different temperatures and frequencies could be superimposed (now referred to as time-temperature superposition), enabling a master curve to be created for a reference temperature (1977). Master curves have since become a useful tool to translate laboratory results to one reference temperature, as is done in the MEPDG.

Laboratory testing has since evolved with the ASTM specification, “D3497-79 (2003) Standard Test Method for Dynamic Modulus of Asphalt Mixtures” (2003). This method requires the application of a haversine compressive stress pulse to a cylindrical specimen at three temperatures, 41, 77, and 104^{o}F, as well as three frequencies, 1, 4, and 16 Hz. The sinusoidal load is applied to the specimen for a minimum of 30 seconds, but not to exceed 45 seconds. Strain gages bonded to the mid-height of the specimen measure axial strain from which the dynamic modulus is computed as the ratio of axial stress to recoverable axial strain.

The most recent and widely used laboratory test for E* is the AASHTO TP62-07 standard method (2007). Again a cylindrical specimen is used, to which haversine axial compressive stress is applied at a given temperature and frequency. Five temperatures, 14, 40, 70, 100, and 130^{o}F and six frequencies, 0.1, 0.5, 1.0, 5, 10, and 25 Hz are specified for testing. Linear variable differential transformers (LVDT) are mounted as a minimum in two locations to measure axial deformation, from which recoverable strain

is calculated. Dynamic modulus is defined in this procedure as the ratio of the stress magnitude to average strain magnitude. Furthermore, phase angle computations are outlined in this procedure.

2.2.2 Factors Affecting E*

Dynamic modulus has been sufficiently proven to be dependent on two parameters: temperature and frequency. The decrease in dynamic modulus with an increase in temperature and decrease in loading frequency has been consistently reported by researchers for many years (e.g., Bonnaure et al., 1977; Flintsch et al., 2007; Tashman and Elangovan, 2007; Mohammad et al., 2007). Looking at the test specimen itself, it is evident that there are many parameters that may present variability in the dynamic modulus. HMA has two main components: aggregate and binder. Each component has numerous properties which influence the overall response of the mixture. Thus, it is only logical that the properties of each component may further influence dynamic modulus.

This sentiment was echoed in research findings at the Virginia Tech Transportation Institute (VTTI) (Flintsch et al., 2007). Dynamic modulus tests produced different master curves for the various mixtures tested, causing Flintsch and colleagues to conclude that “the dynamic modulus test is sensitive to variation in the mix properties” (Flintsch et al., 2007). In recent research conducted for the Washington State Department of Transportation (WSDOT) different mixes were found to possess statistically significantly different dynamic moduli (Tashman and Elangovan, 2007). The objective of this study was to determine typical dynamic moduli values for their Superpave mixes as well as the sensitivity to mix properties. Seven job mix formulas

(JMF) were investigated with aggregates of different type and source. Dynamic modulus tests were completed using the Asphalt Performance Mixture Tester (AMPT), formerly the Simple Performance Tester (SPT) from which master curves were created, illustrated in Figure 2.2. Although variations in dynamic moduli were evident in Figure 2.2, statistical measures (Type I p-value) confirmed that overall the seven different Superpave mixtures were significantly different (Tashman and Elangovan, 2007). Comparing the mixes side-by-side, using a Tukey pair-wise comparison, the results shown indicated that only some mixes were significantly different than others (presented in bold font) (Tashman and Elangovan, 2007). Because these mixtures were tested using the same procedure, AASHTO TP-62-03 (e.g. same temperatures and frequencies), the differences in the aggregate properties, as well as the differences in asphalt properties may account for the variations in dynamic moduli.

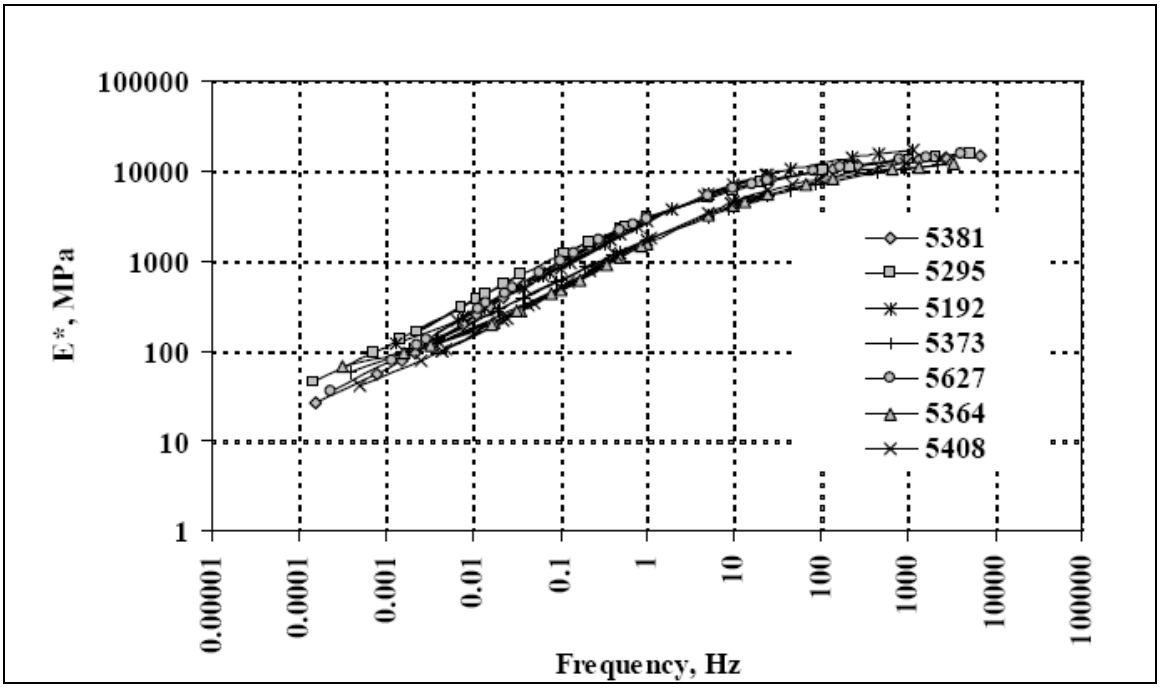

FIGURE 2.2 E* Master Curves by JMF (Tashman and Elangovan, 2007).

2.2.2.1 *Effect of Aggregate Properties*

Previous investigations into dynamic moduli revealed that some aggregate properties are more influential than others. At the very simplest level, the amount of aggregate significantly influences the mix design and its performance. Likewise, Bonnaure and colleagues found that the percent of aggregate by volume also influences the stiffness (dynamic modulus) of the mix (Bonnaure et al., 1977). The percent by volume of air voids was also observed to influence the stiffness of the mix (Bonnaure et al., 1977). Research for WSDOT into aggregate gradation found that small variations (±2% from the JMF) in the percent passing the #200 sieve did not consistently show significant differences in the dynamic modulus of the mix (Tashman and Elangovan, 2007). A look into asphalt mixtures in Louisiana revealed that nominal maximum aggregate size (NMAS) contributed to variations in dynamic moduli (Mohammad et al., 2007). Shown in Figure 2.3, is the trend of increasing dynamic moduli among mixes with higher NMAS. Mixes with a 25mm NMAS were found to be associated with higher dynamic moduli than those mixes with a 19mm or 12.5mm NMAS within each mixture category. Mohammad and colleagues attributed this trend to the stronger stone-to-stone contact among larger aggregates (Mohammad et al., 2007).

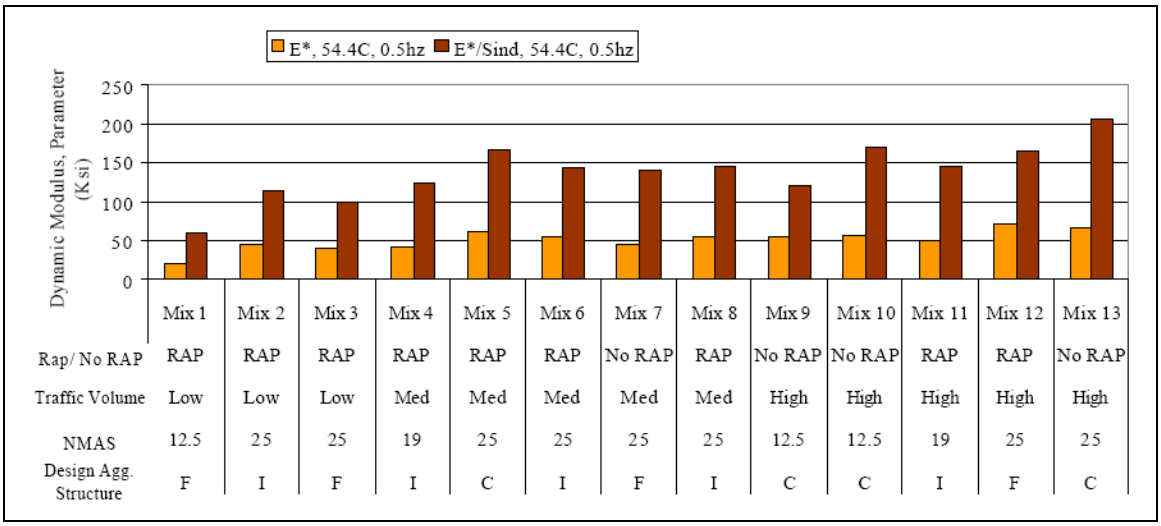

FIGURE 2.3 E* and E*/sinδ for Louisiana Asphalt Mixtures (Mohammad et al., 2007).

The effect of confining pressure was investigated as part of a larger investigation into dynamic moduli of HMA mixtures in Tennessee (Huang et al., 2007). At higher temperatures the effect of aggregate properties was more significant, causing the dynamic moduli to increase with confining pressure. For more rounded aggregate such as gravel, confining pressure was more influential in the improvement of dynamic moduli. From this, Huang and colleagues concluded that the effect of confining pressure on dynamic moduli was "dependent on the role of aggregate structures in asphalt mixtures" (Huang et al., 2007).

Aggregate interactions were found to also influence the phase angle associated to the dynamic moduli. In research conducted at VTTI, phase angles were found to increase up to a certain frequency, and beyond that frequency, phase angles began to decrease for a temperature of 100ºF (Flintsch et al., 2007). Whereas at 130ºF, phase angles consistently increased with increased frequencies. "The predominant effect of aggregate interlock" was credited for the observed behavior (Flintsch et al., 2007).

In addition to aggregate gradation, shape, and interaction, the type of aggregate was also found to contribute to variations in dynamic modulus values of asphalt mixtures. Research at the Florida Department of Transportation (FDOT) was conducted on several mixes in which the binder type remained constant, while aggregate properties varied (Ping and Xiao, 2007). Because the binder type was consistent among all mixes, the differences in HMA stiffness were attributed to the different aggregate types (Ping and Xiao, 2007). Asphalt mixtures containing either granite or RAP were found to be stiffer (higher E*) than the limestone mixtures (Ping and Xiao, 2007).

2.2.2.2 *Effect of Binder Properties*

Some properties associated with the asphalt binder used in HMA mixtures have been found to influence the dynamic modulus values. The PG grade of an asphalt binder is related to its performance under certain temperature ranges. Higher graded binders are generally stiffer to prevent deformation under hot weather conditions. The stiffer binder would likely contribute to the overall stiffness of the mix. Findings from Huang and his associates were consistent with this, as an increase in dynamic moduli was observed as the PG grade progressed from PG 64-22 to PG 70-22 to PG 72-22 for a given temperature (Huang et al., 2007). However for a different type of aggregate (gravel rather than limestone), they found the trend was reversed, such that the dynamic moduli decreased with an increase in binder grade, shown in Figure 2.4.

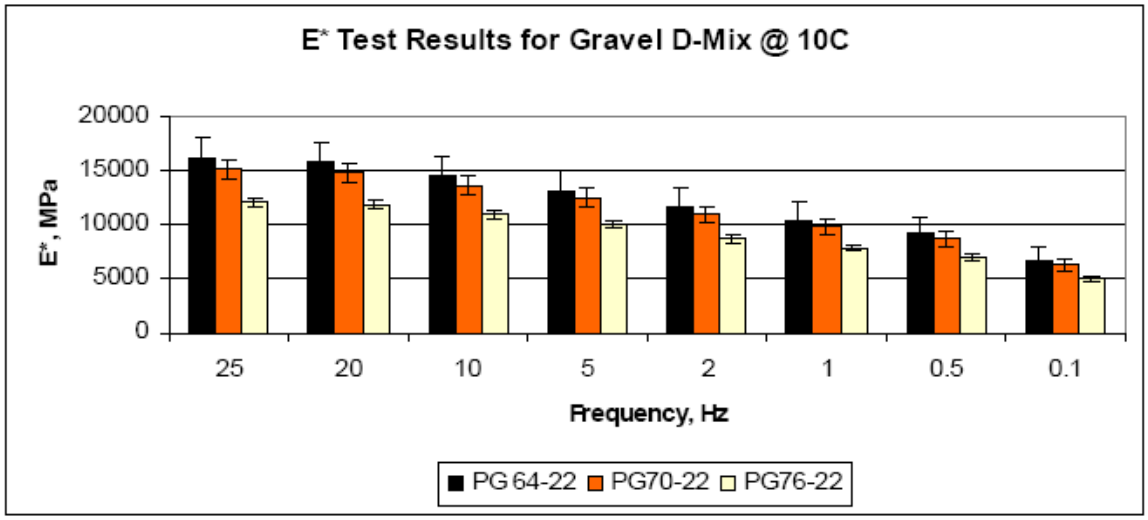

FIGURE 2.4 Dynamic Modulus Results for Gravel at 10ºC (Huang et al., 2007).

Further investigation on the Tennessee plant produced mixes revealed that the asphalt content was influencing the stiffness of the mix as well (Huang et al., 2007). The mixes containing gravel had different asphalt contents for each binder grade used, and overall higher binder contents than the limestone mixes. It was found that the lower dynamic moduli values were associated with higher asphalt contents, leading them to conclude that small variations in binder content influenced the dynamic modulus values (Huang et al., 2007). The sensitivity of the dynamic modulus to asphalt content found in Tennessee mixes was consistent with findings at VTTI (Flintsch et al., 2007). By comparing mixes of the same type, Flintsch et al. also found that the mix with the highest asphalt content exhibited the lowest dynamic modulus (2007). The findings by both these researchers reiterate those from early research by Bonnaure et al., in which sensitivity to the percent of bitumen, the hardness of the bitumen and the temperature susceptibility of the bitumen in the mix were reported (1977).

Reclaimed asphalt pavement (RAP) is often used in mixes across the country to reduce costs. Using RAP in a mixture reduces the amount of new binder required in the

mix because of the contributing asphalt content of the RAP. The aged binder (and therefore higher binder stiffness) from the RAP has been credited with contributing to higher dynamic modulus for Louisiana HMA mixtures (Mohammad et al., 2007).

2.3 PREDICTING E* FROM OTHER PARAMETERS

Although E* can be determined in the laboratory, it is time-consuming and requires expensive specialized equipment and operator training. As a result, the development of equations to predict E* strictly from mix properties have been attempted for many decades. The predictive models, according to Bari and Witczak (2006), developed in the last 60 years are as listed in Table 2.1.

TABLE 2.1 List of E* Predictive Models (Bari and Witczak, 2006)

Model No.	E* Predictive Model	Year (Published)
1	Van der Poel Model	1954
2	Bonnaure Model	1977
3	Shook and Kallas' Models	1969
4	Witczak's Early Model, 1972	1972
5	Witczak and Shook's Model	1978
6	Witczak's 1981 Model	1981
7	Witczak, Miller and Uzan's Model	1983
8	Witczak and Akhter's Models	1984
9	Witczak, Leahy, Caves and Uzan's Models	1989
10	Witczak and Fonseca's Model	1996
11	Andrei, Witczak and Mirza's Revised Model	1999
12	Hirsch Model of Christensen, Pellinen and Bonaquist	2003

Although not the first attempt to model E*, in 1977 Bonnaure et al. developed a nomograph to model E* as a function of the volume of the binder, the volume of the mineral aggregate and stiffness modulus of the binder in Figure 2.5 (1977). This nomograph is commonly referred to as the Shell nomograph, as it was developed for Shell International Petroleum. Additionally, from the same findings, Bonnaure et al., developed a computer program, Module, to predict the stiffness modulus (dynamic modulus) of the mix using the following equations (1977):

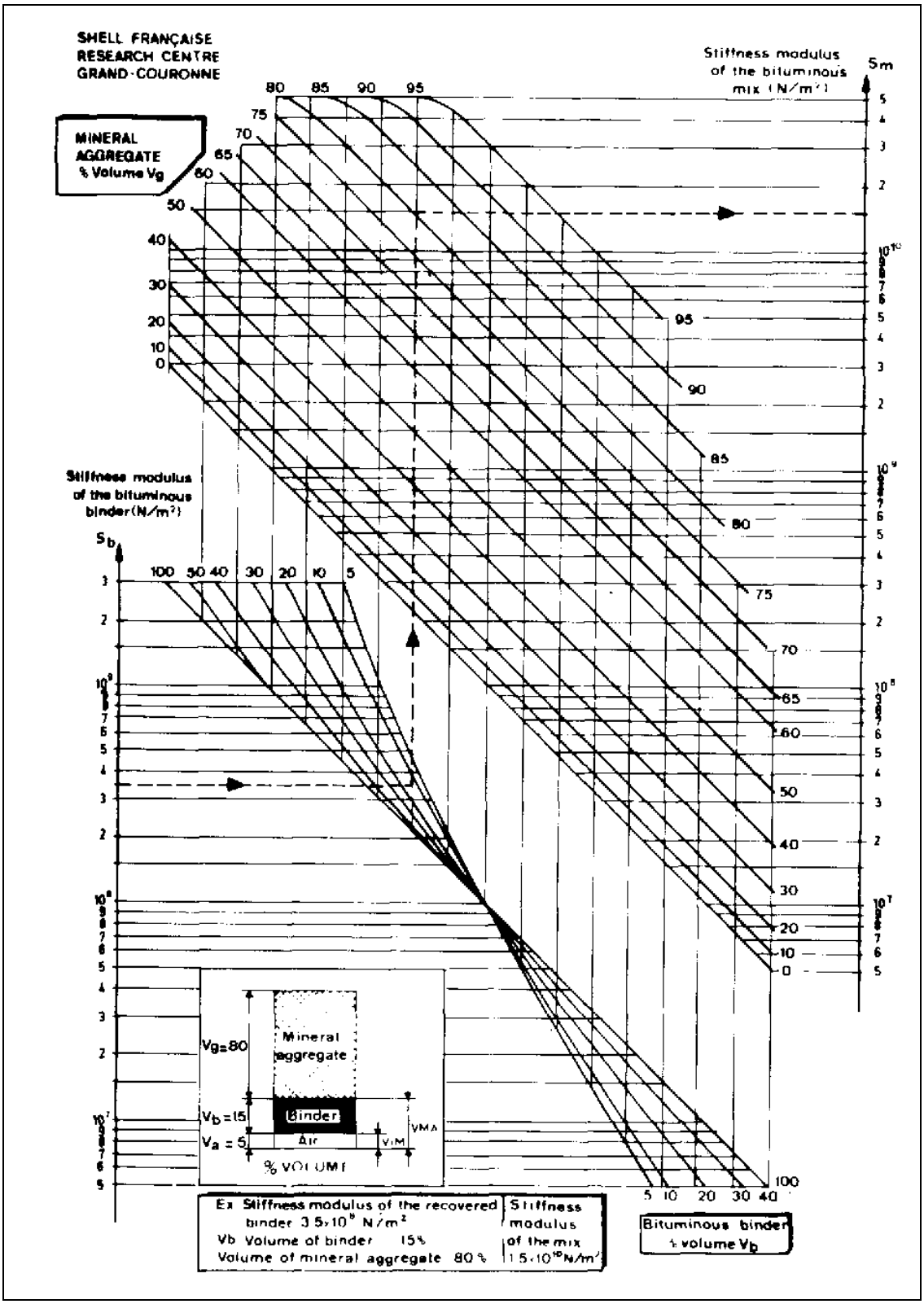

FIGURE 2.5 Nomograph for Predicting Stiffness Modulus of Bituminous Mixes (Bonnaure et al., 1977).

$$\beta_1 = 10.82 - \frac{1.342(100 - V_g)}{V_g + V_b} \quad (2\text{-}3)$$

$$\beta_2 = 8.0 + 0.00568V_g + 0.0002135V_g^2 \quad (2\text{-}4)$$

$$\beta_3 = 0.6\log\left(\frac{1.37V_b^2 - 1}{1.33V_b - 1}\right) \quad (2\text{-}5)$$

$$\beta_4 = 0.7582(\beta_1 - \beta_2) \quad (2\text{-}6)$$

For 5 x 10^6 N/m^2 < S_b < 10^9 N/m^2,

$$\log S_m = \frac{\beta_4 + \beta_3}{2}(\log S_b - 8) + \frac{\beta_4 - \beta_3}{2}\left|\log S_b - 8\right| + \beta_2 \quad (2\text{-}7)$$

For 10^9 N/m^2 < S_b < 3 x 10^9 N/m^2,

$$\log S_m = \beta_2 + \beta_4 + 2.0959(\beta_1 - \beta_2 - \beta_4)(\log S_b - 9) \quad (2\text{-}8)$$

where:

S_m = stiffness modulus of the mix (dynamic modulus) (N/m^2)

V_g = percent volume of aggregate (%)

V_b = percent volume of binder (%)

S_b = stiffness modulus of the bitumen (N/m^2)

The Asphalt Institute (A.I.) developed a method for design in which the dynamic modulus is determined from the following equations, as presented in Huang's Pavement Analysis and Design textbook (1993):

$$|E^*| = 100{,}000 \times 10^{\beta_1} \quad (2\text{-}9)$$

$$\beta_1 = \beta_3 + 0.000005\beta_2 - 0.00189\beta_2 f^{-1.1} \quad (2\text{-}10)$$

$$\beta_2 = \beta_4^{0.5} T^{\beta_5} \quad (2\text{-}11)$$

$$\beta_3 = 0.553833 + 0.028829(P_{200} f^{-0.1703}) - 0.03476V_a + 0.070377\lambda + 0.931757 f^{-0.02774} \quad (2\text{-}12)$$

$$\beta_4 = 0.483V_b \quad (2\text{-}13)$$

$$\beta_5 = 1.3 + 0.49825 \log f \quad (2\text{-}14)$$

$$\lambda = 29{,}508.2(P_{77^\circ F})^{-2.1939} \quad (2\text{-}15)$$

where:

E* = dynamic modulus (psi)

f = loading frequency (Hz)

T = temperature (°F)

V_a = volume of air voids (%)

λ = asphalt viscosity at 70°F, or use equation 2-15 (10^6 poise)

P_{200} = percentage by weight of aggregate passing the No. 200 sieve (%)

V_b = volume of bitumen (%)

$P_{77°F}$ = penetration at 77°F

While the equations developed for Module and the nomograph (Bonnaure et al., 1977) incorporate the volume of all of the aggregate, the A.I. equations utilize only the volume of the fines (percent passing the No. 200 sieve). This indicates possible dependency on the percent of fines, which is contrary to laboratory results in the WSDOT study that found small variations in P_{200} did not significantly affect the dynamic moduli (Tashman and Elangovan, 2007). Although both consider the percent of bitumen in the mix, the A.I. equations also incorporate the viscosity of the bitumen as well as the temperature of the bitumen. Furthermore, the A.I. equations utilize loading frequency as a factor in the

determination of the dynamic modulus of the mix. Although loading frequency is used to compute E*, it is assumed to be 10 Hz for the A.I. design charts (Huang, 1993).

Since, the development of the A.I. method and associated E* predictive model, there have been many more models developed to supplement laboratory testing. Over the last sixty years, these models have progressed by the factors used to determine E* and the overall accuracy of the models. The three most recent models include the Andrei, Witczak and Mirza's Revised Model (1999), the Hirsch Model of Christensen, Pellinen and Bonaquist (2003), and the new revised version of the Witczak E* predictive model (2006). Each of the three is discussed in more detail below.

2.3.1 Andrei, Witczak and Mirza's Revised Model (Witczak 1-37A Model)

The Andrei, Witczak and Mirza's revised model was developed in 1999 (called the Witczak 1-37A model from this point forward), as an update to the previous E* predictive equation, by Witczak and Fonseca in 1996 (Andrei et al., 1999). The previous model considered the binder properties by means of the asphalt viscosity, and effective asphalt content. The model also includes the loading frequency as a variable. Other parameters included air voids, and aggregate gradation information. Laboratory E* test results were used to re-calibrate the previous model by the addition of various mix properties. This was done by establishing a new database consisting of 56 additional mixes, 34 of which were composed of modified asphalt binders, for a total of 1,320 new data points. While the new database had E* test results for only 5 different aggregate gradations, it had a much wider range of viscosity values, as 5 temperatures were tested for the 20 binders. By combining the new database with the database used to develop the previous model, a re-calibration of the previous model was completed, with the revised

model listed below in Equation 2-16 (Bari and Witczak, 2006). As shown in Equation 2-16, the same factors as used for the previous model were utilized for the revised predictive equation. It should be noted that the equation listed in Equation 2-16 was reported by Bari and Witczak in the most recent document regarding the revised Witczak E* predictive equations and it appears that the sixth coefficient is contrary to other sources. The coefficient, listed below as "-0.0822", is contrary to the "-0.08022" reported by Andrei et al. (1999) as well as in other comparative studies (Dongre et al., 2005; Ping and Xiao, 2007). Given that this was the most recent resource by one of the developers of the model and that the difference is negligible, the -0.0822 coefficient was taken as the correct value.

$$\log E^* = -1.25 + 0.029\rho_{200} - 0.0018(\rho_{200})^2 - 0.0028\rho_4 - 0.058V_a - 0.0822\frac{V_{beff}}{V_{beff} + V_a} + \frac{3.872 - 0.0021\rho_4 + 0.004\rho_{38} - 0.000017(\rho_{38})^2 + 0.0055\rho_{34}}{1 + e^{(-0.603313 - 0.313351\log(f) - 0.393532\log(\eta))}} \quad (2\text{-}16)$$

where:

E* = dynamic modulus of mix, 10^5 psi

η = viscosity of binder, 10^6 poise

f = loading frequency, Hz

ρ_{200} = % passing #200 sieve

ρ_4 = cumulative % retained on #4 sieve

ρ_{38} = cumulative % retained on 3/8 in. sieve

ρ_{34} = cumulative % retained on 3/4 in. sieve

V_a = air voids, % by volume

V_{beff} = effective binder content, % by volume

For use in this model (Andrei et al., 1999), the viscosity of the binder is determined by a linear relationship between log-log viscosity and log temperature, illustrated by Equations 2-17 (Bari and Witczak, 2006). In plotting the log-log of the viscosity versus the log of temperature, the slope of the line is the parameter VTS, and the intercept is A. If viscosity information is not obtainable, viscosity can be determined by the relationship with the binder shear complex modulus and binder phase angle, shown in Equation 2-18 (Bari and Witczak, 2006).

$$\log\log\eta = A + VTS\log T_R \tag{2-17}$$

where:

η = viscosity of binder, centipoise (cP)

A, VTS = regression parameters

T_R = temperature, ºRankine

$$\eta = \frac{|G_b^*|}{10}\left(\frac{1}{\sin\delta_b}\right)^{4.8628} \tag{2-18}$$

Where:

G_b* = dynamic shear modulus of binder, psi

δ_b = phase angle of G_b*, degrees

In comparing this model with previous predictive equations, it is evident that it is much more detailed in terms of both aggregate and binder composition of the mix. Similar to the A.I. equations (Huang, 1993), the Witczak 1-37A model requires the percent of fines, air voids, and loading frequency. Like the equations behind the Shell nomograph

(Bonnaure et al., 1977), this model also utilizes the stiffness of the binder, in terms of the shear complex modulus used to determine the viscosity. Rather than considering the percent binder as does the previous equations, this model makes use of the effective binder content, incorporating the ability of the aggregate to absorb the binder. Additionally, the Witczak 1-37A model requires more detailed gradation information beyond the percent of fines needed by previous equations.

2.3.1.1 *Accuracy of the Witczak 1-37A Model*

This model was developed through regression analyses based on the measured dynamic moduli of mixtures ranging in gradation, "from sand-asphalt mixtures to dense-graded mixes," asphalt cements, both conventional and modified, and their degree of aging (Andrei et al., 1999). A coefficient of determination of 0.886 in arithmetic space and 0.941 in logarithmic space was reported for the model (Andrei et al., 1999). Although the model proved to accurately predict the E* values from the database, it is necessary to determine its ability to predict E* for other gradation and binder variations not included in the database, before suggesting its use globally. Several comparison studies have been completed to assess the quality of this model, with various results.

Comparisons were drawn from AMPT laboratory E* testing conducted by the FHWA mobile laboratory with calculated E* values for the properties of the specimens tested (Dongre et al., 2005). For each measured value, three E* values were calculated given the same conditions (temperature and frequency) as the measured values; varying only the binder information for the three different aging scenarios. The three different aged conditions were the original, rolling thin film oven (RTFO), and pressure aging vessel (PAV). Five different mixes, composed of four different binders (PG 64-22, PG

58-28, PG 64-28, and PG 70-22) were tested in this investigation. From this study, it was reported that the Witczak 1-37A model using RTFO aged binder most closely estimated the measured E* values among the three aged conditions (Dongre et al., 2005). Furthermore, the Witczak 1-37A model was found to overestimate E* for the specimens tested at moduli values below 125,000 psi (Dongre et al., 2005). Causes for overpredictions of E* were assumed to be associated with the A and VTS parameters (Dongre et al., 2005). Originally those parameters were developed prior to Superpave specifications, however, Dongre utilized G* results and the associated phase angles to determine viscosity, through Equation 2-18, and thus citing this difference as a potential cause for overprediction (2005). The A and VTS parameters were also credited for the decreased precision ($R^2 = 0.88$) of this model when applied to an expanded database which added 5,820 data points to the database used to create the Witczak 1-37A model (Bari and Witczak, 2006). Furthermore, Bari and Witczak stated "The inherent problem with the ASTM Ai-VTSi relationship is that it does not consider the effect of loading frequency (or time) on the stiffness of the binder itself (2006)."

The overestimation of E* at lower moduli values reported by Dongre and his associates (Dongre et al., 2005), was echoed in later investigations. In a comparison study on Louisiana asphalt mixtures, the Witczak 1-37A model generally underestimated the measured values, except at high temperatures and/or low frequencies (Mohammad et al., 2007). At these lower measured E* values, the model was found to overpredict dynamic moduli values for the thirteen Superpave mixtures tested (Mohammad et al., 2007). Although Dongre et al. reported overprediction for the mixes tested at moduli values of 125,000 psi and less, Azari and colleagues observed

overprediction across the board, with the overprediction more significant at 500,000 psi and lower (Azari et al., 2007). In a comparison study at the VTTI, the Witczak 1-37A was found to overestimate measured values in some instances, with a predicted value reported nearly twice the measured value (Flintsch et al., 2007). Wide ranges were reported for the ratio of predicted to measured E* for each of the eleven mixes investigated; the minimum and maximum ratios are listed in Table 2.2 for each mix (Flintsch et al., 2007). Overestimating low dynamic moduli values could present potential design failures as higher strains result from low moduli, thereby causing premature distresses. Thus, the repeated observed overprediction of dynamic moduli at low frequency and high temperatures is a point of concern.

TABLE 2.2 Minimum and Maximum Values for the Ratio of Predicted to Measured E* (Flintsch et al., 2007)

Ratio	SM1	SM2	SM3	IM1	IM2	IM3	IM4	BM1	BM2	BM3	BM4
Min	0.54	0.58	0.75	0.60	0.60	0.48	0.64	0.54	0.52	0.45	0.68
Max	0.90	1.07	1.56	0.90	1.01	0.75	1.24	0.80	1.90	0.84	1.05

A study on Louisiana asphalt mixtures was completed, in which measured E* values of various mixtures were compared with predicted values from the Witczak 1-37A model (Mohammad et al., 2007). The thirteen mixtures tested included Superpave mixes designed for high, medium and low volume roads, SMA mixes, and Marshall mixes. Three types of binder were used: PG 76-22M, PG 70-22M and PG 64-22, of which the first two were modified. Aggregate structures varied with NMAS ranging from 12.5 mm to 25.0 mm, and various amounts of RAP were used in the mixtures. Mohammad et al. reported generally good agreement between measured and predicted values, with coefficients of determination greater than 0.90 in logarithmic space (2007).

However, it should be noted that logarithmic space can be deceiving and the goodness of fit for arithmetic space was not reported.

As mentioned previously, Mohammad and colleagues reported sensitivity to NMAS in laboratory tests. The Witczak 1-37A model also exhibited sensitivity to NMAS as it produced more accurate predictions for larger NMAS. For the 12.5, 19.0, and 25 mm NMAS mixtures, the predicted modulus was found to be 0.75, 0.93 and 1.01 of the measured values, respectively (Mohammad et al., 2007).

In addition to aggregate gradation, aggregate type was also found to influence the accuracy of the prediction using Witczak's 1-37A model. In a study conducted on Florida DOT mixes, twenty Superpave mixes containing three different aggregate types were investigated using the same binder in all of the mixes (Ping and Xiao, 2007). For mixes containing granite or RAP material, the predictive equation was found to be conservative, as the measured values were slightly underestimated (Ping and Xiao, 2007). Predicted values for mixes containing limestone materials fell above the line of equality when compared with measured values, indicating a slight overprediction for this aggregate type (Ping and Xiao, 2007).

2.3.2 Hirsch Model for Estimating HMA Modulus

The Hirsch model for estimating HMA modulus is based on a law of mixtures for composite materials (Christensen et al., 2003). The law of mixtures, called the Hirsch model, was developed by T.J. Hirsch in the 1960s and combines phases of a material by the arrangement of its elements (Christensen et al., 2003). The elements of a material may be in parallel or series arrangement. The Hirsch model allows for the prediction of a material property (commonly the modulus) of a composite material from

the sum of the same material property of two separate phases of the material, shown in Equation 2-19 in parallel, and Equation 2-20 in series.

$$E_c = \nu_1 E_1 + \nu_2 E_2 \quad (2\text{-}19)$$

$$1/E_c = \nu_1 / E_1 + \nu_2 / E_2 \quad (2\text{-}20)$$

where:

E_c = modulus of the composite material

ν_1, ν_2 = the volume fraction of a given phase

E_1, E_2 = moduli of each phase

In applying the Hirsch model to HMA, Christensen et al. developed a model to predict the modulus of HMA, E*, from the shear modulus of the binder, G*, and volumetric properties of the mix (2003).

This model was developed in part to meet the objectives of the NCHRP Projects 9-25 and 9-31 for Superpave requirements, and to analyze the effects of air voids, voids in mineral aggregate (VMA) and other volumetric properties on E* (Christensen et al., 2003). According to Christensen, the Hirsch model was selected for application to HMA because "asphalt concrete tends to behave like a series composite at high temperature, but more like a parallel composite at low temperatures (2003)." The resulting model for estimating HMA modulus is for "a simple three-phase system of aggregate, asphalt binder, and air voids (Christensen et al., 2003)." The aggregate phase in the parallel portion of the model represents that portion of the aggregate particles in intimate contact with each other, termed aggregate contact volume, Pc (Christensen et al., 2003). Temperature dependency of HMA is partially represented by Pc, such that high values of Pc are related to mixtures with high stiffness and strength, typical at low

temperatures, whereas low values of Pc represent mixtures with low strength and stiffness, typical at high temperatures (Christensen et al., 2003). A database consisting of 18 different mixtures, with 8 different binders and 5 different gradations was utilized in the development of the model, as presented in Equation 2-21 (Christensen et al., 2003). In addition to a predictive equation for E*, an equation to predict the phase angle was also developed, although it is not presented here.

$$\left|E^*\right|_{mix} = Pc\left[4{,}200{,}000\left(1-\frac{VMA}{100}\right)+3\left|G^*\right|_b\left(\frac{VFA\times VMA}{10{,}000}\right)\right]+$$
$$\left(1-Pc\right)\left[\frac{1-\left(VMA/100\right)}{4{,}200{,}000}+\frac{VMA}{3VFA\left|G^*\right|_b}\right]^{-1} \quad (2\text{-}21)$$

where:

$$Pc=\frac{\left(20+\frac{VFA\times 3\left|G^*\right|_b}{VMA}\right)^{0.58}}{650+\left(\frac{VFA\times 3\left|G^*\right|_b}{VMA}\right)^{0.58}}$$

where:

$\left|E^*\right|_{mix}$ = dynamic modulus, psi

VMA = voids in mineral aggregate, %

VFA = voids in aggregate filled with mastic, %

VFA = 100*(VMA-V_a)/VMA

V_a = air voids, %

$\left|G^*\right|_b$ = dynamic shear modulus of binder, psi

In comparison with the Witczak 1-37A predictive equation, and other previous models, this model is much simpler, requiring only three parameters (G*, VMA and VFA). Rather than incorporating frequency and temperature directly into the Hirsch predictive equation, they are inherent to the shear modulus of the binder. Also, the need to translate viscosity data to shear modulus is eliminated, which not only simplifies the equation but is also intuitive given the Superpave Performance Grading system for which G_b* testing is conducted. This could possibly reduce errors highlighted by Dongre and colleagues in their evaluation of the Witczak 1-37A model (2005).

2.3.2.1 *Accuracy of Hirsch Model*

The database used to develop the Hirsch predictive model captured a wide range of measured E* values (183 to 20,900 MPa) from test temperatures of -9, 4, 21, 38, and 54ºC, but only two frequencies, 0.1 and 5 Hz (Christensen et al., 2003). Although the database reflected various conditions, it lacked in the robustness of the test mixes. The range of air voids leaned towards the high end of the spectrum, with only 5.6% air voids (Christensen et al, 2003) tested at the low end. The coefficient of determination of the model was reported as 98.2% (in log space) for the measured E* values in the database (Christensen et al., 2003).

Christensen also applied the Hirsch predictive model to mixes used in a sensitivity study by Witczak, as well as comparing results with measured values and predictions made by Witczak's 1-37A predictive equation (2003). These comparisons revealed that the Hirsch model resulted in a standard error of 41%, a slight improvement over the standard error for the Witczak 1-37A model of 45% (Christensen et al., 2003).

In a comparison study conducted by Dongre and his associates, findings similar to Christensen's were reported, in which predictions by the Hirsch model for E* were closer to the laboratory measured values than those predicted by the Witczak 1-37A model (Dongre et al., 2005). Dongre observed that overall the Hirsch model showed a slight improvement over the Witczak 1-37A model with R^2 values of 0.96 and 0.92 respectively, and S_e/S_y (where S_e is standard error and S_y is standard deviation) values of 0.192 and 0.284 respectively in logarithmic scale (2005). Witczak and colleagues applied the Hirsch model first to their smaller original database of 206 data points and second to the expanded database of 7400 data points (2006). An excellent goodness of fit, $R^2 = 0.98$ in logarithmic scales, was reported when applied to the first database (Witczak et al., 2006). However, when applied to the second, the Hirsch model did not accurately predict the E* values, returning a coefficient of determination of 0.61 in logarithmic scale and 0.23 in arithmetic scale (Witczak et al., 2006).

2.3.3 Newly Revised Witczak Model

Upon the expansion of the database used to enhance the original Witczak predictive model, resulting in the Witczak 1-37A model, Witczak discovered a decrease in accuracy of the 1-37A model (2006). As a result of this decrease, $R^2 = 0.88$ compared to $R^2 = 0.94$ for the development of the 1-37A model, a new model was developed from the expanded database, called the Witczak 1-40D predictive equation from this point forward. The 1-40D model is presented in Equation 2-22.

$$\log E^* = -0.349 + 0.754\left(\left|G_b^*\right|^{-0.0052}\right) \times \left(\begin{array}{l} 6.65 - 0.032\rho_{200} + 0.0027(\rho_{200})^2 + 0.011\rho_4 \\ -0.0001(\rho_4)^2 + 0.006\rho_{38} - 0.00014(\rho_{38})^2 \\ -0.08V_a - 1.06\left(\dfrac{V_{beff}}{V_a + V_{beff}}\right) \end{array} \right)$$

$$+ \frac{2.56 + 0.03V_a + 0.71\left(\dfrac{V_{beff}}{V_a + V_{beff}}\right) + 0.012\rho_{38} - 0.0001(\rho_{38})^2 - 0.01\rho_{34}}{1 + e^{(-0.7814 - 0.5785\log\left|G_b^*\right| + 0.8834\log\delta_b)}}$$

(2-22)

where:

E* = dynamic modulus of mix, psi

$|G_b^*|$ = dynamic shear modulus of binder, psi

ρ_{200} = % passing #200 sieve

ρ_4 = cumulative % retained on #4 sieve

ρ_{38} = cumulative % retained on 3/8 in. sieve

ρ_{34} = cumulative % retained on 3/4 in. sieve

V_a = air voids, % by volume

V_{beff} = effective binder content

The combined database used to develop the 1-40D model expanded the mix properties and incorporated various aging conditions including short-term oven aging, laboratory aging, plant aging, and field aging (Witczak et al., 2006). This was an improvement from the previous database that included only un-aged laboratory blended mixes. Discrepancies in the accuracy of the 1-37A model for the combined database

were believed to be due to the representation of stiffness of the binder and extrapolation of the model beyond the initial range of variables (Witczak et al., 2006).

The 1-37A model requires viscosity by means of the A-VTS relationship shown in Equation 2-17, however, this relationship, as Witczak states, "does not consider the effect of loading frequency (or time) on the stiffness of the binder itself (2006)." This was accounted for in the 1-40D model by replacing the viscosity by means of the A-VTS relationship with a direct input of the complex shear modulus of the binder, G_b*, which "can more effectively take care of the binder rheology with changing temperature and loading rate (Witczak et al., 2006)." Furthermore, the associated binder phase angle, δ_b, was also incorporated into the new model. Similar to the 1-37A model, the 1-40D model also makes use of aggregate gradation, air voids, effective binder volume, voids in mineral aggregate, and voids filled with asphalt to predict E*.

2.3.3.1 *Accuracy of the Witczak 1-40D Model*

The database which enabled the development of the Witczak 1-40D predictive equation used 7400 data points from 346 mixes, from which a coefficient of determination of 0.90 was reported in logarithmic scale, and 0.80 in arithmetic scale (Witczak et al., 2006). This was an improvement over the 1-37A model for the same database, as was the ratio of standard error to standard deviation (Se/Sy) which was reported for the 1-40D model as 0.32 in logarithmic scale and 0.45 in arithmetic scale (Witczak et al., 2006). In looking at the coefficients of determination, it is evident that the 1-40D model ($R^2 = 0.90$) offers a slight improvement over the 1-37A model ($R^2 = 0.88$) for the wide range of mix properties, including varying binder types and aging conditions tested.

Both the 1-37A and 1-40D Witczak equations were evaluated for pavements at the FHWA's Accelerated Loading Facility (ALF) (Azari et al., 2007). Both equations were found to be good predictors of the measured E* values contained in the study. The 1-40D model, however, returned a slightly higher coefficient of determination, 0.936 (in logarithmic scale) than the 1-37A model, which produced an R^2 of 0.917 (also in logarithmic scale) (Azari et al., 2007). Although this reiterates the improvement reported by Witczak (2006), the overestimation at low modulus values reported in numerous evaluations of the 1-37A model (Dongre et al., 2005; Mohammad et al., 2007; Azari et al, 2007) was not improved by the 1-40D model in the study completed by Azari (2007).

2.4 E* IN THE MECHANISTIC-EMPIRICAL PAVEMENT DESIGN GUIDE

The MEPDG offers three levels of design which are dependent on the user's available data and desired accuracy of the design. One significant difference in the three levels of design is the determination of the dynamic modulus. Upon the determination of E*, a master curve is created at a reference temperature of 70^{o}F. The degree of complexity required for material property inputs is dictated by the level of design chosen. A brief description of the methods to estimate E* at each level is listed in Chapter Two of Part Two of the Guide for the MEPDG, presented in Table 2.3 (ARA Inc., 2004). At the highest level of complexity, level one requires laboratory E* and G* results. At levels two and three, laboratory test results for E* are replaced by the estimation of E* from either the 1-37A or 1-40D Witczak predictive equation. At the current stage of development of the MEPDG, the user can select which E* predictive model is run. However, this is likely to change in the future, given the improvement of the 1-40D model over the 1-37A model.

TABLE 2.3 Asphalt Dynamic Modulus (E*) Estimation at Different Hierarchical Input Levels for New and Reconstruction Design (ARA Inc., 2004)

Input level	Description
1	• Conduct E* (dynamic modulus) laboratory test (NCHRP 1-28A) at loading frequencies and temperatures of interest for the given mixture • Conduct binder complex shear modulus (G*) and phase angle (δ) testing on the proposed asphalt binder (AASHTO T315) at ω = 1.59 Hz (10 rad/s) over a range of temperatures. • From binder test data estimate Ai-VTSi for mix-compaction temperature. • Develop master curve for the asphalt mixture that accurately defines the time-temperature dependency including aging.
2	• No E* laboratory test required. • Use E* predictive equation. • Conduct G*-δ on the proposed asphalt binder (AASHTO T315) at ω = 1.59 Hz (10 rad/s) over a range of temperatures. The binder viscosity of stiffness can also be estimated using conventional asphalt test data such as Ring and Ball Softening Point, absolute and kinematic viscosities, or using the Brookfield viscometer. • Develop Ai-VTSi for mix-compaction temperature. • Develop master curve for asphalt mixture that accurately defines the time-temperature dependency including aging.
3	• No E* laboratory testing required. • Use E* predictive equation. • Use typical Ai-VTS – values provided in the Design Guide software based on PG viscosity, or penetration grade of the binder. • Develop master curve for asphalt mixture that accurately defines the time-temperature dependency including aging.

For a level one design, E* laboratory testing must be completed for a range of frequencies and temperatures. G* testing on RTFO-aged binder must also be completed, however, at a fixed loading frequency of 1.59 Hz for a range of temperatures. The recommended temperatures and frequencies for these tests are listed in Table 2.4.

TABLE 2.4 Recommended Frequencies and Temperatures for E* and G*, at Level One Design (ARA Inc., 2004)

	Mixture E* and δ				Binder G* and
Temperature (ºF)	0.1 Hz	1 Hz	10 Hz	25 Hz	δ, 1.59 Hz
10	X	X	X	X	
40	X	X	X	X	X
55					X
70	X	X	X	X	X
85					X
100	X	X	X	X	X
115					X
130	X	X	X	X	X

In Table 2.3, the A-VTS relationship is mentioned as a requirement for a level one design, as well as levels two and three. The A-VTS relationship is described by Equation 2-17 and characterizes the effect of temperature on viscosity for a particular binder. It is used mainly in a level one design to complete the master curve. To obtain viscosity, conventional binder testing can be completed, as listed in Table 2.5, or Equation 2-18 can be used to convert G_b* test results (at f = 1.59 Hz) to viscosity. Once viscosity is obtained the A-VTS relationship is obtained through a linear regression on the viscosity-temperature data, allowing the determination of viscosity at any temperature.

TABLE 2.5 Conventional Binder Tests to Achieve Viscosity (ARA Inc., 2004)

Test	Temp, ºC	Conversion to Viscosity, Poise
Penetration	15	See Equation 2-23
Penetration	25	See Equation 2-23
Brookfield Viscosity	60	None
Brookfield Viscosity	80	None
Brookfield Viscosity	100	None
Brookfield Viscosity	121.1	None
Brookfield Viscosity	135	None
Brookfield Viscosity	176	None
Softening Point	Measured	13,000Poise
Absolute Viscosity	60	None
Kinematic Viscosity	135	Value x 0.948

$$\log\eta = 10.5012 - 2.2601\log(Pen) + 0.00389\log(Pen)^2 \quad (2\text{-}23)$$

where:

η = viscosity, Poise

Pen = penetration for 100 g, 5 sec loading, mm/10

A level two design uses one of the two models previously discussed to estimate E*, requiring volumetric properties, gradation information and depending on which model is selected, either G* testing or viscosity testing. For the Witczak 1-37A model, viscosity is required and can be obtained in the same manner as described above for a

level one design. Although G* testing (at f = 1.59 Hz) can be used for the Witczak 1-37A model, it is not required. For a level two design using the Witczak 1-40D model, G* testing is necessary. Rather than testing at a fixed loading frequency, G* testing must be completed for a range of frequencies and temperatures.

A level three design also utilizes volumetric properties, and gradation information, however no laboratory testing is required. If the user selects the Witczak 1-37A model to estimate E*, viscosity values are estimated from typical temperature-viscosity relationships, programmed into the MEPDG, for the selected binder grade. Similarly, the Witczak 1-40D E* model selects typical G* values from the temperature-viscosity relationship for the binder grade.

2.5 FACTORS AFFECTING LOAD DURATION AND STRAIN

It is known from laboratory testing that HMA modulus is frequency and temperature dependent. In the field the dynamic modulus of HMA characterizes how a particular mixture is likely to respond to a moving load under varying pavement temperatures. Neither E* nor frequency can be measured directly in the field; however time of loading is measurable. Due to time-frequency relationships, time significantly influences the HMA stiffness, and therefore should be investigated. Pavement responses under moving loads are heavily dependent on the HMA modulus. From the defining equation (2-1) for E*, it is evident that strain is inversely influenced by E*. Therefore, it is important that the factors affecting strain be detailed in order to better understand the factors affecting E*.

2.5.1 Load Duration

Historically, time of loading has been defined by either a stress pulse or a strain pulse and found to be dependent on speed and depth. Through the use of finite element and elastic layer theory, Barksdale estimated the shape and length of compressive stress pulses under a rolling wheel load (Barksdale, 1971). He concluded that compressive stress pulse durations are a function of pavement depth and vehicle speed and could be characterized by either a sinusoidal or triangular pulse for vehicle speeds up to 45 mph depending on the depth within the pavement. Further investigation by Brown extended Barksdale's research to stress pulses in three directions, using again elastic layered theory and sinusoidal curves to estimate the length of such pulses (Brown, 1973). From this research Brown developed Equation 2-24, such that the loading time represents the average pulse times of the three orthogonal stresses (vertical, radial, and tangential) which resulted in a loading time equal to 0.48 times that of Barksdale's.

$$\log(t) = 0.5d - 0.2 - 0.94\log(v) \quad (2\text{-}24)$$

where:

d = depth (m)

v = vehicle speed (km/hr)

Measuring load durations in the field has presented challenges in defining the boundaries of the load pulse. More recent research by Loulizi et al. at the Virginia Smart Road facility characterized the effects of speed, depth and temperature on measured vertical compressive stress pulse times (2002). Pulse durations were measured for truck speeds ranging from 8 km/h (5 mph) to 72 km/h (45 mph) at various pavement depths. Similar testing conducted at a later date was used for temperature comparisons, resulting

in maximum in-situ temperature differences between test dates of 13.2ºC (55.8ºF) and 6.8 ºC (44.2 ºF) for the two pavement types investigated. Due to the lack of symmetry in the stress pulses, the loading time was taken to be twice the time of the rising normalized vertical compressive stress pulse beginning at a normalized stress of 0.01 (Loulizi et al., 2002). Loulizi et al. concluded that normalized compressive stress pulse durations generally increased with depth and were related to vehicle speed by a power function (2002). For the conditions tested, no significant relationship with temperature was determined (Loulizi et al., 2002).

In 2008, Garcia and Thompson utilized strain pulses to measure the loading times, reporting that load durations for strain pulses were also influenced primarily by load speed and pavement thickness (2008). A traffic load simulator, the Advanced Transportation Loading Assembly (ATLAS), was employed to apply loads with no lateral displacement under a single tire inflated to 110 psi (Garcia and Thompson, 2008). For the strain measurements recorded during ATLAS testing, the longitudinal and transverse strain pulses were of different shapes, requiring two different definitions for strain pulse duration. In the longitudinal direction, it was taken to be the time that the pavement experienced only tensile strain, whereas in the transverse direction, it was taken to be twice the rising portion (in the tensile region) of the pulse using the unloaded condition as a reference point.

ATLAS testing was conducted at very low speeds, 2 mph, 6 mph, and 10 mph for loads ranging from 5-11 kips. Load duration measurements were taken at various depths in the pavement; however in-situ pavement temperatures were not considered. Generally speaking, pulse durations were found to increase with depth and decrease with

speed, consistent with prior research on stress pulses (Garcia and Thompson, 2008). Specifically, in the longitudinal direction, loading durations were compared with Ullidtz's method for calculating loading times from vertical stress pulses (Garcia and Thompson, 2008). As presented by Garcia and Thompson, the method outlined by Ullidtz is described in Equations 2-25 and 2-26 (2008). From this comparison it was found that for the conditions tested, the Ullidtz method very accurately estimated the measured strain pulse times, over estimating measured longitudinal strain pulse durations by only 2.21% (Garcia and Thompson, 2008).

$$L_{eff} = 200 + 2z \tag{2-25}$$

where:

L_{eff} = effective length (mm)

z = actual depth (mm)

$$t = \frac{L_{eff}}{v} \tag{2-26}$$

where:

t = time of loading

L_{eff} = effective length (mm)

v = vehicle speed

The newly-developed Mechanistic-Empirical Pavement Design Guide (MEPDG) considers depth, vehicle speed and temperature in the determination of loading time (ARA Inc., 2003). The MEPDG assumes the time of loading to be the duration of a haversine stress pulse (ARA Inc., 2003). The method outlined by the MEPDG is similar to the method of Ullidtz as described by Garcia and Thompson (2008), in that an

effective length, L_{eff}, of the load pulse is calculated as a function of the depth, and that time is then a function of the effective length and vehicle speed. However, the MEPDG uses effective depth, Z_{eff}, to compute L_{eff} by considering the modulus of each layer as well as the thickness of each layer above the point of interest. Additionally, the MEPDG takes into account the actual contact radius of the applied load. Given that the HMA modulus is frequency and temperature dependent, and that the MEPDG calculates time of loading ultimately as a function of the HMA modulus, the process is an iterative one. The MEPDG procedure for calculating load duration is described in greater detail in Chapter 6.

2.5.2 Strain

Pavement responses, specifically tensile strain, can be difficult to characterize due to the viscoelastic nature of HMA. Because of its viscous properties, HMA responses are time-dependent, such that as a load is applied, a response is not immediately induced throughout the pavement. Additionally, it is dependent on temperature, causing increased flexibility under warmer temperatures and increased stiffness under colder temperatures. The prediction model becomes increasingly complex when the pavement is under dynamic loading, such as the loading that occurs with live traffic.

Researchers and engineers have characterized these time-temperature relationships both theoretically and through physical measurement. Although developing a temperature-strain relationship was not the primary area of investigation in Mateos and Snyder's validation of a response model from the Minnesota Road Research (Mn/ROAD) test facility, a trend of increasing strain with increasing pavement

temperatures was illustrated in their findings (2002). Observations from the National Center for Asphalt Technology (NCAT) Test Track have reported that an increase in temperature has resulted in an increase in horizontal tensile strain. This relationship was found to be well-modeled by a power function of the mid-depth pavement temperature (Priest and Timm, 2006).

Investigations at the PACCAR Technical Center into the effects of vehicle speed on strain have revealed a reduction in tensile strain with increasing speed (Chatti et al., 1996). For tensile strain in the longitudinal direction at the bottom of the HMA layer, a maximum reduction of 30-40% was reported as vehicle speeds were increased from creeping motion to 64 km/h (Chatti et al., 1996). Similarly, transverse strain at the bottom of the HMA layer was also reported to decrease with speed, although not as significantly (Chatti et al., 1996). Mateos and Snyder (2002) also recorded a decrease in tensile strains in both the transverse and longitudinal direction with changes in vehicle speed.

2.6 SUMMARY

HMA is a viscoelastic material that responds differently to varying conditions. When a load is applied to HMA, the response, strain, is not immediately induced, but rather a time lag exists between the applied stress and induced strain. The dynamic modulus, E*, characterizes this viscoelasticity through its dependency on frequency and temperature. E* is defined as the ratio of peak recoverable stress to peak recoverable strain when HMA is under sinusoidal loading. There have been numerous laboratory tests developed over the years to determine the dynamic modulus of HMA, the most recent and commonly used is the AASHTO TP 62-07 (2007).

Although it has been established that the dynamic modulus is frequency and temperature dependent, laboratory testing has shown that E* is also influenced by mix properties. Aggregate properties such as the type of aggregate, NMAS, air voids and aggregate interactions were found to influence E*. Furthermore, the binder grade, asphalt content, and RAP content were reported as contributing parameters as well.

There have been numerous attempts over the last sixty years with varying degrees of success to develop a means to predict E* without conducting an E* laboratory test. Nomographs and predictive equations have been developed using gradation information, volumetric and binder properties to estimate E*. The three most recently developed equations include the Witczak 1-37A E* predictive model, the Hirsch E* predictive model, and the Witczak 1-40D E* predictive model. The accuracy of the 1-37A model has been reported to vary among NMAS, and aggregate type. The Hirsch E* model was found to be an improvement over the 1-37A model for some databases, but was found to be poor for the database used to create the 1-40D model. Both the 1-37A and 1-40D were reported to overpredict E* at low moduli values.

E* is an important parameter that is essential to accurate pavement designs. The method to determine E* varies among the levels of design in the MEPDG. The hierarchical levels of design (1-3) dictate the extent of required material properties. Levels two and three are particularly useful to those State DOTs which do not have E* laboratory equipment because E* laboratory results are supplemented with E* predictions. At the most complex level, level one, laboratory test results for E* and G* are required. At levels two and three the user may select which model, the Witczak 1-37A or the Witczak 1-40D, is employed to estimate E* from mix properties. At level

two, design gradation information and volumetric properties are required regardless of which model is selected. If the 1-37A model is selected, G* testing at a frequency of 1.59 Hz or viscosity testing is required. For the 1-40D model G* testing at a range of frequencies and temperatures is necessary. At a level three design only gradation and volumetric information is required as the necessary binder information is selected based on typical temperature-viscosity relationships for the selected binder grade.

It is important to be able to link field performance with material properties to further refine the accuracy of M-E pavement design. However, E* cannot be measured in the field. However, two important parameters can be measured: time of loading and strain. Understanding these parameters under varying conditions may lend insight into how E* is characterized under field conditions. Tensile strain has been found to increase under high temperatures and decrease with an increase in vehicle speed. Load durations are influenced by vehicle speed, as well as depth in the pavement. Load durations have been measured by stress and strain pulses, although the MEPDG considers it to be characterized by a haversine stress pulse.

CHAPTER THREE

TEST FACILITY

3.1 INTRODUCTION

The National Center for Asphalt Technology at Auburn University has a full-scale test facility for the evaluation of flexible pavements under live traffic. The test facility is located in Opelika, Alabama, and consists of a 1.7 mile oval test track, with applied traffic similar to open access highways using real trucks and human drivers. The Test Track has enabled its sponsors, state Departments of Transportation (DOT) from the Southeast region and beyond, the Federal Highway Administration (FHWA) and other contributors from the industry to collaborate on advancing HMA technology through the construction and evaluation of flexible pavements in an accelerated pavement testing framework. The Test Track is comprised of 46 200-ft pavement sections with varying cross-sections. Some sections have embedded instrumentation for the evaluation of pavement response and Mechanistic-Empirical analysis. Three complete testing cycles have been completed in the years 2002, 2005, and 2008 respectively. For this investigation, only data from the third cycle, constructed in 2006 and completed in 2008, were utilized, focusing only on those test sections that were newly constructed in the 2006 Test Track structural study.

3.2 2006 STRUCTURAL STUDY

Assessments of the first two test cycles highlighted the sponsors' need for further investigation into structural pavement response (Timm, 2008). To address this need, the third test cycle (2006-2008) included 11 test sections as part of the structural study. The 11 test sections were equipped with embedded instrumentation to capture pavement response under live loading. Of the 11 sections, five (N3, N4, N5, N6, and N7) were left in place from the 2003-2006 test cycle to continue evaluation under additional traffic, and six sections (N1, N2, N8, N9, N10, and S11) were newly constructed with embedded instrumentation in 2006 (Timm, 2008). Additionally, N5 was milled and inlaid with 2 inches of HMA to correct previous top-down cracking in the section. Under normal testing operations, pavement responses were captured on a weekly basis throughout the testing cycle for analysis. Also, the surface performance of each test section was monitored on a weekly basis.

3.3 PAVEMENT CROSS-SECTIONS

Each of the 11 test sections was designed based on the individual sponsor's need and common practices. As a result, the cross-sections varied by the HMA mixtures and unbound materials utilized in the structures. The cross-sections of each are shown in Figure 3.1, labeled by its associated sponsor and whether it was left in place from the 2003-2006 test cycle or newly constructed in 2006.

One commonality among the test sections was the local unbound material used to construct the sections. All 11 pavement sections utilized the local soil at the Test Track, referred to as "Track soil," which is classified as an AASHTO A-4(0) soil

containing large cobbles and stones (Timm, 2008). Excluding section N8 and N9, all of the test sections utilized this material as a compacted subgrade. Sections N8 and N9 instead used a compacted soft subgrade material, on top of the uncompacted Track soil (not shown in Figure 3.1) and the compacted Track soil as a base material. The soft subgrade material was imported from Seale, Alabama and had a high clay content which closely replicates subgrade materials typically encountered in Oklahoma. A Limerock base quarried in Florida and typically used by the Florida DOT was placed in sections N1 and N2. The Granite base used in sections N3-N7, and S11 was quarried in Columbus, Georgia, and is typically utilized by ALDOT for road construction in the Southeastern part of Alabama. Section N10 used a Missouri Type 5 base material. Laboratory testing and backcalculation was conducted on each of the unbound materials to determine the resilient modulus, M_R, as a function of the state of stress (Taylor, 2008). Discussion of these results appears in Chapter Six of this thesis.

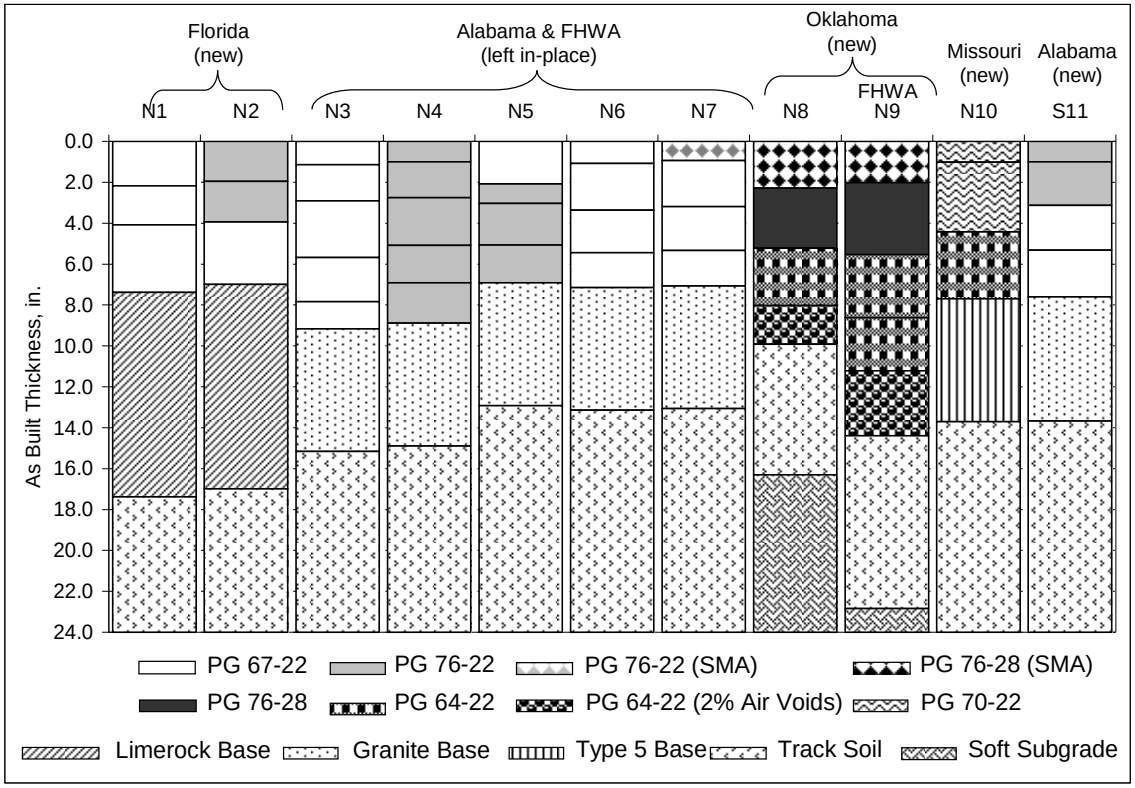

FIGURE 3.1 2006 Test Track Structural Study Test Sections (Timm, 2008).

In terms of HMA mixtures, five different binder types were used to create unique mixes by varying aggregate gradations, air voids, and binder contents. HMA layers in seven sections, N1, N2, N3, N5, N6, N7, and S11 employed a PG 67-22 unmodified binder. The PG 76-22 binder used in the HMA layers in sections N2, N4, N5, and S11 was modified with styrene-butadiene-styrene (SBS) (Timm, 2008). The surface course of N7 also used a PG 76-22; however it was a stone-matrix asphalt (SMA) mix. PG 76-28 binder was used in sections N8 and N9 in the surface course SMA and in the second HMA layers. These sections used PG 64-22 binder in the bottom two HMA layers. Although the binder type was common to both layers, the bottom layer was designed for only 2% air voids, referred to as a "rich bottom" layer. Lastly, the PG 70-22 binder was used for one HMA layer in section N10. As-built properties of each layer were

recorded, as well as the designed properties. For the sections constructed in 2006, including the top layer of section N5, binder testing was completed to determine the dynamic shear modulus, G*, and viscosity values. Additionally, laboratory tests were completed to determine the dynamic modulus, E*, of the HMA layers. As mentioned previously, only the datasets from the newly constructed 2006 sections and the top lift in N5 were utilized for this investigation. Detailed information about these laboratory test results is discussed in Chapter Four of this thesis.

3.4 INSTRUMENTATION

In order to characterize pavement response, instrumentation was embedded within each section at the time of construction, providing extensive information on temperature, stress and strain within the structures. Embedded within each of the 11 sections was at a minimum, one pair of earth pressure cells, twelve strain gages, and four temperature probes. Based on the research objectives of the corresponding sponsors, some sections included more extensive instrumentation. Figures 3.2, 3.3, and 3.4 illustrate the arrangement of the pressure cells and strain gages for the various sections, though this investigation focused primarily on Section N9 (Figure 3.4).

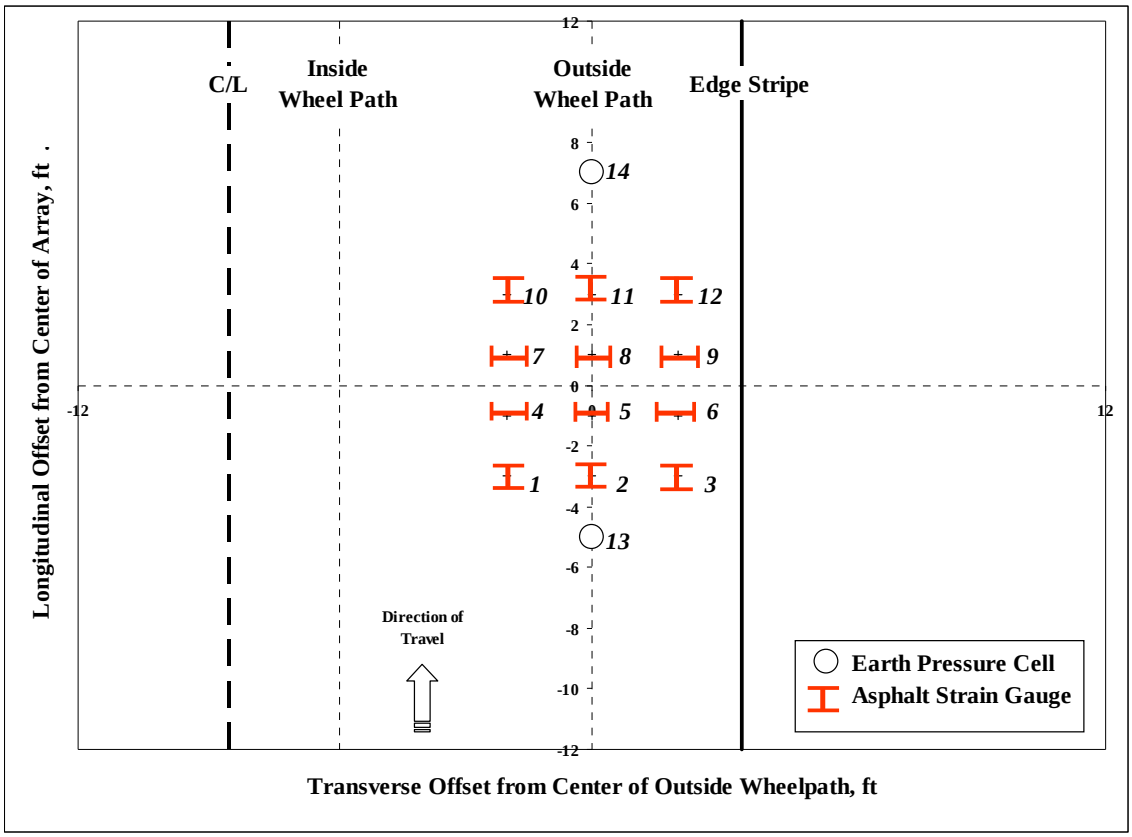

FIGURE 3.2 Location of Gages, Sections N1-N6, N8, N10, S11 (Timm, 2008).

Strain gages were installed to capture the induced tensile strain in both the longitudinal and transverse directions. Regardless of the year of construction, 2003 or 2006, the same type of gage was consistent. The gages were purchased from Construction Technologies Laboratories, Inc. (CTL). They were designed for most pavement cross-sections with a maximum range of 1,500 με, well within typical strain magnitudes experienced in most pavement cross-sections (Timm, 2008). A strain gage array, gages 1-12, was installed in each of the sections at the bottom of the HMA layer. The gages were installed in groups of three by direction, oriented either longitudinally or transversely. Within a group, one gage was aligned with the centerline of the outside wheel path, and the remaining two were offset to the right and left of the outside wheel path. Doing so helped to account for wheel wander, allowing the best hit to be captured.

Two groups each of strain gages were installed in both the longitudinal and transverse directions to create redundancy in the system.

Figure 3.2 illustrates the configuration of gages for sections N1-N6, N8, N10 and S11. Additional strain gages, gages 18-21 were installed in section N7 at a depth of 5 inches, located along the centerline of the outside wheel path atop the gages installed at the bottom of the HMA layers, as shown in Figure 3.3. Carrying this idea further, Section N9 included twelve strain gages in addition to the gage array at the bottom of the HMA layers. The additional twelve were installed in groups of four along the centerline of the outside wheel paths at various depths, downstream from the three by four gage array, illustrated in Figure 3.4. Within each array, two each longitudinal and transverse gages were installed inline with the outside wheel path. Gages 16-19 were installed at the bottom of the fourth HMA layer (11.04 inches), gages 20-23 were placed at the bottom of the third HMA lift, 8.76 inches deep and lastly, gages 24-27 were placed at the bottom of the second HMA lift, 6.00 inches deep. These depths were determined using surveying equipment.

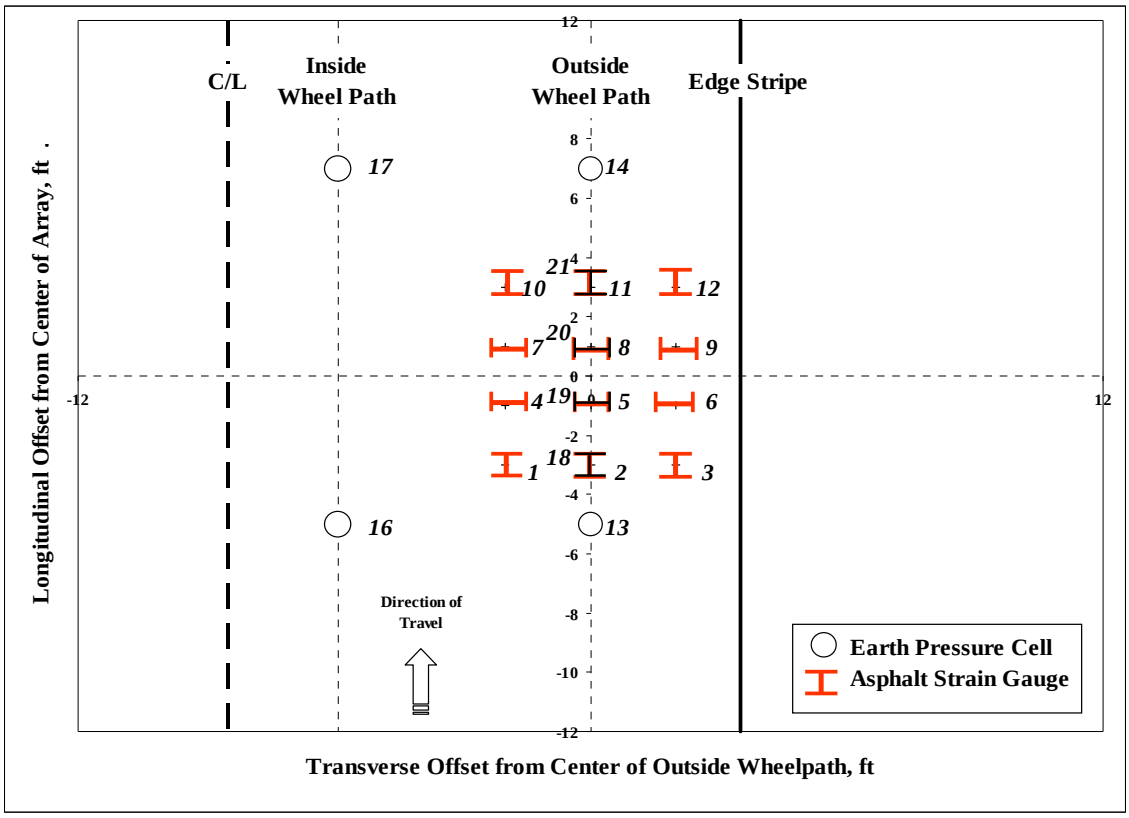

FIGURE 3.3 Location of Gages, Section N7 (Timm, 2008).

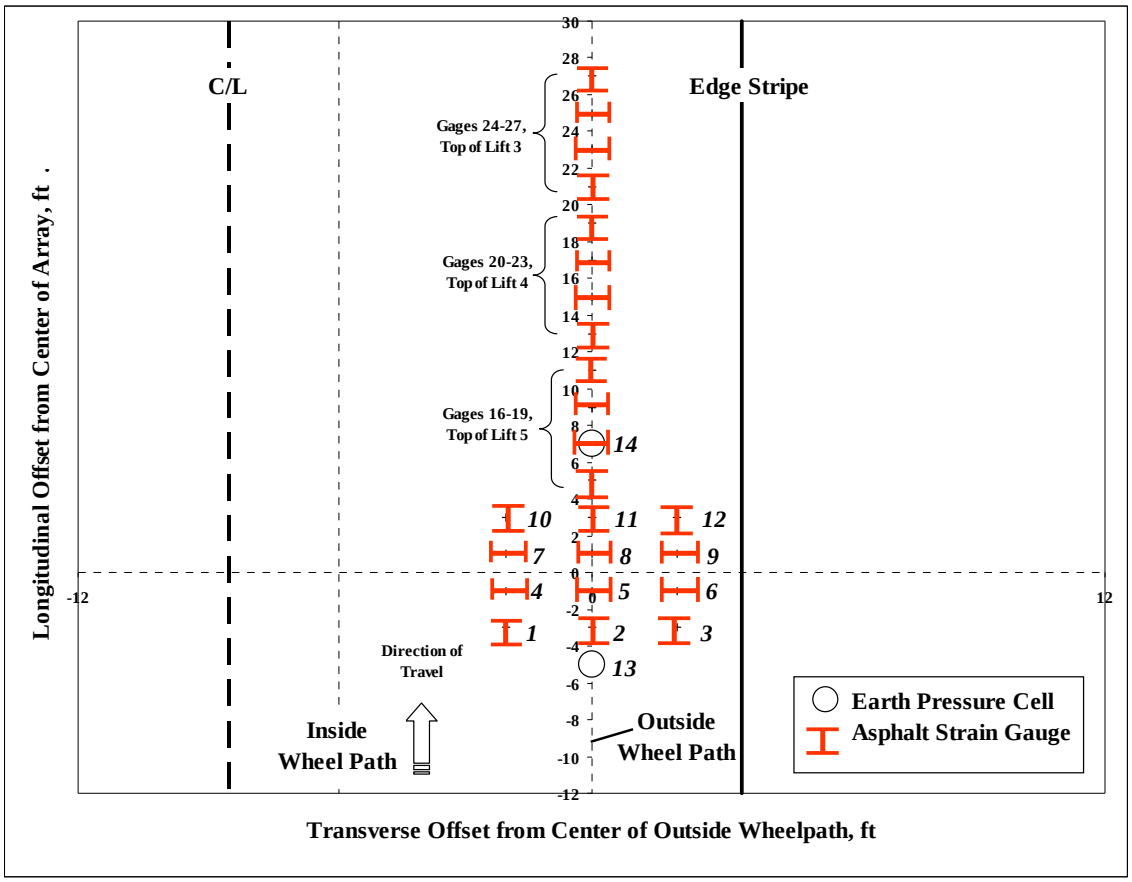

FIGURE 3.4 Location of Gages, Section N9 (Timm, 2008).

Temperature probes were installed at various depths within the structure, creating a complete temperature profile for each. For consistency, Campbell-Scientific model 108 temperature thermistors were installed in the sections constructed in both 2003 and 2006. Four thermistors were placed as a minimum in each section, as listed in Table 3.1. Sections N3-N7 (those left in place from the 2003-2006 cycle) were installed at consistent depths, regardless of the cross-section. However, for the sections constructed in 2006, one thermistor each was installed at the surface, mid-depth and bottom of the HMA layer and three inches into the base layer (Timm, 2008). Section N9 employed additional thermistors, installed at the depths listed in Table 3.2, which provided a much more detailed view of the temperature gradients experienced.

TABLE 3.1 Location of Thermistors

	Depth of Probe, inches			
Section	T1	T2	T3	T4
N1	0.0	3.7	7.4	10.4
N2	0.0	3.5	7.0	10.0
N3	0.0	2.0	4.0	10.0
N4	0.0	2.0	4.0	10.0
N5	0.0	2.0	4.0	10.0
N6	0.0	2.0	4.0	10.0
N7	0.0	2.0	4.0	10.0
N8	0.0	5.0	10.0	13.0
N9	0.0	7.2	14.4	17.4
N10	0.0	3.9	7.7	10.7
S11	0.0	3.8	7.6	10.6

TABLE 3.2 Location of Additional Probes in Section N9

Probe	Depth, in.
T5	0.0
T6	1.0
T7	2.0
T8	3.7
T9	5.4
T10	6.9
T11	8.4
T12	9.6
T13	10.8
T14	12.4
T15	14.1
T16	17.1

3.5 TRAFFIC

Live traffic was applied at the Test Track on a daily basis. Heavy trucks were operated by truck drivers for 16-hours a day, 5 days a week, totaling nearly 10 million Equivalent Single Axle Loads (ESALs) in the 3-year testing cycle. The trucks had approximately a 12-kip steer axle, 40-kip tandem axle, and 5 trailing 20-kip single axles. The Test Track operates five different trucks with the following axle spacing and axle weights listed in Tables 3.3 and 3.4.

TABLE 3.3 Spacing Between Axles (Taylor, 2008)

		Distance Between Axles (ft)						
Truck #	Steer	Front Tandem	Rear Tandem	Single 4	Single 5	Single 6	Single 7	Single 8
1	0.0	13.6	4.3	18.7	11.2	20.0	11.2	20.0
2	0.0	13.6	4.3	17.1	17.0	17.0	17.0	17.0
3	0.0	13.6	4.3	17.1	17.0	17.0	17.0	17.0
4	0.0	13.6	4.3	17.1	17.0	17.0	17.0	17.0
5	0.0	13.6	4.3	14.8	12.4	17.2	11.0	17.2

TABLE 3.4 Axle Weight by Truck (Taylor, 2008)

		Axle Weights (lb)						
Truck #	Steer	Front Tandem	Rear Tandem	Single 4	Single 5	Single 6	Single 7	Single 8
1	9,400	20,850	20,200	20,500	20,850	20,950	21,000	20,200
2	11,200	20,100	19,700	20,650	20,800	20,650	20,750	21,250
3	11,300	20,500	19,900	20,500	20,500	21,000	20,650	21,100
4	11,550	21,200	19,300	21,000	21,050	21,000	20,750	20,800
5	11,450	20,900	19,400	20,100	20,450	21,000	20,050	20,650

3.6 DATA ACQUISITION

Wireless data transmission was utilized in the 2006 Test Track structural study to transmit pavement response measurements. However, data were collected through hard-connection at roadside data acquisition enclosures during the 2003-2006 testing cycle. For consistency the same data acquisition devices were utilized in both the sections from the 2003-2006 testing cycle and those constructed in 2006. To do so meant upgrading the left-in-place sections with new devices to meet the needs of the 2006 wireless system. This enabled safe data acquisition wirelessly from an enclosed building away from the track and live traffic, which was a significant improvement given the frequency of data collection. For normal operations, data were collected on each of the structural sections on a weekly basis. Weekly data collection consisted of recording the in-situ pavement temperatures and strain responses under three passes of live traffic. As mentioned previously, an additional field study was conducted utilizing section N9. To

do so, data was collected on four different test dates over a one month testing period. For this testing strain responses were measured under a variety of speeds, rather than at the normal 45 mph. The details of the N9 field investigation are discussed in more detail in Chapter Five of this thesis.

3.7 SUMMARY

This chapter served in describing the test facility. The test facility encompasses the application of live traffic over 46 different pavement cross-sections on a 1.7 mile test track. Approximately 10 million ESALs were applied via the five 132-kip trucks operated at the Test Track. Eleven of the 46 test sections were included in the 2006 Test Track structural study which utilized embedded instrumentation to record pavement responses at various critical locations within a structure. On a weekly basis strain and stress data were collected from these sections through the use of data acquisition devices and wireless transmittal. Laboratory testing was conducted on the sections constructed in 2006 as well as the top lift of N5 which was milled and inlaid in 2006. Testing included G*, E*, and viscosity testing. Also, detailed as-built information regarding the volumetric properties of each section was recorded. Using those datasets for these six sections (plus N5 top lift), further analysis was completed on the accuracy of E* models. Additional analysis was completed on the relationship between E* and pavement response, as discussed in Chapters Five and Six.

CHAPTER FOUR

LAB INVESTIGATION

4.1 INTRODUCTION

There are three levels of design that one can choose from when using the MEPDG for flexible pavement design (ARA Inc., 2004). One significant difference in the three levels of design is how the dynamic modulus of HMA is computed and therefore the degree of complexity required for material property inputs. Level one is the most complex degree of design, requiring laboratory test results for both mixture dynamic modulus (E*) and binder shear modulus (G_b*). However, dynamic modulus laboratory testing is time consuming and expensive. Therefore, it is likely that many state DOTs will opt to use levels two or three design which do not require E* test results, but rather estimate E* from predictive equations. The required material property inputs for these levels are minimal and are parameters that are typically measured as part of a specification. Level two, the second most complex design, utilizes either the 1-37A or the 1-40D Witczak Predictive E* equation (at the discretion of the user) as a function of binder information, gradation information, and other volumetric information. Level three, the least complex of the three designs also utilizes either the 1-40D or the1-37A Witczak Predictive E* equation, however laboratory binder test results are not required. Interestingly, when using the MEPDG, the designer is simply presented with the option of running either equation, but no guidance to aid in this decision.

Although the MEPDG utilizes the Witczak equations in its determination of E*, there are many other equations that have been developed over the years to predict E* from similar properties. One such model, the Hirsch E* predictive model was developed in 2003 as a response to the objectives of the NCHRP 9-25 and 9-31 projects (Christensen et al., 2003). It is among the most recently developed models used to predict E* from mix properties. Although the Hirsch E* predictive model is not currently used in the MEPDG, it should be evaluated to offer comparisons with the MEPDG methods and to determine the most effective predictive model for pavement designers.

Due to the lack of finances and means to run difficult laboratory tests, there is a need to validate the MEPDG's procedure in calculating E* at the two lowest levels of design. To evaluate the accuracy of these two designs, three E* predictive equations were analyzed and compared with E* laboratory test results. E* testing on the mixtures in the newly-constructed 2006 Test Track structural study formed the basis of this investigation.

4.2 MODELS TO DETERMINE E*

Three E* predictive equations were utilized to assess the accuracy of the MEPDG, both Witczak equations contained within the program and a third equation, the Hirsch model for estimating E*. As part of the NCHRP 1-37A project, a predictive model for E* was developed utilizing rudimentary mix information including basic binder test results to be included in the MEPDG (Bari and Witczak, 2006). An initial model was developed in 1996 by Witczak and Fonseca, however it was quickly updated, expanding the dataset and re-calibrating the model. This model, updated by Witczak and

Andrei, was implemented for use in both levels two and three of the MEPDG in 1999 (Bari and Witczak, 2006). To alleviate confusion, this model will be referred to as the Witczak 1-37A E* predictive equation, given that it was developed under the NCHRP 1-37A project. In 2005, a third Witczak equation was developed under the NCHRP 1-40D initiative which again updated Witczak's E* predictive equation (Bari and Witczak, 2006). This third equation, termed here as the Witczak 1-40D E* predictive equation, was implemented in the MEPDG version 1.0 allowing the user to select between the 1-37A and 1-40D equation for use in level two and three design. However, the user is heeded that the 1-40D equation has not yet been nationally calibrated.

Aside from the 1-37A and 1-40D equations, there have been many other E* predictive equations developed over the years. One of the more recent models is the Hirsch E* predictive model developed in 2003 (Christensen et al., 2003). In meeting the objectives of this thesis, the two Witczak models embedded within the MEPDG, the Witczak 1-37A and the Witczak 1-40D E* predictive equations were analyzed as well as the Hirsch E* predictive model.

The information required for each model is listed in Table 4.1. As mentioned previously, the level of complexity of the material property inputs varies among the three models. Two of the three require G_b* testing, while only one requires the phase angle associated with G_b*. It is worthy of noting that while both the Witczak models incorporate the gradation of the mix, the Hirsch model does not. In fact, the Hirsch model relies only on four properties of the mix.

TABLE 4.1 Material Property Requirements by Model

Information	Witczak (1-37A)	Witczak (1-40D)	Hirsch
Gradation:			
ρ_{200} pass.	X	X	
ρ_4 ret.	X	X	
ρ_{38} ret.	X	X	
ρ_{34} ret.	X	X	
VMA			X
V_a	X	X	X
VFA			X
V_{beff}	X	X	
f	X		
η	X		
G_b*		X	X
δ_b		X	

4.2.1 Witczak 1-37A E* Predictive Equation

The original Witczak model was developed in 1996 by Dr. Witczak and his colleagues using 149 unaged HMA mixtures (Bari and Witczak, 2006). The binder types utilized in the mixtures were conventional binders only (i.e., unmodified), which severely limits the use of this model. This equation was revised in 1999, by expanding the dataset and deriving an equation that more accurately fit a wider range of gradations, binder stiffness and air voids (Andrei et al., 1999). The revised equation, the Witczak 1-37A E* predictive equation (Bari and Witczak, 2006), listed in Equation 4-1, is a function of gradation of the aggregate, air voids, effective binder content, viscosity of the binder, and loading frequency:

$$\log E^* = -1.25 + 0.029\rho_{200} - 0.0018(\rho_{200})^2 - 0.0028\rho_4 - 0.058V_a - 0.0822\frac{V_{beff}}{V_{beff} + V_a}$$
$$+ \frac{3.872 - 0.0021\rho_4 + 0.004\rho_{38} - 0.000017(\rho_{38})^2 + 0.0055\rho_{34}}{1 + e^{(-0.603313 - 0.313351\log(f) - 0.393532\log(\eta))}} \quad (4\text{-}1)$$

where:

E^* = dynamic modulus of mix, 10^5 psi

η = viscosity of binder, 10^6 poise

f = loading frequency, Hz

ρ_{200} = % passing #200 sieve

ρ_4 = cumulative % retained on #4 sieve

ρ_{38} = cumulative % retained on 3/8 in. sieve

ρ_{34} = cumulative % retained on 3/4 in. sieve

V_a = air voids, % by volume

V_{beff} = effective binder content

Equation 4-1 is currently used for a level two design in the MEPDG (ARA Inc., 2004). It is also employed for the level three design with the use of typical viscosity values of the binder based on the binder grading (ARA Inc., 2004). The viscosity can be determined by conventional binder tests or from a dynamic shear modulus (G_b^*) test. When using the G_b^* to determine viscosity, G_b^* and its associated phase angle must be measured at a variety of temperatures for a loading frequency of 1.59 Hz or 10 rad/sec, from which Equation 2-18 is employed to calculate viscosity (ARA Inc., 2004). The loading frequency for G_b^* testing should not be confused with the loading frequencies required for the 1-37A model, as the loading frequencies selected for the model are typical of an E^* laboratory test (0.1, 1, 10, 25 Hz, etc.). Viscosity can also be determined from conventional binder tests: Penetration, Softening Point, Absolute Viscosity,

Kinematic Viscosity or Brookfield Viscosity. However some require a conversion to achieve a viscosity in Poise.

4.2.2 Witczak 1-40D E* Predictive Equation

The Witczak 1-37A E* predictive model was revised in 2006, again expanding the dataset beyond the original model, using a total of 346 HMA mixes to calibrate the model (Bari and Witczak, 2006). One important difference to note between the 1-37A E* predictive model and the 1-40D E* predictive model is the replacement of the viscosity and loading frequency parameters with the dynamic shear modulus of the binder, G_b^*, and its associated phase angle, δ_b, as shown in Equation 4-2 (Bari and Witczak, 2006):

$$\log E^* = -0.349 + 0.754\left(|G_b^*|^{-0.0052}\right)\times\left(\begin{array}{l} 6.65 - 0.032\rho_{200} + 0.0027(\rho_{200})^2 + 0.011\rho_4 \\ -0.0001(\rho_4)^2 + 0.006\rho_{38} - 0.00014(\rho_{38})^2 \\ -0.08V_a - 1.06\left(\dfrac{V_{beff}}{V_a + V_{beff}}\right) \end{array}\right) + \frac{2.56 + 0.03V_a + 0.71\left(\dfrac{V_{beff}}{V_a + V_{beff}}\right) + 0.012\rho_{38} - 0.0001(\rho_{38})^2 - 0.01\rho_{34}}{1 + e^{(-0.7814 - 0.5785\log|G_b^*| + 0.8834\log\delta_b)}} \quad (4\text{-}2)$$

where:

E* = dynamic modulus of mix, psi

$|G_b^*|$ = dynamic shear modulus of binder, psi

ρ_{200} = % passing #200 sieve

ρ_4 = cumulative % retained on #4 sieve

ρ_{38} = cumulative % retained on 3/8 in. sieve

ρ_{34} = cumulative % retained on 3/4 in. sieve

V_a = air voids, % by volume

V_{beff} = effective binder content

δ_b = phase angle of binder associated with $|G_b^*|$, degrees

This newly established Witczak equation (Bari and Witczak, 2006), the Witczak 1-40D E* Predictive equation was implemented in the MEPDG for use in level two and three design. As mentioned previously, the user has the option of selecting the 1-37A or the 1-40D model for design. At a level three design, typical G_b^* and δ_b values are estimated within the program depending on the selected grade of the binder. Although the loading frequency parameter has been omitted in the new model, the time and temperature dependency of dynamic modulus is characterized by G_b^* and δ_b. Witczak and colleagues attempt to define the time-frequency relationship used to characterize G_b^* and δ_b, however, the relationships are unclear and inconsistent throughout the document (Bari and Witczak, 2006). Therefore, it is assumed that the loading frequency used in G_b^* testing is equivalent to loading frequency for the mixture modulus test, E*.

4.2.3 Hirsch E* Predictive Model

The Hirsch E* predictive equation is similar to the Witczak equations in that it also utilizes volumetric information and G_b^* laboratory test results. However, this model requires only two volumetric properties: VMA and VFA, as a function of V_a. The Hirsch E* model was developed based on the law of mixtures, also referred to as the Hirsch model, for composite materials (Christensen et al., 2003). The Hirsch E* predictive equation for asphalt mixtures, as developed by Christensen and his colleagues is:

$$\left|E^*\right|_{mix} = Pc\left[4{,}200{,}000\left(1-\frac{VMA}{100}\right)+3\left|G^*\right|_b\left(\frac{VFA\times VMA}{10{,}000}\right)\right]+$$

$$(1-PC)\left[\frac{1-(VMA/100)}{4{,}200{,}000}+\frac{VMA}{3VFA\left|G^*\right|_b}\right]^{-1}$$

where:

$$Pc=\frac{\left(20+\frac{VFA\times 3\left|G^*\right|_b}{VMA}\right)^{0.58}}{650+\left(\frac{VFA\times 3\left|G^*\right|_b}{VMA}\right)^{0.58}}$$

(4-3)

where:

$\left|E^*\right|_{mix}$ = dynamic modulus, psi

VMA = voids in mineral aggregate, %

VFA = voids in aggregate filled with mastic, %

VFA = 100*(VMA-V_a)/VMA

V_a = air voids, %

$\left|G^*\right|_b$ = dynamic shear modulus of binder, psi

Just as in the 1-40D model, the time and temperature dependency of E* is characterized in the Hirsch E* predictive model by G_b*. According to Christensen, the G_b* "should be at the same temperature and loading time selected for the mixture modulus, and in consistent units (Christensen et al., 2003)." For this evaluation, it was assumed that the frequency-time relationship is consistent for both G_b* and E* tests such that a selected frequency applies the load for the same time in either test. Therefore, the loading frequencies and temperatures selected associated with G_b* were the same as those from

the measured E* values, which enabled a direct comparison of predicted to measured E* values.

4.3 TESTING PROTOCOL

To complete the dynamic modulus testing for each unique mix listed, the testing protocol outlined by AASHTO TP 62-07 was followed (AASHTO, 2007). An Asphalt Mixture Performance Tester (AMPT), formerly called the Simple Performance Testing machine (SPT), shown in Figure 4.1, was utilized to apply haversine compressive loading for a range of frequencies and temperatures. For this investigation E* results at three temperatures, 40, 70, and 100ºF and seven frequencies, 0.5, 1, 2, 5, 10, 20, and 25 Hz were obtained.

FIGURE 4.1 The AMPT Machine and Close-up of Specimen.

Viscosity was obtained for the various binders using the Brookfield Viscometer. The test procedure was in compliance with the ASTM D2983-04a (ASTM, 2004). The

binders were aged in a Rolling Thin-Film Oven (RTFO) and Brookfield viscosities were obtained at two temperatures, 135 and 165ºC.

Dynamic shear modulus, G_b*, testing, in accordance with AASHTO T 315-06 (AASHTO, 2006), was also conducted on RTFO aged binders using a Dynamic Shear Rheometer (DSR). Although testing was conducted at four temperatures, 4, 21, 37.8, and 54.4ºC (40, 70, 100, and 130ºF), results at 4ºC (40ºF) were inconsistent and unreliable due to the inability to maintain a constant temperature and thus excluded from the analysis. A frequency sweep, in which thirteen frequencies (0.1, 0.2, 0.3, 0.4, 0.6, 1.0, 1.6, 2.5, 4.0, 6.3, 10.0, 15.9, and 25 Hz) were applied, was completed at each of the four temperatures.

4.4 MIXTURES TESTED

E* laboratory testing was completed for the mixes in each section constructed in 2006 as part of the structural study. The mixes investigated are described in Table 4.2, listed by the section and layer in which it was placed. Four different mix types were incorporated in the investigation including Superpave mixes (super), stone matrix asphalt mixes (SMA), and a rich bottom layer (RBL). Each mixture is described by a unique mix number and unique binder number. The gradation information acquired from as-built records (quality control laboratory tests at time of construction), as well as the nominal maximum aggregate size (NMAS) for each mix number is listed in Table 4.3. The air voids associated to the specimens produced for E* testing were used to predict E* following each of the models, enabling a direct comparison to measured E*. Using the maximum specific gravity of the mix (Gmm) recorded in quality control as-builts, the bulk specific gravity of the mix (Gmb) was back calculated for each specimen tested

using the associated air voids. The remaining volumetric properties, voids filled with asphalt (VFA), voids in mineral aggregate (VMA), and effective binder content (V_{beff}) were calculated using the Gmb of each specimen, and the known bulk specific gravity of the aggregate (Gsb), and percent aggregate (Ps) from quality control as-builts. The VMA of the specimens tested ranged from 13.14% to 21.77%, the VFA ranged from 48.67% to 65.15%, and the air voids were between 6% and 8.6%. Due to the large number of data points, these individual, specimen-specific data (V_a, VMA, VFA) are not listed. As shown in Table 4.2, a total of ten unique mixes were evaluated, however, some unique mixes were used in multiple pavement layers. Associated with a unique binder number is the performance grade (PG), viscosity and G* test results (including phase angle values, δ_b); these values are listed for each binder in Tables 4.4 through 4.12. A total of nine binders were used in the HMA layers investigated, and similar to the unique mix number, some unique binders were used in multiple pavement layers.

For this evaluation a Brookfield viscometer was used to determine the viscosity of various binders at 135 and 165°C. After the test temperatures were converted to °Rankine, Equation 2-17 was utilized to extrapolate viscosity for the temperatures (40, 70, and 100°F) at which E* testing was completed. Viscosity values were not obtained for unique binder #4, which was contained only in unique mix #7. From these data the dynamic moduli of the mixes, aside from mix #7, were predicted for the 1-37A E* predictive model at three temperatures and seven loading frequencies. G_b* and δ_b values were obtained at multiple temperatures and frequencies. However, to compare laboratory E* values with E* predictions from either the Hirsch or 1-40D E* predictive models, the loading frequencies and test temperatures for G_b* must equal those used in

the E* laboratory test. As a result, the 1-40D and Hirsch E* predictive models were evaluated at two temperatures, 70 and 100ºF, and three frequencies, 1, 10, and 25 Hz.

TABLE 4.2 HMA Mixes by Section and Layer

Section	Layer	Sponsor	Mix Type	Binder	Unique Binder #	Unique Mix #
N1	1	FL	Super	67-22	1	1
N1	2	FL	Super	67-22	1	1
N1	3	FL	Super	67-22	14	2
N2	1	FL	Super	76-22	2A	3
N2	2	FL	Super	76-22	2A	3
N2	3	FL	Super	67-22	14	2
N8	1	OK	SMA	76-28	3	4
N8	2	OK	Super	76-28	3	5
N8	3	OK	Super	64-22	4A	6
N8	4	OK	RBL	64-22	4	7
N9	1	OK	SMA	76-28	3	4
N9	2	OK	Super	76-28	3	5
N9	3	OK	Super	64-22	4A	6
N9	4	OK	Super	64-22	4A	6
N9	5	OK	RBL	64-22	4	7
N10	1	MO	Super	70-22	5	8A
N10	3	MO	Super	64-22	6	9
S11	1	AL	Super	76-22	13	28A
S11	3	AL	Super	67-22	14	2
S11	4	AL	Super	67-22	14	2

TABLE 4.3 Gradation Information by Mix #

Unique Mix #	Unique Binder #	ρ200 % passing	ρ4 % retained	ρ38 % retained	ρ34 % retained	NMAS (mm)
1	1	8.79	39.61	16.44	0.00	12.5
2	14	5.48	45.82	25.19	4.47	19
3	2A	8.10	38.61	16.62	0.00	12.5
4	3	10.71	68.55	28.62	0.00	12.5
5	3	6.90	34.80	19.53	4.71	19
6	4A	6.90	36.31	21.13	5.48	19
7	4	10.51	39.93	13.68	0.00	12.5
9	6	6.28	51.79	25.60	1.81	19
8A	5	5.40	47.71	16.83	0.79	12.5
28A	13	8.59	13.98	0.10	0.00	9.5

TABLE 4.4 Binder Information (Section N1)

Unique Binder #	Temp, F	Frequency, Hz	G*, psi	Delta, º	Viscosity, cP
1	40	-	-	-	44,720,000,000
1	70	1	246.64	55.49	623,700,000
1	70	10	520.55	56.86	623,700,000
1	70	25	473.71	58.09	623,700,000
1	100	1	24.61	62.77	21,870,000
1	100	10	91.80	61.25	21,870,000
1	100	25	138.46	60.05	21,870,000

TABLE 4.5 Binder Information (Section N2)

Unique Binder #	Temp, ºF	Frequency, Hz	G*, psi	Delta, º	Viscosity, cP
2A	40	-	-	-	1.553E+11
2A	70	1	261.73	55.64	2,068,000,000
2A	70	10	565.94	57.48	2,068,000,000
2A	70	25	590.01	58.21	2,068,000,000
2A	100	1	29.71	59.78	68,120,000
2A	100	10	103.04	59.91	68,120,000
2A	100	25	156.75	58.73	68,120,000

TABLE 4.6 Binder Information (Sections N8 & N9)

Unique Binder #	Temp (F)	Frequency, Hz	G*, psi	Delta, º	Viscosity, cP
3	40	-	-	-	3.527E+11
3	70	1	325.09	53.89	4,147,000,000
3	70	10	667.87	55.76	4,147,000,000
3	70	25	692.95	54.5	4,147,000,000
3	100	1	38.69	57.81	123,500,000
3	100	10	129.85	56.28	123,500,000
3	100	25	207.21	49.12	123,500,000

TABLE 4.7 Binder Information (Section N8 & N9)

Unique Binder #	Temp (F)	Frequency, Hz	G*, psi	Delta, º	Viscosity, cP
4	40	-	-	-	-
4	70	25	1232.21	45.94	-
4	100	25	177.77	58.69	-

TABLE 4.8 Binder Information (Sections N8 & N9)

Unique Binder #	Temp (F)	Frequency, Hz	G*, psi	Delta, º	Viscosity, cP
4A	40	-	-	-	595,100,000
4A	70	1	251.43	56.12	28,820,000
4A	70	10	560.86	57.4	28,820,000
4A	70	25	581.59	58.07	28,820,000
4A	100	1	24.87	63.06	2,506,000
4A	100	10	94.93	61.08	2,506,000
4A	100	25	148.19	59.04	2,506,000

TABLE 4.9 Binder Information (Section N10)

Unique Binder #	Temp (F)	Frequency, Hz	G*,psi	Delta, º	Viscosity, cP
5	40	-	-	-	11,950,000,000
5	70	1	284.925	60.01	257,400,000
5	70	10	641.48	61.22	257,400,000
5	70	25	619.15	62.04	257,400,000
5	100	1	23.78	65.96	12,290,000
5	100	10	100.166	65.18	12,290,000
5	100	25	158.775	63.4	12,290,000

TABLE 4.10 Binder Information (Section N10)

Unique Binder #	Temp (F)	Frequency, Hz	G*,psi	Delta, º	Viscosity, cP
6	40	-	-	-	26,150,000,000
6	70	1	245.48	56.16	431,700,000
6	70	10	555.64	57.42	431,700,000
6	70	25	577.68	58.17	431,700,000
6	100	1	23.81	62.74	17,060,000
6	100	10	92.51	61.12	17,060,000
6	100	25	144.80	59.35	17,060,000

TABLE 4.11 Binder Information (Section S11)

Unique Binder #	Temp (F)	Frequency, Hz	G*,psi	Delta, º	Viscosity, cP
13	40	-	-	-	306,100,000
13	70	25	573.19	60.07	26,720,000
13	100	25	133.34	59.37	3,530,000

TABLE 4.12 Binder Information (Section S11)

Unique Binder #	Temp (F)	Frequency, Hz	G*,psi	Delta, º	Viscosity, cP
14	40	-	-	-	76,590,000,000
14	70	1	258.24	55.68	936,600,000
14	70	10	571.01	57.03	936,600,000
14	70	25	585.80	57.89	936,600,0009
14	100	1	26.29	62.13	29,800,000
14	100	10	98.96	60.59	29,800,000
14	100	25	152.54	59.11	29,800,000

4.5 RESULTS AND DISCUSSION

In following Equation 4-1 to evaluate the Witczak 1-37A E* model, 644 data points were produced from mixture properties of each individual specimen. The values were plotted against the laboratory measured log E* values in Figure 4.2. For the Witczak 1-40D and Hirsch E* models, 177 data points were evaluated for each, again

using individual mix properties of the specimen, and were plotted against measured log E* values in Figure 4.2. Ideally, all points would fall along the line of equality, but this clearly is not the case. Upon visual inspection, it can be concluded that overall the 1-40D E* model consistently overpredicts the measured values, with 99% of the data points lying above the line of equality. While there is a large amount of scatter in the data, the 1-37A E* model generally follows the line of equality, with data points both above and below this line. Similarly, the Hirsch E* model also generally follows this line, although there is much less scatter in these data. Some of the scatter evident in this plot may be related to inherent errors in measured values, as E* laboratory testing is not a flawless test and has limitations, particularly at high frequencies.

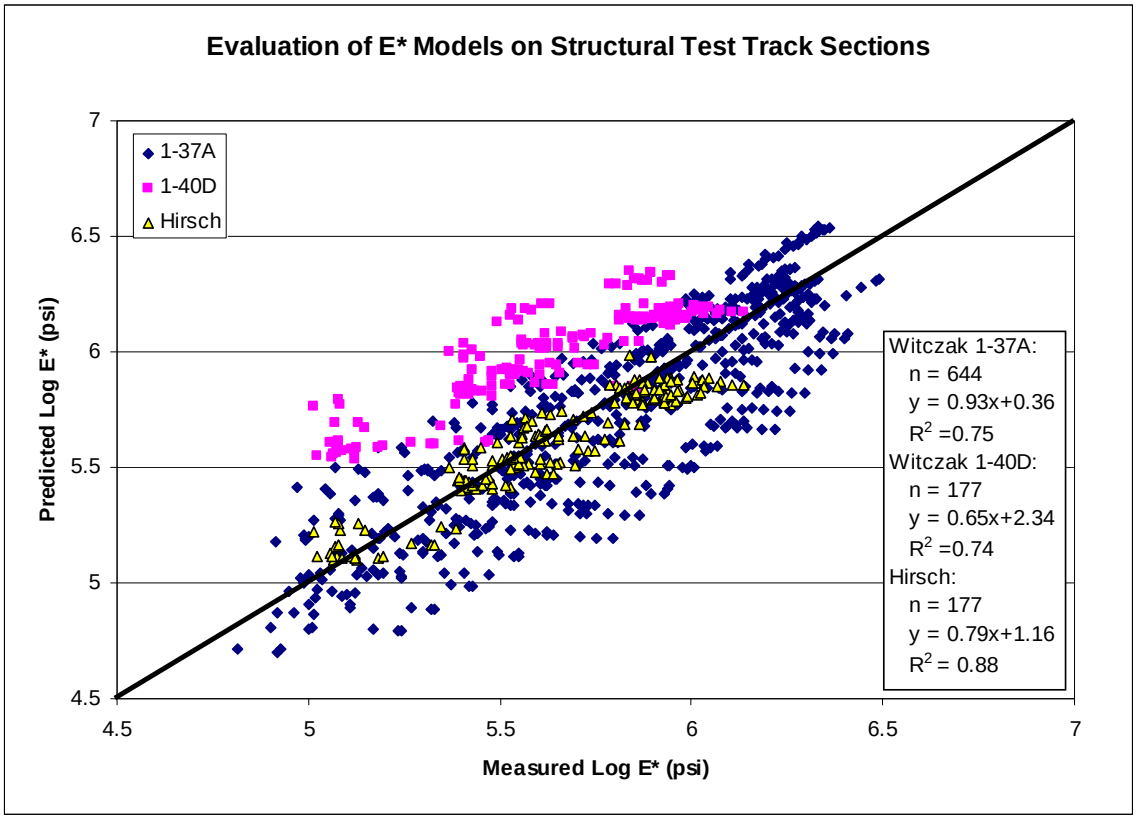

FIGURE 4.2 Comparison of Predicted E* to Measured E* by Predictive Models.

Attaching a linear regression equation indicates how precisely the modeled values are linearly related to the measured values, in log space. Some researchers (Bari and Witczak, 2006; Dongre et al., 2005, Andrei et al., 1999, Christensen et al, 2003; Azari et al., 2007; Mohammad et al., 2007) have used the coefficient of determination from this relationship as an indication of the quality of the model. Inset in Figure 4.2 are the sample sizes, linear regression equations and associated coefficients of determination in log scale for each model evaluated. All three models produced predictions that correlated well to the measured values by a linear relationship. The Hirsch E* model produced the highest R^2 value, 0.88 in log scale, while the Witczak 1-40D produced the lowest, 0.74 in log scale. This is contrary to previous findings in which the 1-40D model was found to be an improvement over both the Hirsch and 1-37A model (Bari and Witczak, 2006; Azari et al., 2007). All three models, 1-37A, 1-40D, and Hirsch, returned significantly lower R^2 values than reported in their development, 0.941, 0.90, and 0.982 in log scale, respectively (Andrei and Witczak, 1999; Bari and Witczak, 2006, Christensen et al., 2003). Although these models were found to linearly correlate very well with the measured values used to create them, they may not be applicable to mixtures not included in their original database. This is of concern since the purpose of these equations is to provide a reasonable estimation of E* without having to run the E* test.

The coefficient of determination is a measure of how precisely the linear regression equation matches the data. For the model to be accurate, the linear regression equation should be as close to $y = x$ as possible, therefore the slope and intercepts of the

regression equations should also be investigated. Table 4.13 lists the linear regression coefficients and goodness of fit in arithmetic scale for each of the models.

TABLE 4.13 Linear Regression Coefficients for Each Model

Model	Slope	Intercept (psi)	R^2
Witczak 1-37A	0.90	48,623	0.66
Hirsch	0.64	125,416	0.80
Witczak 1-40D	1.25	447,561	0.60

According to these lines of best fit, the Witczak 1-37A has the smallest difference in slopes from the line of equality, deviating above the line by only 12.22%. Additionally, the y-intercept is the smallest of the three models. However, indicated by the R^2 and Figure 4.2, the 1-37A E* model does not consistently predict the measured values accurately. The Hirsch model is more consistent than the Witczak 1-40D model, however, the slope for the Hirsch model deviates from one the most. In looking at Figure 4.2, the data for both the Hirsch and 1-40D models appear to level out, approaching a slope close to zero at intermediate measured moduli values (725,000-1,400,000 psi) and at lower moduli values (100,000-250,000 psi). When the data are plotted in arithmetic scale, this trend at intermediate and low moduli values is more predominant in the Hirsch model (shown in Figure 4.3) than the 1-40D model (Figure 4.4), which may explain the large deviation in slope from the line of equality.

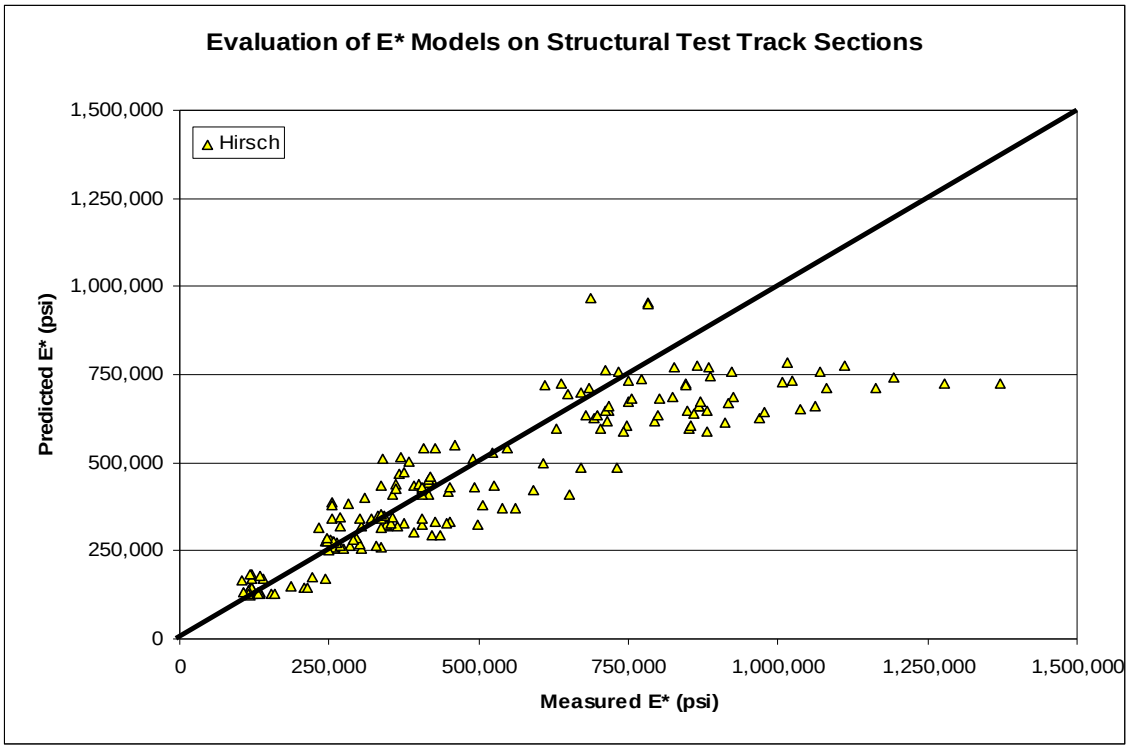

FIGURE 4.3 Comparison of Predicted E* to Measured E* for the Hirsch E* Model.

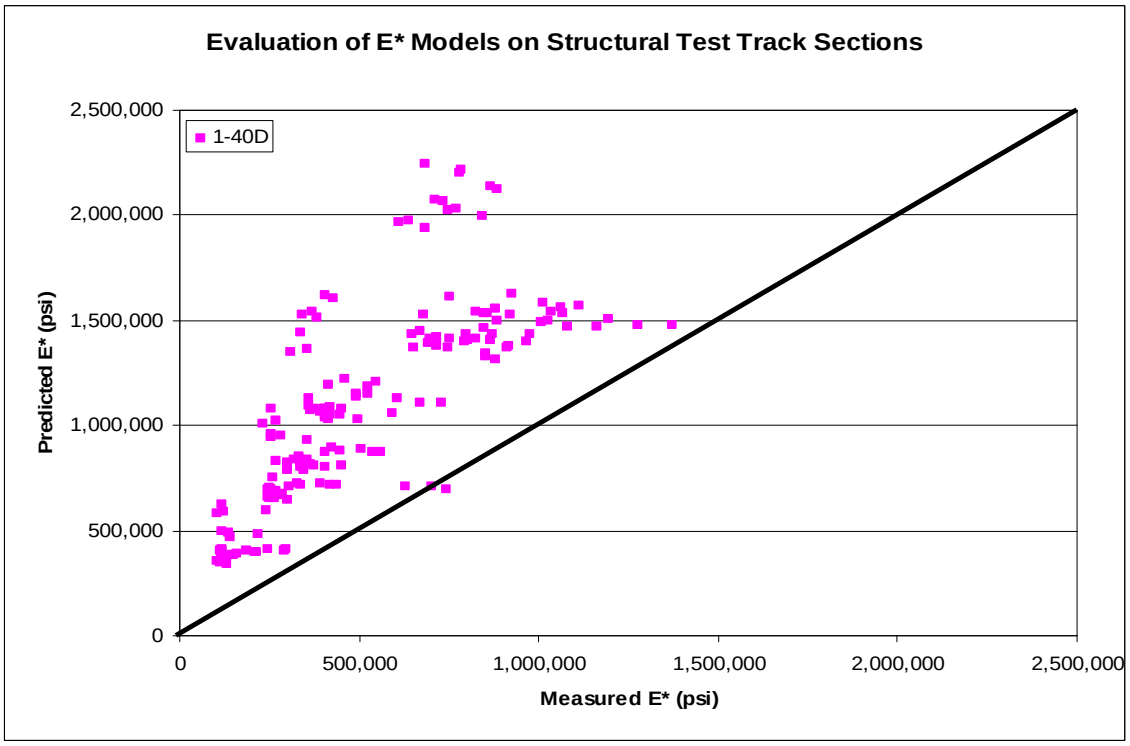

FIGURE 4.4 Comparison of Predicted E* to Measured E* for the 1-40D E* Model.

Given that both of these models follow this trend and utilize G_b*, such inconsistencies could be related to the use of G_b* values. This could indicate errors in G_b* test results at high frequencies and the low end of the temperature range, 70ºF. Similar to E* testing, G_b* testing also has limitations, particularly at high frequencies. Although, testing errors may exist, no obvious errors were noted during testing, thus, this trend may also be due in part to the use of G_b* in the development of these two models. Table 4.14 lists the percentage of E* values that are underpredicted by the Hirsch model for each of the frequencies and temperatures used for the comparisons. As the frequency increases for either temperature, the percent of predicted E* values that are less than its measured counterpart increases. This trend is contrary to the time-dependency of HMA, such that increases in frequency should result in higher E* values. Additionally, at the higher temperature, 100ºF, the percent of values underpredicted at 10 and 25 Hz are less than at the lower temperature. The number of E* values that are under predicted by the Hirsch model are greatest at a temperature of 70ºF and 25 Hz. In general, it appears that the Hirsch E* model predicts the measured values most accurately and precisely for lower dynamic moduli (250,000-725,000 psi).

TABLE 4.14 Percent of Total E* Values Underpredicted by Hirsch Model

Frequency	70ºF	100ºF
1 Hz	5%	6%
10 Hz	12%	8%
25 Hz	18%	10%

Consistent with previous research (Azari et al., 2007), the 1-40D E* model grossly overpredicts dynamic moduli at low values which are characterized by high temperatures and/or low frequencies. To further investigate this trend, the ratio of

predicted to measured E* values was calculated by frequency and temperature. Table 4.15 lists the minimum, maximum and average ratios.

TABLE 4.15 Ratio of Predicted to Measured E* for Witczak 1-40D E* Model

			70ºF			100ºF
Frequency	Min	Max	Avg	Min	Max	Avg
1 Hz	1.5	4.5	2.7	1.9	5.6	3.2
10 Hz	1.3	3.2	2.0	1.6	4.3	2.6
25 Hz	0.9	3.3	1.7	1.4	4.3	2.5

Of the 177 data points, only one underpredicts the measured value, by just 2%, corresponding to a ratio of 0.9. At the highest temperature (100ºF) and lowest frequency (1 Hz) which corresponded to low measured moduli; the 1-40D model produces dynamic moduli 3.2 times greater, on average. Table 4.15 reveals that at a low frequency (1 Hz) and a high temperature (100ºF) the model overpredicts the greatest among test frequencies and temperatures, reiterating previous findings. At the minimum, the 1-40D model overpredicts by 1.9 times at low frequencies (1 Hz) and high temperatures (100ºF). Similarly, among the three frequencies tested at an intermediate temperature, 70F, the model results in predicted values drastically greater than the corresponding measured values.

The models were further analyzed by mixture parameters: mixture type, binder type, gradation, and NMAS. Initially three mixture types were included in the evaluation: SMA, Superpave, and RBL. The RBL mixture was excluded from further analysis, due to the lack of viscosity values for the associated binder and the small sample size (only six data points) for the Hirsch and 1-40D predictive models. Despite the small sample sizes for SMA mixtures, the trends discussed earlier were not found to be independent of mixture type, illustrated by Figures 4.5 and 4.6.

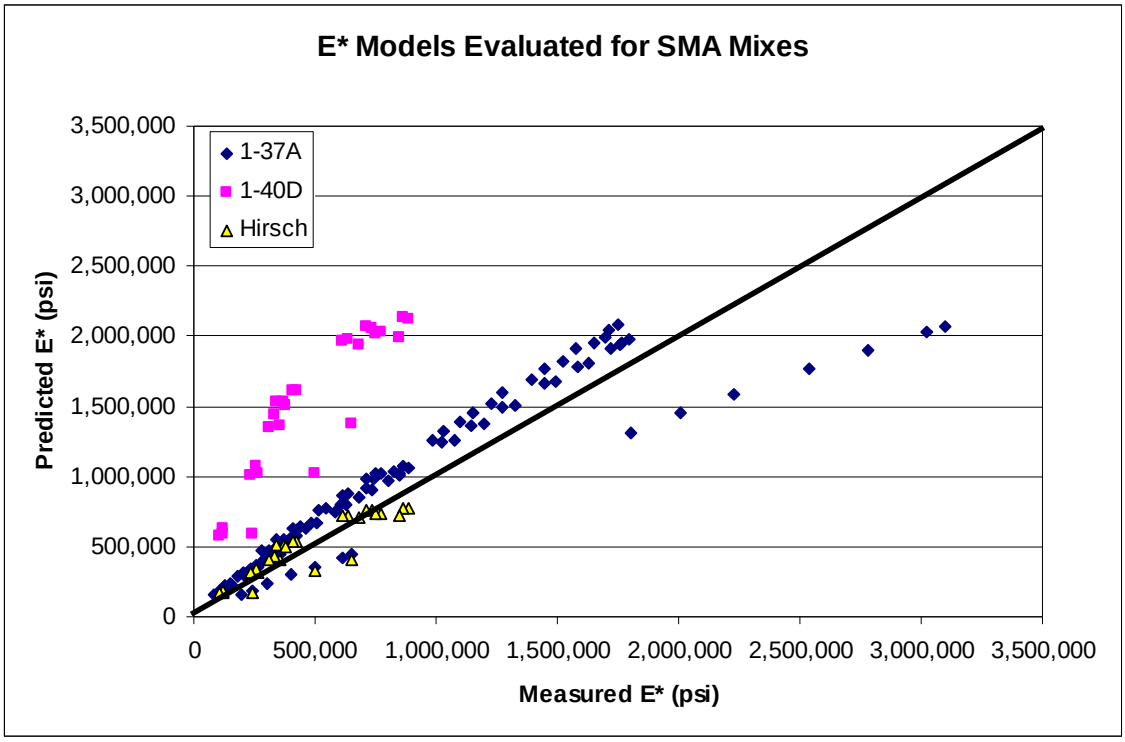

FIGURE 4.5 Comparison of Measured E* to Predicted E* for SMA Mixes.

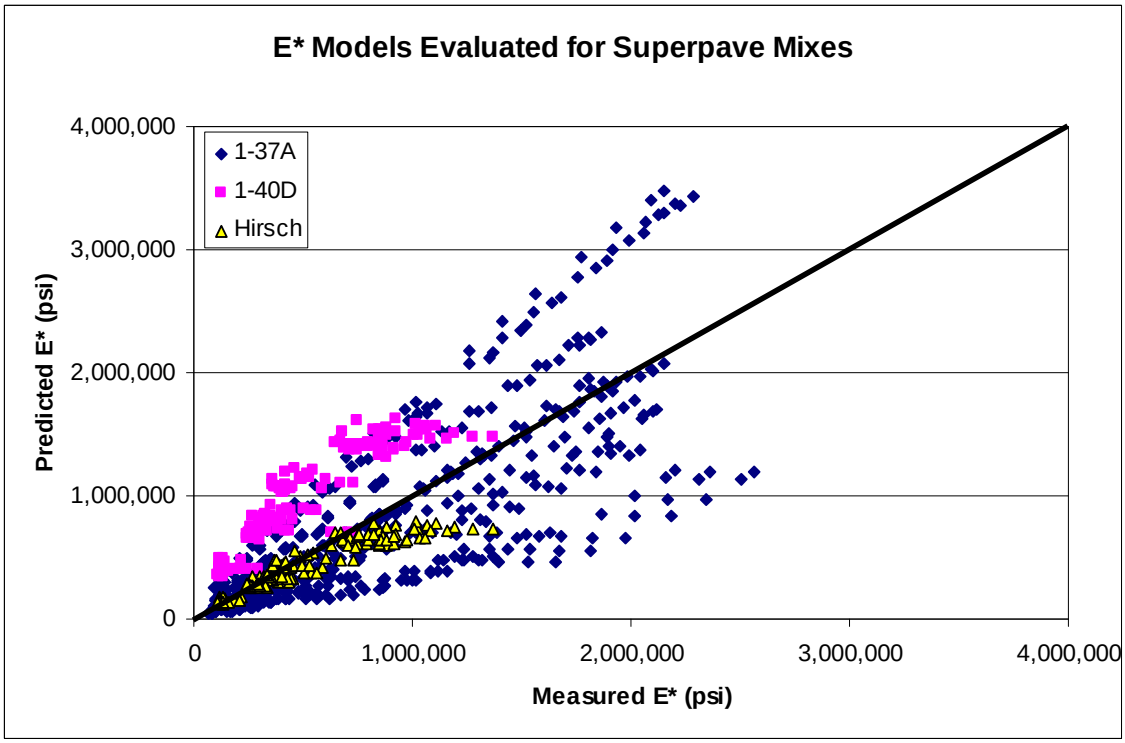

FIGURE 4.6 Comparison of Measured E* to Predicted E* for Superpave Mixes.

As was found earlier, the 1-37A model is largely scattered about the line of equality, neither consistently over nor underpredicting E*. The 1-40D model was found to return E* values much larger than those measured in the laboratory. The Hirsch model generally follows the unity line for both mixtures. Figure 4.6 again illustrates the leveling out of the data for both the 1-40D and Hirsch models.

Similar to the evaluation of mixture types, measured moduli were plotted against predicted values for each of the five binder types included in the study. Comparisons were plotted for two binder types, PG 64-22 and PG 76-28 in Figures 4.7 and 4.8, respectively.

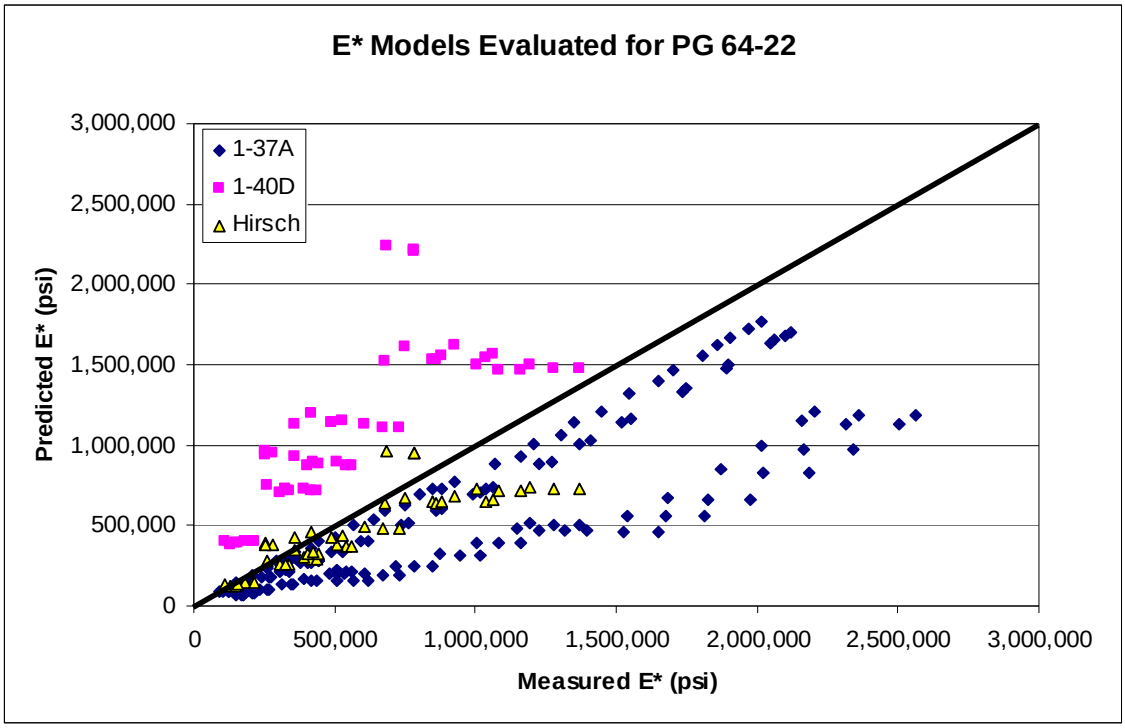

FIGURE 4.7 Comparison of Measured E* to Predicted E* for Mixes with PG 64-22 Binder.

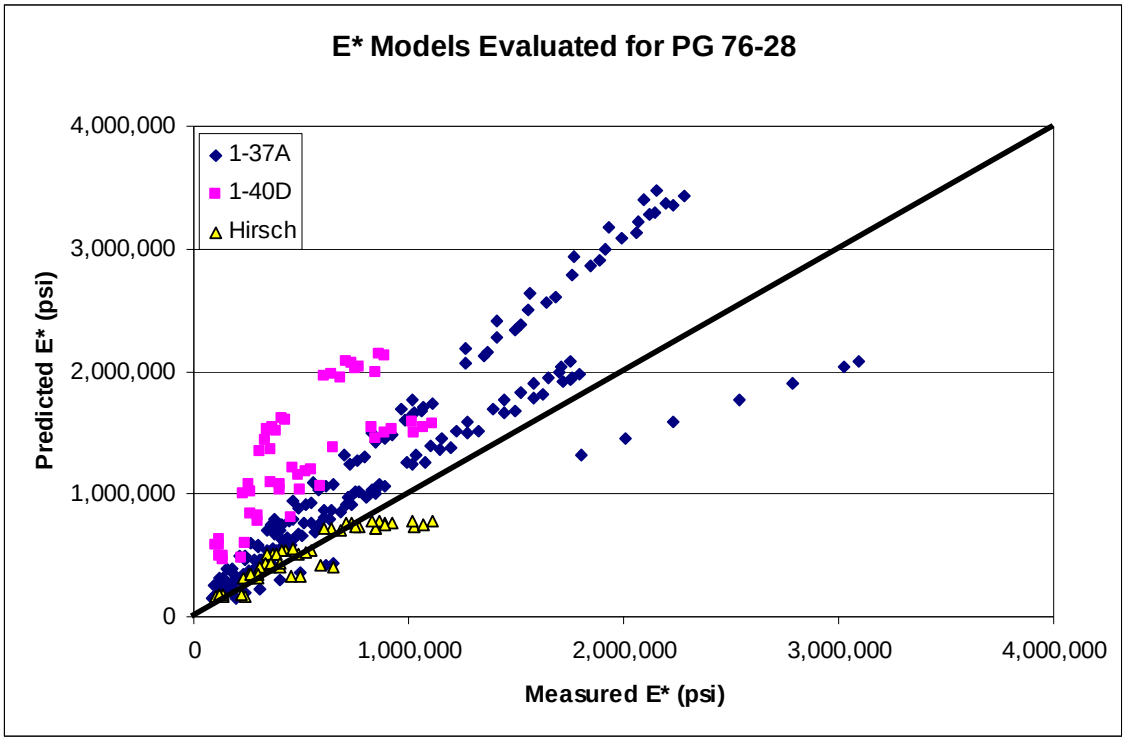

FIGURE 4.8 Comparison of Measured E* to Predicted E* for Mixes with PG 76-28 Binder.

The same general trends discussed previously were again evident: large scatter in the 1-37A predictions, overestimation by the 1-40D model, and fairly accurate predictions by the Hirsch model. Although not shown, the Witczak 1-37A model improved for binder types PG 67-22 and PG 70-22, predicting E* most accurately, while the other two models preformed in accordance with previously noted trends. However, for these two binder types only one mixture each was represented. Therefore, it was concluded that binder types have no discernible affect on E* predictions for the three models evaluated.

Plotting measured moduli against predicted moduli for coarse and fine mixes showed that the same trends existed regardless of the gradation of the mixture. Likewise for NMAS, the same trends spotted in Figure 4.2 were exhibited no matter the NMAS. Although mixture properties such as binder shear modulus, and gradation (percent

retained or passing specific sieves) inherently influence model predictions, no relationship between model accuracy and binder type or coarseness of the aggregate was found to exist.

4.6 SUMMARY

Three E* predictive models were evaluated for asphalt mixtures from the southeastern region. The dynamic moduli of ten different HMA mixtures from the 2006 Test Track were measured in the laboratory and compared with moduli predicted by the 1-37A, 1-40-D, and Hirsch E* predictive models. Following the Witczak 1-37A E* model, E* was estimated for three temperatures (40, 70, and 100°F) and seven frequencies (0.1, 1, 2, 5, 10, 20, and 25 Hz). E* was also estimated using the Witczak 1-40D and Hirsch E* predictive models for two temperatures (70, and 100°F) and three frequencies (1, 10, 25 Hz). The findings from these comparisons are summarized below:

- The Witczak 1-37A E* model was found to be unreliable with a large amount of scatter.
- The Hirsch E* model was found to be the most precise model, with the highest coefficient of determination, 0.707 in log scale and 0.766 in arithmetic scale.
- The Witczak 1-40D E* model consistently overpredicts E* particularly for low dynamic moduli.
- The Hirsch E* model is most accurate at low dynamic moduli values (250,000-700,000 psi).

- At an intermediate test temperature (70ºF), both the Witczak 1-40D E* and Hirsch E* models flatten out, thus misrepresenting the time-dependency of E*.

- Mixture parameters, such as mixture type, binder type, gradation (coarse/fine) or NMAS of the mix were not found to significantly influence the accuracy of E* predictions by any of the three models.

At the current state of the MEPDG, Witczak E* predictive equations, 1-40D and 1-37A, are employed to determine dynamic modulus given volumetric, gradation and binder properties of a mixtures. In applying these models to ten mixtures included in the 2006 Test Track Structural study, neither model consistently estimated laboratory dynamic moduli values to a high degree of accuracy. Because both the 1-37A and 1-40D models were found to be unreliable and the 1-40D model largely overpredicts dynamic modulus, it is recommended that the Hirsch E* model be used. It should be used with caution however, as discrepancies at lower temperatures and/or higher frequencies were observed.

CHAPTER FIVE

FIELD DATA

5.1 INTRODUCTION

Further investigation into E* was conducted through a field experiment. Section N9 was utilized to explore various factors on strain and loading duration. As mentioned previously, load duration ultimately affects E*; E* in turn influences tensile strain levels. Since E* cannot be measured in the field, factors affecting it such as temperature, and load duration at various depths were measured under live traffic at the Test Track. Strain levels were also recorded to evaluate the effects of temperature and velocity.

5.2 TESTING

In order to understand E* in the field, a better understanding of pavement responses was necessary. Section N9 was selected for further investigation given its deep HMA cross-section and multiple strain gages at various depths. Field testing was conducted in the spring of 2007, on four separate test dates over the course of a one month testing period. A minimum of four speeds were tested on any given test day, ranging from 15 mph to 55 mph. On the first two dates, April 6 and 10, 2007, testing was completed for five speeds: 15, 25, 35, 45, and 55 mph. Testing at the highest speed, 55 mph, was abandoned for the last two dates, April 25 and May 2, 2007, for safety reasons, as the Test Track was designed for only 45 mph. Live traffic was applied to the section in three passes of each truck, following the findings of previous research at the

Test Track, enabling the best hit to be detected by the instrumentation (Timm, 2006). As mentioned previously, live traffic was applied with the heavy trucks employed by the Test Track, composed of a steer axle, tandem axle and five trailing single axles. A minimum of four trucks traveled over the section at each speed tested. The in-situ pavement temperatures were recorded, enabling a complete evaluation of strain measurements and load durations for a variety of speeds and temperatures.

5.3 STRAIN RESPONSES

Strain measurements were evaluated to determine the effects of temperature and speed on tensile strain to give a broader understanding of E*. Tensile strain measurements were analyzed for the strain induced at the bottom of the HMA layers, 13.9 inches deep, as this is the most critical location for tensile strain and the prevention of fatigue cracking. Measurements were recorded in both the longitudinal and transverse directions by gages 1-12, as discussed in Chapter Three. The layout of these twelve gages is displayed in the inset of Figure 5.1. Temperatures were recorded at the surface (T1), mid-depth (T2) and bottom (T3) of the HMA layer, also illustrated in Figure 5.1. Temperature probes were also embedded within each HMA layer, as described in Chapter Three, Table 3.2. From these measurements relationships were analyzed for tensile strain with temperature and speed.

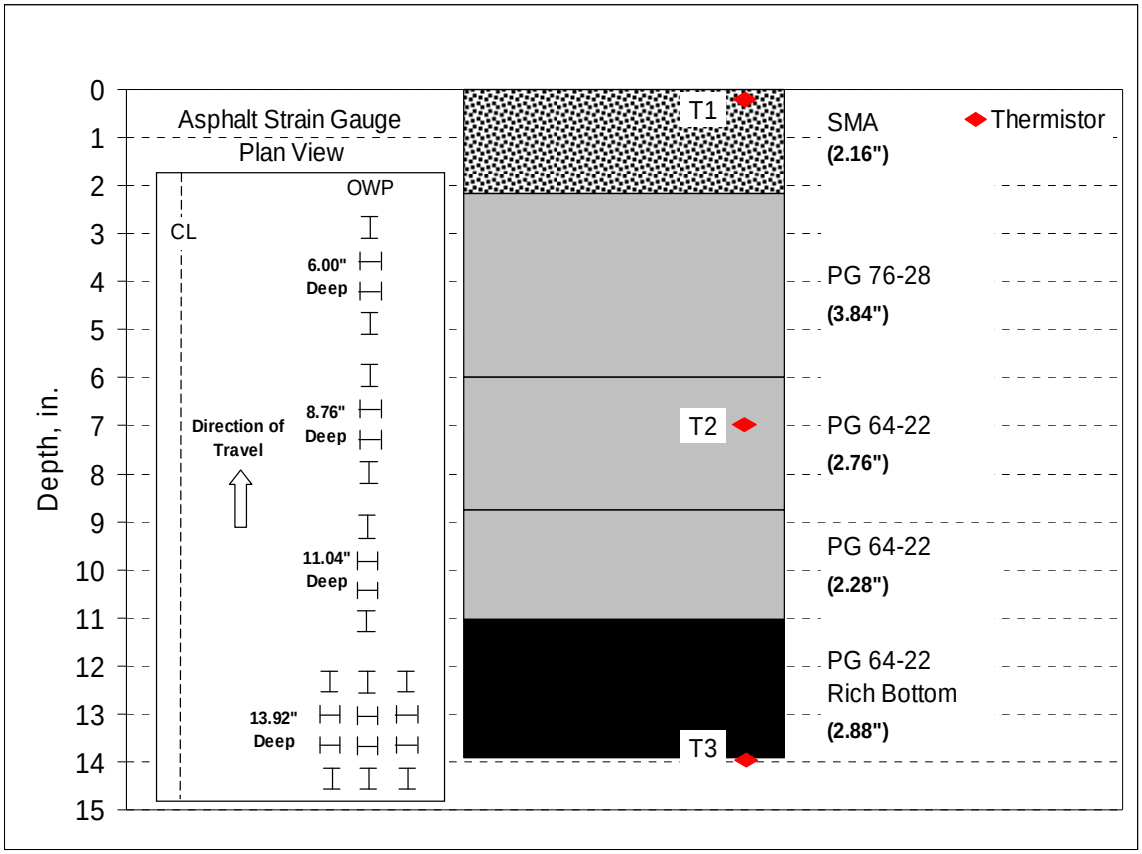

FIGURE 5.1 Cross-section of N9.

5.3.1 Definition of Strain

To analyze the effect of temperature and speed on tensile strain, the recorded strain pulses were first evaluated. Figure 5.2 illustrates the longitudinal strain induced under a single axle of a moving load. It was found that as the load approached the strain gage, compressive strain was experienced first, and as the HMA layers began to bend under loading, the strain pulse transitioned into the tensile realm. At the peak of the strain pulse, the HMA layers experienced maximum tensile strain, $\varepsilon_{t,\,max}$, at which time the load was directly over or nearly directly over the strain gage. Figure 5.2 reveals that the tensile strain lessened as the load moved further away from the gage, eventually

transitioning into compressive strain, ε_c, again before it returned to the baseline strain level.

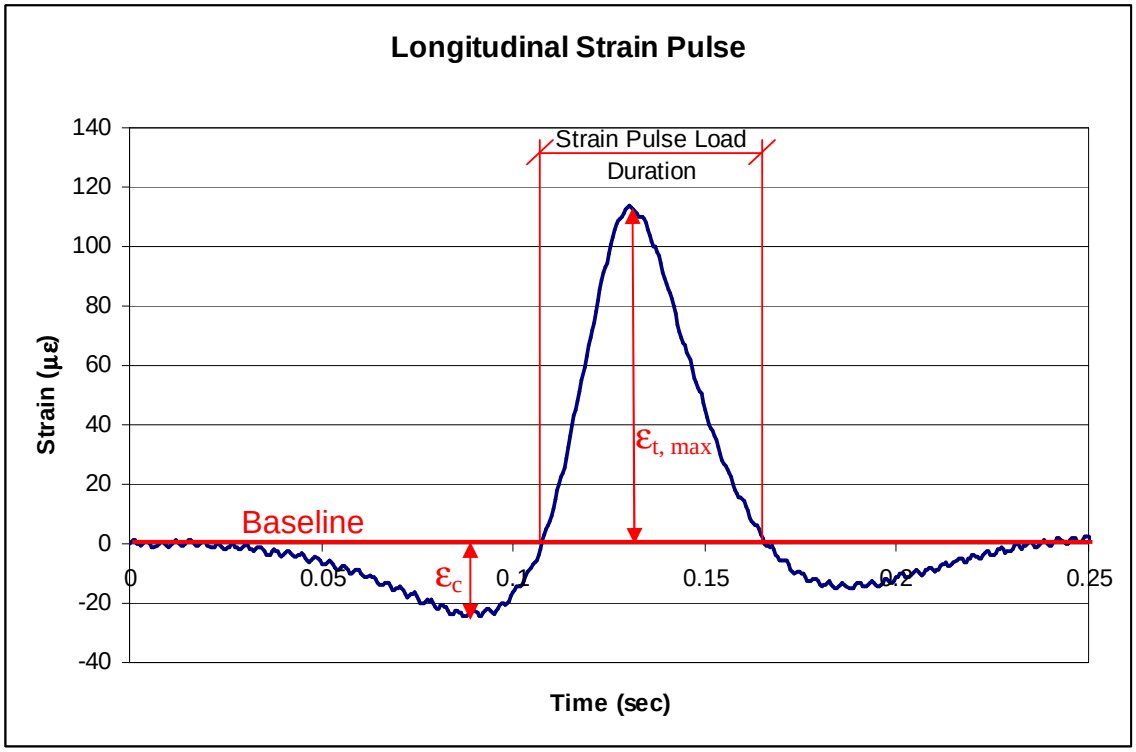

FIGURE 5.2 Longitudinal Strain Pulse.

Strain induced in the transverse direction was slightly different than in the longitudinal direction, displayed in Figure 5.3 for an entire truck pass. The HMA layers experienced only tensile strain in the transverse direction. As the truck approached the gage, the strain went directly into tension. As the load was directly or nearly directly atop the gage, maximum tensile strain was induced in the transverse direction just as it was in the longitudinal. However, once the load moved past the gage, the strain remained in tension until it returned and remained at the baseline strain level. Since the maximum tensile strain values are most critical, they were utilized to evaluate the effects of temperature and speed on tensile strain under a moving load. It was found that the maximum tensile strain levels in the transverse direction were notably less than that in

the longitudinal direction, consistent with previous research at the Test Track (Timm and Priest, 2008). To account for wheel wander, the "best hit" among the truck passes was used for each condition tested. The "best hit" was considered the maximum tensile strain value recorded among all of the strain gages in a given direction, for a given date, speed and axle type. Using the best hit approach, the effect of temperature and speed on tensile strain in both directions were first analyzed separately. After individual relationships were developed, the combined effects of temperature and speed on tensile strain were quantified.

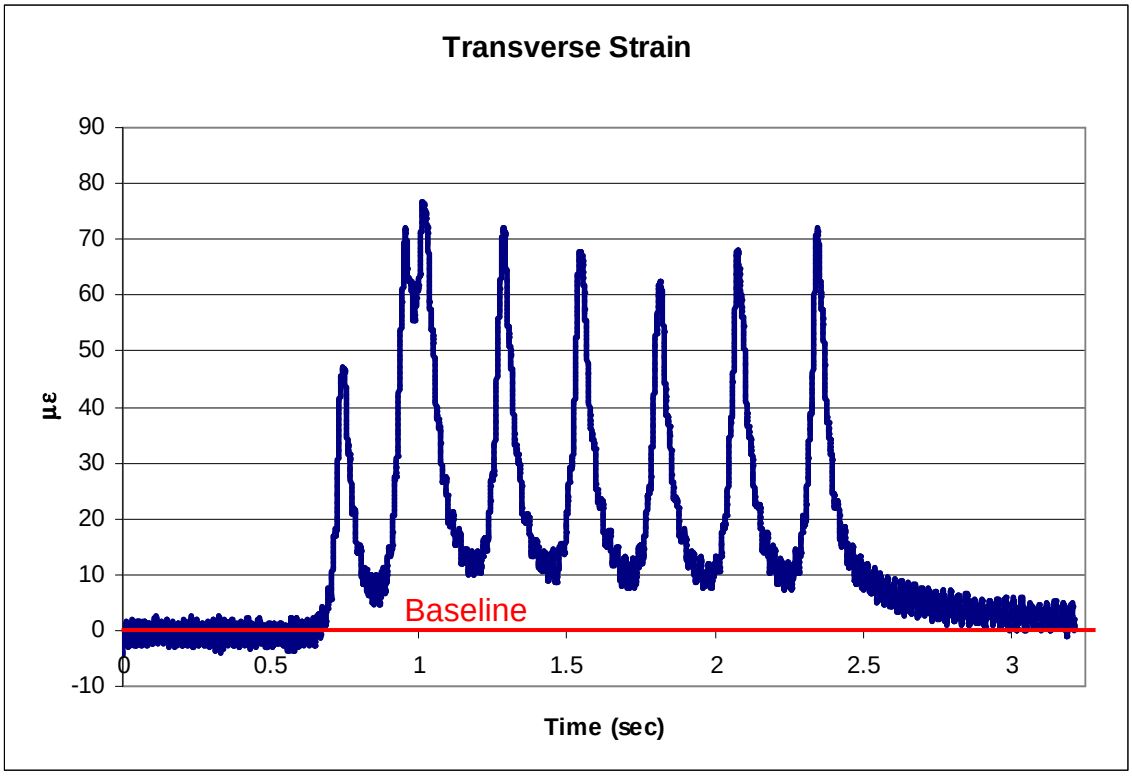

FIGURE 5.3 Transverse Strain Pulse.

5.3.2 Effect of Speed on Tensile Strain

The tensile strains determined from the best hit approach were investigated to determine the effects of speed on tensile strain at the bottom of the HMA layers. To

determine the relationship between speed and tensile strain, strain values in each direction were plotted by speed for each axle type. Figure 5.4 plots the tensile strain values in the longitudinal direction for a single axle. For the first two dates, April 6, and April 10, 2007 the induced longitudinal strain decreases with an increase in speed. The same trend exists for the last two dates; however, the strain decreased at a greater rate than on the first two dates for each increase in speed. This trend was investigated further in Figure 5.5 which plots the rate of change (the slope of each regression line) of the tensile strain with the mid-depth pavement temperature from Figure 5.4. The average mid-depth pavement temperature for each date is listed in Table 5.1. This plot reveals that at high mid-depth temperatures vehicle speed reduced the longitudinal strain at a greater rate. Therefore, at warmer temperatures, vehicle speed has a greater effect on the tensile strain at the bottom of the HMA than at colder temperatures. This was to be expected since warmer temperatures induce a greater viscoelastic behavior from the HMA which would therefore increase the impact of vehicle speed.

TABLE 5.1 Average Mid-Depth Temperatures by Date

Date	Avg. Temperature
4/6/2007	63.9 ºF
4/10/2007	70.8 ºF
4/25/2007	89.0 ºF
5/2/2007	99.0 ºF

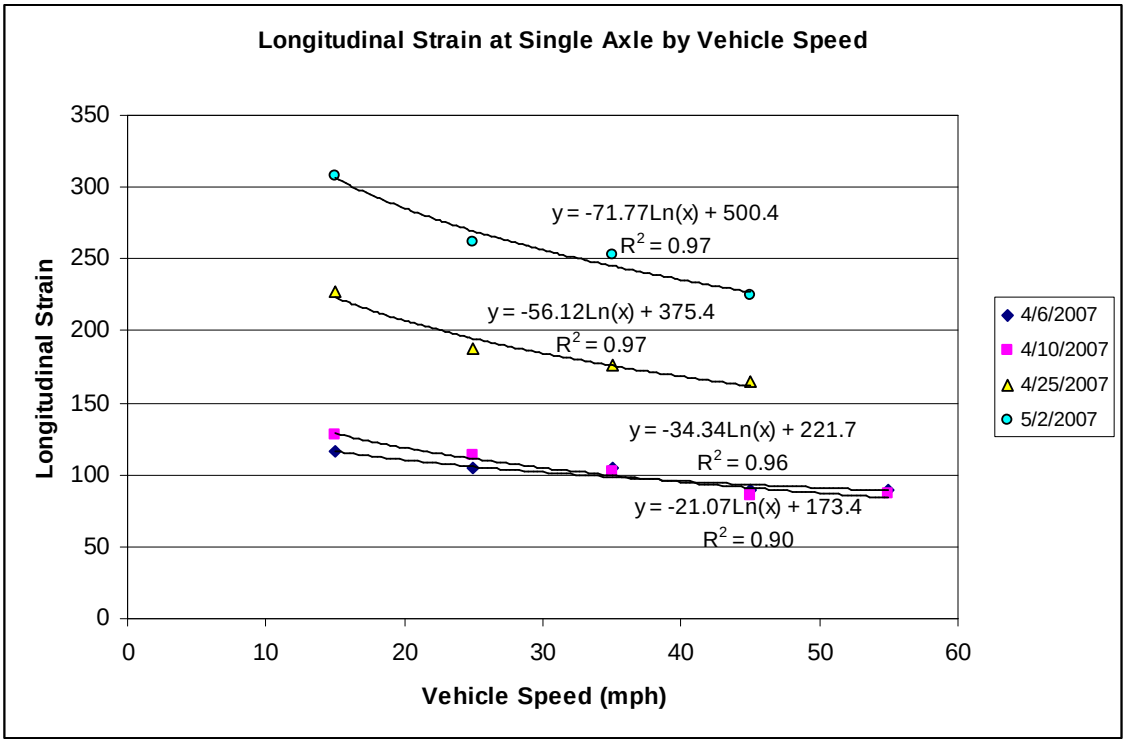

FIGURE 5.4 Effect of Speed on Tensile Strain by Date.

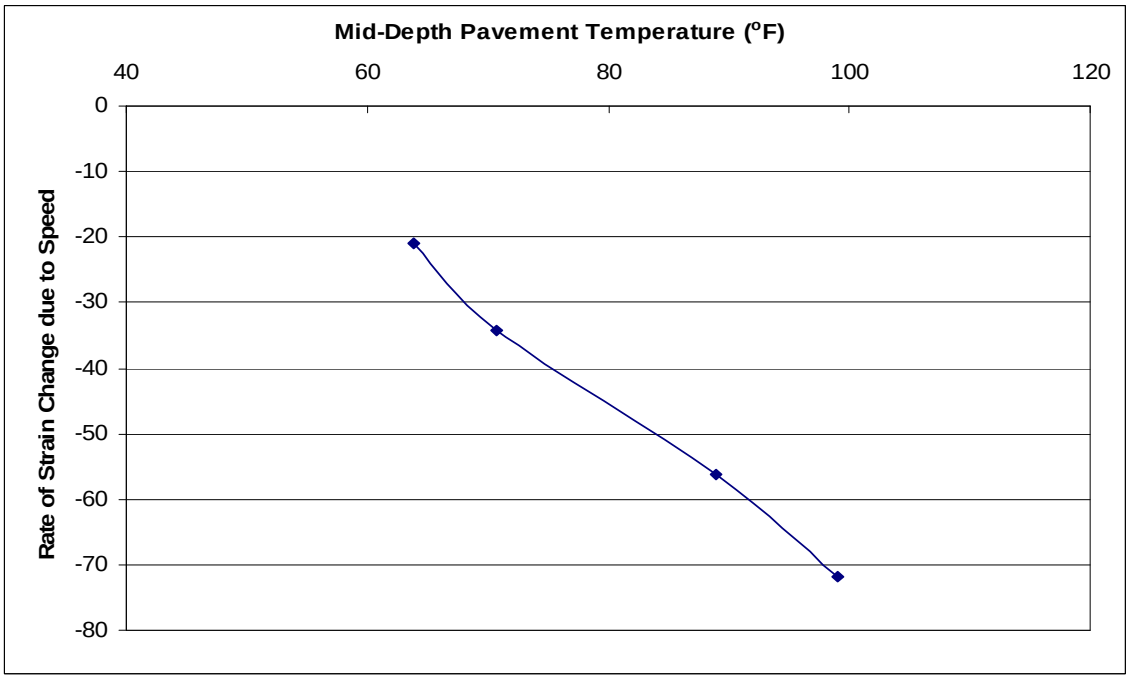

FIGURE 5.5 Rate of Strain Change by Mid-Depth Temperature.

Plots were developed for all three axle types in each direction, from which it was found that regardless of direction or axle type the same general trend existed: increasing the vehicle speed resulted in a decrease in tensile strain levels at the bottom of the HMA. By completing a regression analysis on the data, it became evident that the longitudinal strain was proportional to the natural logarithm of the speed of the applied load, modeled by Equation 5-1. The coefficient of determination, corresponding to the trend line for each axle type on each test date revealed that Equation 5-1 models the relationship for longitudinal strain very well, returning R^2 values ranging from 0.80 to 0.99 with ten of the twelve R^2 values greater than 0.90. The same trends existed for strains under each axle type in the transverse direction, again returning relatively high R^2 values.

$$\varepsilon_t = a \ln v + b \tag{5-1}$$

where:

ε_t = tensile strain ($\mu\varepsilon$)

v = vehicle speed of applied load (mph)

a, b = regression coefficients

5.3.3 Effect of Temperature on Tensile Strain

A broad range of in-situ pavement temperatures were recorded during the one month testing period, with surface temperatures ranging from 78°F to 120°F. This enabled a robust analysis of the relationship between tensile strain and pavement temperature. During testing, pavement temperatures from each of the sixteen temperature probes were recorded at the onset of testing each new speed. As to be

expected, the temperatures throughout the structure rose as the experiment progressed from the start in April to the termination in May. Also, temperature gradients were observed in which the surface temperatures of the asphalt concrete were significantly higher than temperatures at the bottom of the structure.

In determining the effect of temperature on strain, it was necessary to select one of the sixteen thermistors embedded within the structure for analysis. A regression analysis was completed for thermistors T1-T3 which offered a complete temperature profile of the HMA layers. Recorded temperatures from each of the probes were plotted against the resulting strain values in each direction under the steer axle for all speeds tested. Attaching a trend line to each allowed for a comparison of accuracy among the three probes via R^2 values. From this it was found that the temperatures recorded at the mid-depth by thermistor T2 resulted in consistently high R^2 values. This follows the findings of a previous investigation at the Test Track which reported mid-depth temperatures as the best predictor of strain (Priest and Timm, 2006). From this, the mid-depth pavement temperatures were selected for the analysis of the effect of temperature on tensile strain at the bottom of the HMA. The average mid-depth temperatures are listed in Table 5.1.

Plots were developed for tensile strain and mid-depth pavement temperature in each direction, longitudinal and transverse, and for each axle type at the various speeds tested. Figure 5.6 displays the temperature-strain relationship in the longitudinal direction under a single axle.

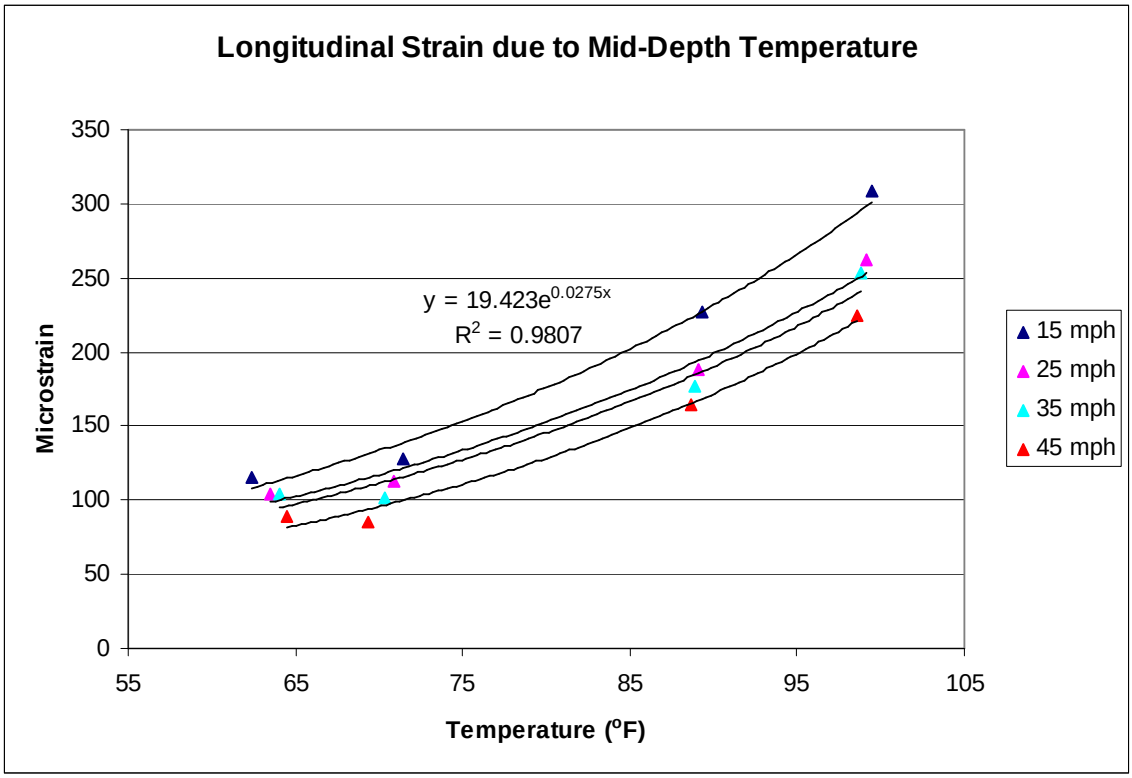

FIGURE 5.6 Effect of Temperature on Longitudinal Strain.

From this plot it is evident that an increase in mid-depth pavement temperature causes a significant increase in tensile strain, a relationship that can be described by an exponential function. In Figure 5.6 the equation for the trend line generated by Excel is displayed for a vehicle speed of 15 mph which illustrates a very high R^2 value indicating that an equation of the form listed in Equation 5-2 is a very good fit for these data. Although only the regression equation and R^2 value for 15mph is displayed, the R^2 values for the relationships at the other three speeds were also very high, ranging from 0.961-0.985. Likewise, plots for temperature-strain relationships under the steer axle and tandem axle also illustrated very close fits with an exponential function described by Equation 5-2. Similarly, in the transverse direction, shown by Figure 5.7 (for a single axle), the temperature-strain relationship was closely fitted by the same exponential

function regardless of axle type. Given the consistently high R^2 values, it was concluded that Equation 5-2 most accurately describes the temperature-strain relationship in both directions for all axle types.

$$\varepsilon_t = ce^{dT} \tag{5-2}$$

where:

ε_t = Tensile strain (micro strain)

T = Mid-depth Temperature (°F)

e = the base of natural logarithm

c, d = regression coefficients

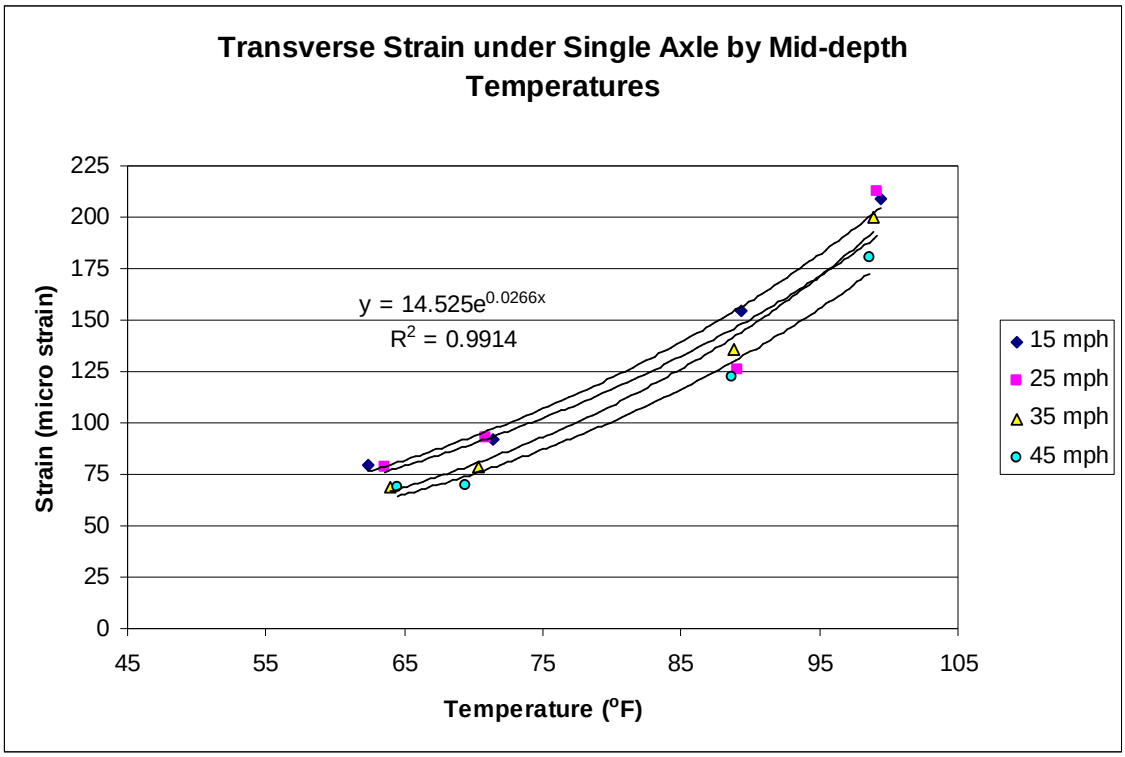

FIGURE 5.7 Effect of Temperature on Transverse Strain.

5.3.4 Combined Effects of Speed and Temperature on Tensile Strain

Although the effects of speed and temperature were first investigated separately, their effects are not independent of each other due to the fact that HMA is a material for which properties are temperature and time-dependent. The investigations into the effects of speed and temperature revealed that tensile strain is directly proportional to the natural logarithm of the vehicle speed and directly proportional to the exponential function of temperature. Furthermore, it was found that the highest strain levels, critical for design, were experienced under slow vehicle speeds and high mid-depth pavement temperatures. To quantify this combined effect, DataFit, a regression analysis software program, was utilized to generate regression equations from the recorded data. DataFit allows the user to enter forms of regression equations not built into Excel. The program then iterates through possible coefficients and checks the validity of the user defined equation by calculating the correlation to the provided data. From this program, Equation 5-3 was selected to represent the effect of speed and temperature on longitudinal strain at the bottom of the HMA layers (13.9 inches deep). The equation of the form listed in Equation 5-3 was selected because it linearly combined the individual effects of speed and temperature (Equations 5-1 and 5-2) with regression coefficients that were statistically significant, and it resulted in high coefficients of determination. It was found that axle type (assuming all axles within each category were of approximately the same weight) influenced strain values; therefore regression equations of the form listed in Equation 5-3 were developed for each axle type as well as each direction, longitudinal and transverse. The regression coefficients for each axle type are listed in Table 5.2. As Table 5.2 illustrates, these equations very closely fit the measured data.

Figure 5.8 also exhibits the accuracy of these regression equations as the measured data points for a single axle in the longitudinal direction lay in close proximity to the line of equality.

$$\varepsilon_t = f \ln v + e^{gT} + h \tag{5-3}$$

where:

ε_t = tensile strain at the bottom of the HMA (13.9 in.) ($\mu\varepsilon$)

v = vehicle speed (mph)

T = mid-depth pavement temperature (°F)

e = base of natural logarithm

f, g, h = regression coefficients

TABLE 5.2 Regression Coefficients by Axle Type and Direction of Strain

		Regression Coefficients			
Gauge Orientation	Axle Type	*f*	*h*	*i*	R^2
Longitudinal	Steer	-24.25	0.047	108.81	0.955
Longitudinal	Tandem	-34.67	0.051	172.93	0.970
Longitudinal	Single	-40.57	0.053	206.67	0.983
Transverse	Steer	-19.70	0.050	101.40	0.986
Transverse	Tandem	-15.05	0.500	112.57	0.971
Transverse	Single	-16.23	0.051	102.18	0.986

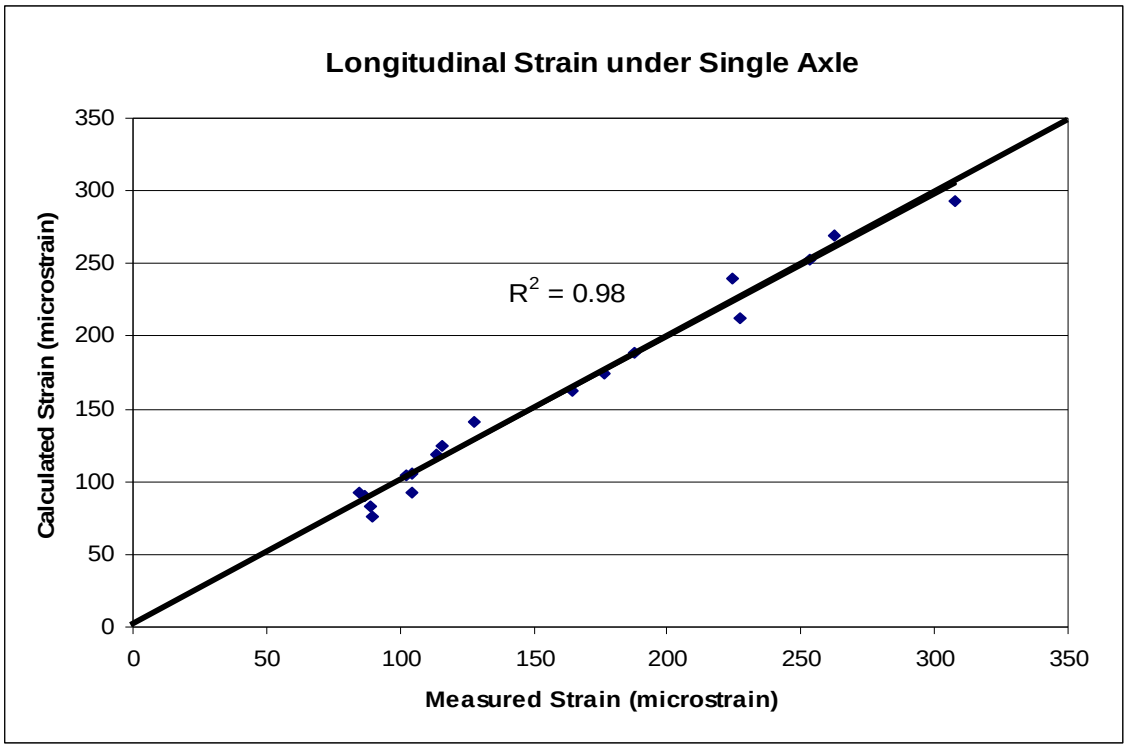

FIGURE 5.8 Calculated vs. Measured Strain.

The above equations were derived for the N9 test section and allow for the prediction of tensile strain under a variety of conditions. This is useful in comparing to critical strain levels essential to perpetual pavement design. Also, quantifying the effects of temperature and speed on tensile strain allow for further investigation into the material property that ultimately affects such responses, E*.

5.4 LOAD DURATION

It is necessary to characterize E* under field conditions to validate mechanistic-empirical design procedures such as the MEPDG. It is has been established through laboratory testing that the HMA stiffness is dependent on temperature and frequency. However, frequency cannot be measured or controlled directly in the field. Given that

frequency is inversely proportional to the time of loading, focus has been placed on modeling load duration in the field. It has been established by previous researchers that time of loading varies with pavement depth and vehicle speed (Barksdale, 1971). Additionally, given the viscoelastic nature of HMA it is expected that load duration also varies with temperature. Thus, further investigation has been conducted in modeling load durations in the field under various temperatures, depths and speeds.

5.4.1 Definition of Load Duration

Previous researchers such as Barksdale, Brown and Loulizi et al., have utilized stress pulses to model time of loading with speed and depth (Barksdale, 1971; Brown, 1973; Loulizi et al., 2002). Stress pulses are often of the haversine waveform, with distinguishable termination points. Although stress pulses enable a fairly easy measurement of load duration at the bottom of the HMA, such time corresponds to a response that is not critical. The critical response at the bottom of the HMA layer that is absolutely imperative to one of the most severe distresses, fatigue cracking, is tensile strain. Therefore, to evaluate the effect of vehicle speed, pavement thickness and temperature on load duration, the time of loading was defined by the strain pulses recorded by the embedded strain gages.

Strain pulses in each direction were described in Figures 5.2 and 5.3 in which strain levels were plotted in time. As previously noted, strain levels were most critical in the longitudinal direction, therefore only load durations from longitudinal strain pulses were examined. The strain pulses experienced in this experiment were very similar to those described by Garcia and Thompson (2008). It is evident from their research (Garcia and Thompson, 2008) as well as Figures 5.2 and 5.3 that strain pulses are not of

a defined waveform, making the task of measuring and modeling load duration more complicated. Given that the strain values asymptotically approach the baseline strain, and the cyclical noise inherent in the signal, it is difficult to define a distinct begin and end of the loading phase of the strain pulse. Although the pavement is loaded from the point it deviates from the baseline strain to the point in which it returns to the baseline strain, it is difficult to determine exactly where the points of deviation and return are located. This is especially true when the strain pulse experienced excessive noise or was located at shallow depths where gages were more sensitive to vibrations and/or were nearing the neutral axis of the pavement that experiences no tensile strain. Due to these difficulties, the definition of load pulse duration described by Garcia and Thompson (2008) was adopted. Figure 5.2 illustrates this definition, as the strain pulse duration was taken as the time that the HMA was experiencing only tensile strain. Using this definition of strain pulse duration, the durations were measured for each of the eight axles (1 steer axle, 2 axles in the tandem axle group and each of the 5 trailing single axles) using the baseline as a reference point to dictate the point at which the strain pulse crossed into the tensile realm. It should be noted that the axles in the tandem axle group were considered separate axles when the trace crossed the baseline strain level in between the two axles. Therefore a total of eight strain pulse durations were measured for each truck.

As discussed in Chapter Three, and shown in Figure 5.1, longitudinal strain gages were embedded at four depths within the pavement: 6.0, 8.8, 11.0, and 13.9 inches. At shallow depths the gages were more sensitive to vibrations, creating noisy traces that in some cases made termination points of the traces completely

undistinguishable. Additionally, strain pulses recorded at 6.0 inches deep illustrated that the strain was mostly compressive, indicating that it was above the neutral axis. At depths above the neutral axis, the strain levels are predominately compressive, whereas, deeper in the structure, the strain is predominately tensile. Strain levels diminish to zero at the neutral axis, making it difficult to measure strain levels when in close proximity to the neutral axis. Thus, strain pulses recorded near the neutral axis were small (approximately 20με compressive), but exhibited primarily compressive strain, as shown in Figure 5.9. In the figure there is a line drawn to help distinguish where the baseline is approximately located, and the small amount of strain that is in the tensile realm (above the baseline). As it might be expected, measuring tensile load duration from a trace similar to that in Figure 5.9 is nearly impossible, therefore strain pulse durations were only measured from gages located at 8.8, 11.0 and 13.9 inches deep where the signal was more discernible.

The effects of speed, depth and temperature on strain pulse duration were characterized first individually. From the individual relationships, the combined effect of these three factors on load duration was then characterized to provide a means to predict the load duration for any set of conditions.

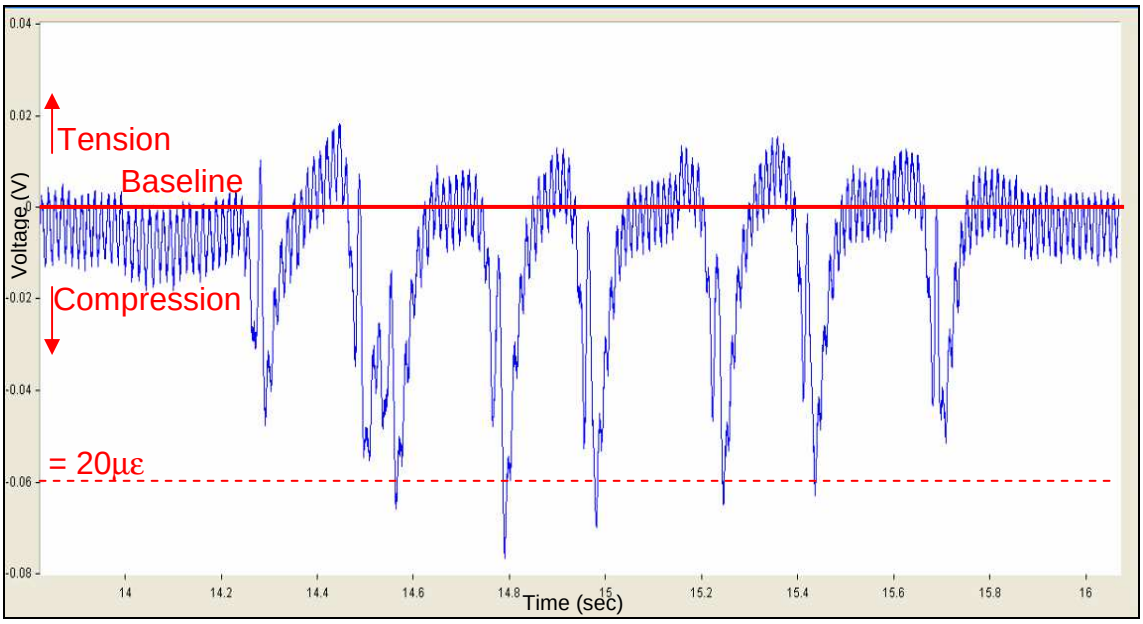

FIGURE 5.9 Strain Pulse Near Neutral Axis.

5.4.2 Effect of Depth on Strain Pulse Duration

To determine the general relationship between strain pulse duration and depth, measured strain pulse durations were plotted against gage depth. Figure 5.10 displays the expected trend of increasing duration with increased depth for a single axle at 35 mph. The same trend was also observed for the remaining axle types and speeds tested. Attaching a line of best fit and its associated regression equation and coefficient of determination showed that the strain pulse duration is a function of the natural logarithm of the gage depth, described by Equation 5-4 for all axle types and speeds. Although only the equation for the data measured on April 6, 2007 is shown, data measured on the remaining dates also illustrated close fitting equations, with similarly high R^2 values.

$$t = j\ln(h) + k \qquad (5\text{-}4)$$

where:

t = strain pulse load duration (sec)

h = depth (in)

j, k = regression coefficients

In looking at Figure 5.10, if the trend lines were extended linearly towards the x-axis, it is evident that at some depth the strain pulse durations would reach zero. This is an indication that the neutral axis has been reached and at the x-intercept zero tensile strain exists. Therefore, at depths shallower than the x-intercept, only compressive strain is experienced. Also, it should be noted that the x-intercept is not the same for each date tested, which may be an indication that temperature is a factor.

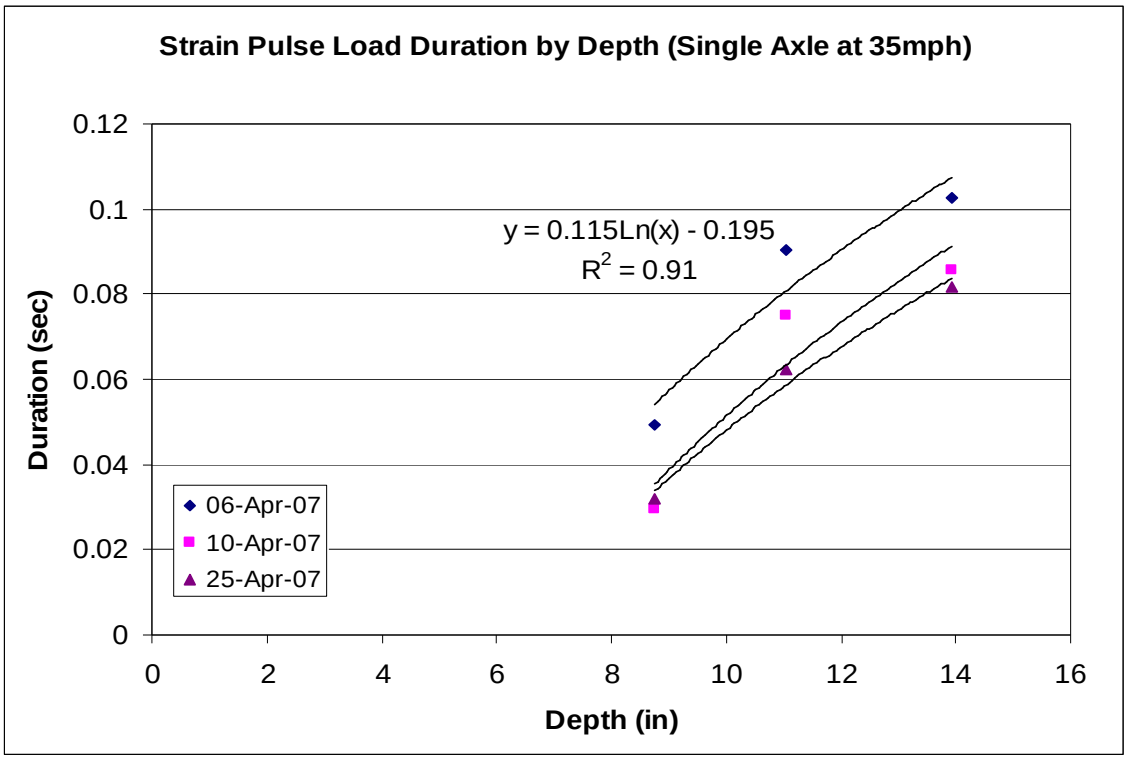

FIGURE 5.10 Strain Pulse Duration by Gage Depth.

5.4.3 Effect of Speed on Strain Pulse Duration

The relationship between speed and strain pulse duration was determined by plotting measured strain pulse durations against vehicle speed. Rather than using the target speeds of the trucks, the actual vehicle speed was calculated from the known distance between gages and the times at which an axle passed over the gages. This was

done to ensure an accurate relationship. Figure 5.11 displays the strain pulse durations with vehicle speed at a gage depth of 11.0 inches for a single axle. As was found with strain levels, increasing vehicle speed resulted in decreased strain pulse durations. It was found that by attaching a trend line that the strain pulse duration is related to the vehicle speed by a power function of the form listed in Equation 5-5. Although only the regression equation for the first test date is shown, Equation 5-5 was found to represent the remaining dates with very high R^2 values. Furthermore, plots at the remaining gage depths showed that Equation 5-5 represents the relationship between strain pulse duration and speed regardless of axle type and gage depth.

$$t = lv^m \tag{5-5}$$

where:

t = strain pulse load duration (sec)

v = vehicle speed (mph)

l, m = regression coefficients

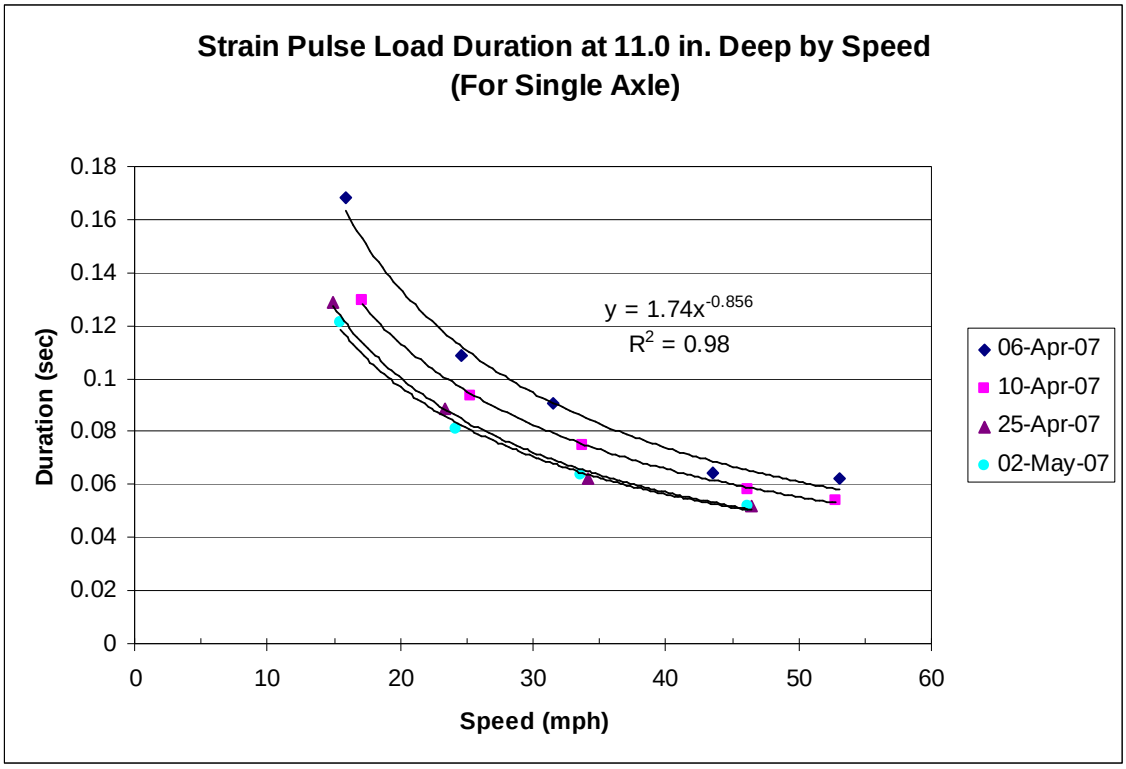

FIGURE 5.11 Effect of Speed on Strain Pulse Duration.

5.4.4 Effect of Temperature on Strain Pulse Duration

The effect of pavement temperature on strain pulse duration was assessed by developing plots for each axle type. To be consistent with the evaluation of field measured strain levels, the mid-depth pavement temperatures were utilized for this analysis as well. Figure 5.12 shows that at the bottom of the HMA layers, the strain pulse duration decreases slowly with an increase in pavement temperature. A power function is shown to fit the data very well for a target vehicle speed of 45 mph. The remaining target speeds can also be fitted with a power function of the same form; however the correlations to the measured data, indicated by the R^2 values, are not as close (at 15 mph, $R^2 = 0.71$). This was also the case for the remaining gage depths. It is evident however; that there is a definite trend, although it might be slight, that the strain

pulse duration decreases with an increase in mid-depth pavement temperature. This trend was evident regardless of axle type or depth in the pavement, and can be described by a power function. Therefore, the power function relationship shown in Equation 5-5 was utilized to characterize strain pulse duration with temperature (rather than speed).

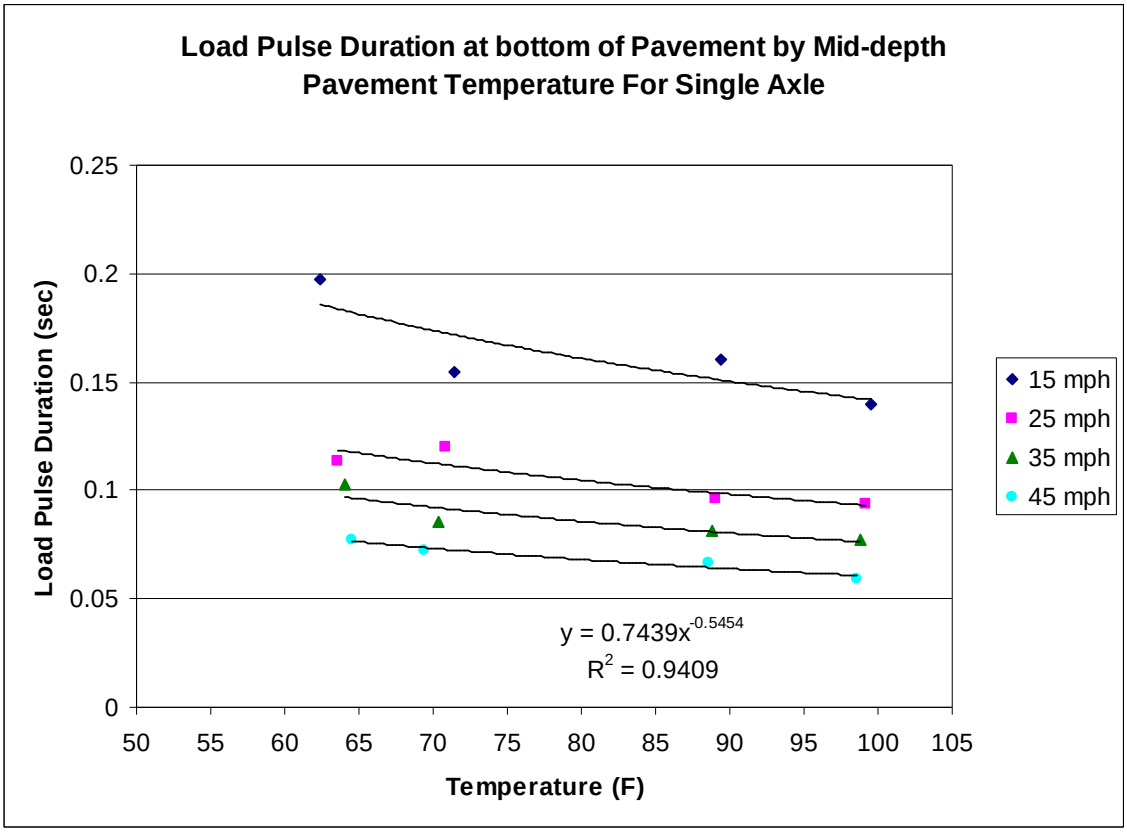

FIGURE 5.12 Effect of Temperature on Strain Pulse Duration.

5.4.5 Modeling Strain Pulse Duration for Field Conditions

Once the individual effects of depth, speed and temperature were evaluated for the measured strain pulse durations, the combined effect of all three variables was quantified. A model was developed using DataFit to account for all three variables by pooling all strain pulse duration measurements regardless of axle type. The resulting model is listed in Equation 5-6 and is a linear combination of the previous relationships,

listed in Equations 5-4 and 5-5. The same process as was discussed in section 5.3.4 to determine the most appropriate model was again followed, in which multiple models were first defined, then based on the statistical output by DataFit, a final model was selected:

$$t = n \ln h + v^p + T^q + r \quad (5\text{-}6)$$

where:

t = strain pulse load duration (sec)

h = depth (in)

v = vehicle speed (mph)

T = mid-depth temperature (°F)

n, p, q, r = regression coefficients

Equation 5-6 was selected for its strong correlation (R^2 value of 83.74%) to the measured data which is displayed in Figure 5.13. Note the measured data clustered around the line of equality in Figure 5.13. Additionally, each of the regression coefficients was found to be statistically significant, evident by the reported p-value, also shown in Figure 5.13.

In Equation 5-6, coefficient "n" adjusts for HMA depth. As previously discussed, increased depth translates to increased load duration, and therefore a positive coefficient is logical. It was found that increasing vehicle speed resulted in decreased load duration, which is accurately represented in the model by a negative exponent, coefficient "p". Similarly, increases in mid-depth temperature induced shorter load durations which are explained by a negative exponent, coefficient "q," in the model.

Using equations of the same form listed in Equation 5-6, individual models were developed by axle type: steer, tandem, and single. Small improvements in correlation to the measured data were found, with R^2 values of 88.83%, 87.62%, and 86.34% respectively. The improvements were slight, and therefore do not suggest that the load duration is heavily dependent on axle type.

By developing a model for strain pulse duration as a function of depth, speed and temperature, predictions can be made for the N9 test section for a set of given conditions. Furthermore, such a model also enables comparisons to be drawn with load durations computed by mechanistic-empirical design procedures, specifically the MEPDG.

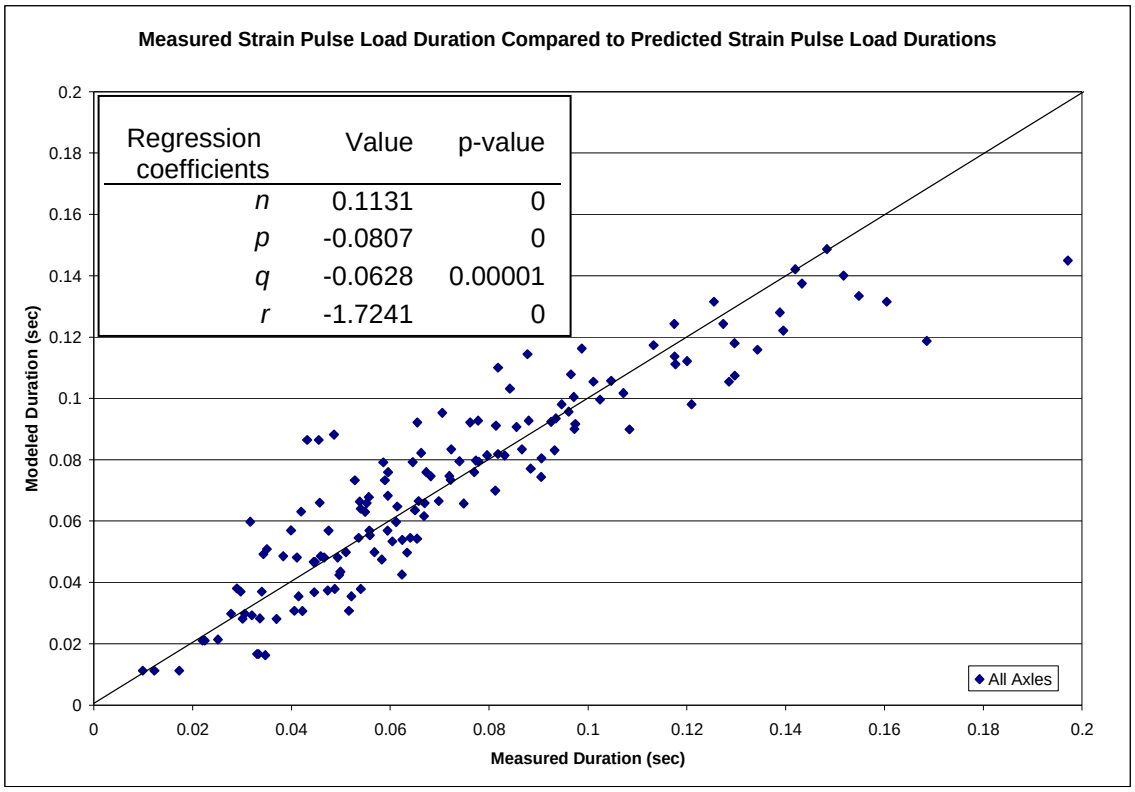

FIGURE 5.13 Goodness of Fit of Predicted Strain Pulse Durations.

5.5 SUMMARY

A field investigation into strain levels and strain pulse durations was completed on section N9 at the NCAT Test Track. Strain pulse traces were recorded by strain gages embedded at multiple depths under live traffic at various speeds and temperatures. From the recorded strain pulse traces the strain levels at the bottom of the HMA layers were evaluated to quantify the effect of speed, and temperature on tensile strain. The strain pulse durations were determined from the recorded traces and utilized to model the effect of pavement depth, vehicle speed, and temperature.

It was found that tensile strain levels at the bottom of the HMA layers are most influenced by mid-depth pavement temperatures. Tensile strain was found to be a function of the natural logarithm of vehicle speed and the exponent of mid-depth pavement temperature. Given the varying weights of the axle groups, the tensile strain levels were found to be heavily dependent on axle type. Additionally, tensile strains in the longitudinal direction were more significant than those in the transverse direction. Given these findings, models were developed separately for tensile strain in the longitudinal and transverse directions to account for vehicle speed, and mid-depth pavement temperature. Furthermore, a model for tensile strain in each direction was developed for each axle type, tallying six models.

Strain pulse durations were defined by the time that the HMA layers experienced only tensile strain under dynamic loading. From the recorded longitudinal strain pulse traces, the durations were measured and related to three variables: pavement depth, vehicle speed, and mid-depth pavement temperature. It was found that strain pulse durations increase with the natural logarithm of pavement depth, and decrease with a

power function of vehicle speed and pavement temperature. Unlike, strain levels, strain pulse durations were not found to be heavily dependent on axle type. One model was developed to account for critical strain pulse durations.

Although the models developed are specific for the N9 test section, it offers a field-measured data set by which to make comparisons to established pavement design procedures that estimate strain levels and load durations. Specifically, comparisons can be made between pavement responses predicted by various methods of computing material properties and the field-measurements. From these comparisons, conclusions can be made on methods of computing material properties, particularly E*, and the quality of these design procedures.

CHAPTER SIX

MEPDG EVALUATION

6.1 INTRODUCTION

It is imperative that the quality of the MEPDG be evaluated in first characterizing material properties and second, in designing against critical distresses, such as fatigue cracking. The mechanism behind fatigue cracking, as mentioned previously, is tensile strain at the bottom of the HMA. To evaluate the quality of the MEPDG, both a field investigation and an investigation into the internal workings of the MEPDG are necessary. The field investigation was completed, and results were discussed in Chapter Five regarding the factors affecting tensile strain at the bottom of the HMA and load durations at various points in the structure. Following the completion of the field investigation, the next step in validating the MEPDG was to follow its procedure to compute load duration which in turn can be used to assess E* predictions and ultimately strain predictions. E* values are computed en route to computing load durations in the method prescribed by the MEPDG. Using these load durations and E* values computed by the MEPDG, results were compared with field measurements and evaluated to determine its usefulness as a design mechanism for state DOTs.

6.2 EVALUATION OF MEPDG LOAD DURATION PROCEDURE

In characterizing the material property, E*, of HMA layers, the MEPDG considers two factors to be the most important: temperature and rate of loading (Eres,

2003). The temperature is determined internally within the program from an enhanced integrated climatic model (EICM) which is calibrated for different regions from historical data (Eres, 2003). The rate of loading, however, is much more complex, due to its direct relationship with time of loading which is influenced by vehicle speed, axle configuration, and properties of the pavement structure (Eres, 2003). Thus, to evaluate the quality of E* estimates, it is necessary to take a detailed look into the procedure to determine the time of loading, as defined by the MEPDG.

6.2.1 MEPDG Load Duration Procedure

The MEPDG uses an iterative procedure to compute the load duration under dynamic loading, shown conceptually in Figure 6.1. The MEPDG assumes the load duration as the length of time for one complete haversine stress pulse in the longitudinal direction for an applied load (Eres, 2003). In following the MEPDG procedure, the load duration is heavily dependent on the pavement structure. Within the procedure, the pavement structure is transformed following Odemark's transformation procedure for layered systems (Eres, 2003). In doing so, the height of each layer is transformed into an effective height based on the ratio of the modulus of that layer to the modulus of the subgrade and the layer height. The effective heights of each layer are used to compute the effective depth, Z_{eff}, of the stress pulse given any point within the structure. The effective depth is the sum of the effective heights of the layers above the point in interest, plus the effective height of the layer where said point resides. Figure 6.1 shows a two layer system in which the point of interest is at the mid-point of the bottom layer. To compute the effective depth, the modulus of each HMA layer is required; however, the modulus of each HMA layer is a function of the time of loading. Since, the time of

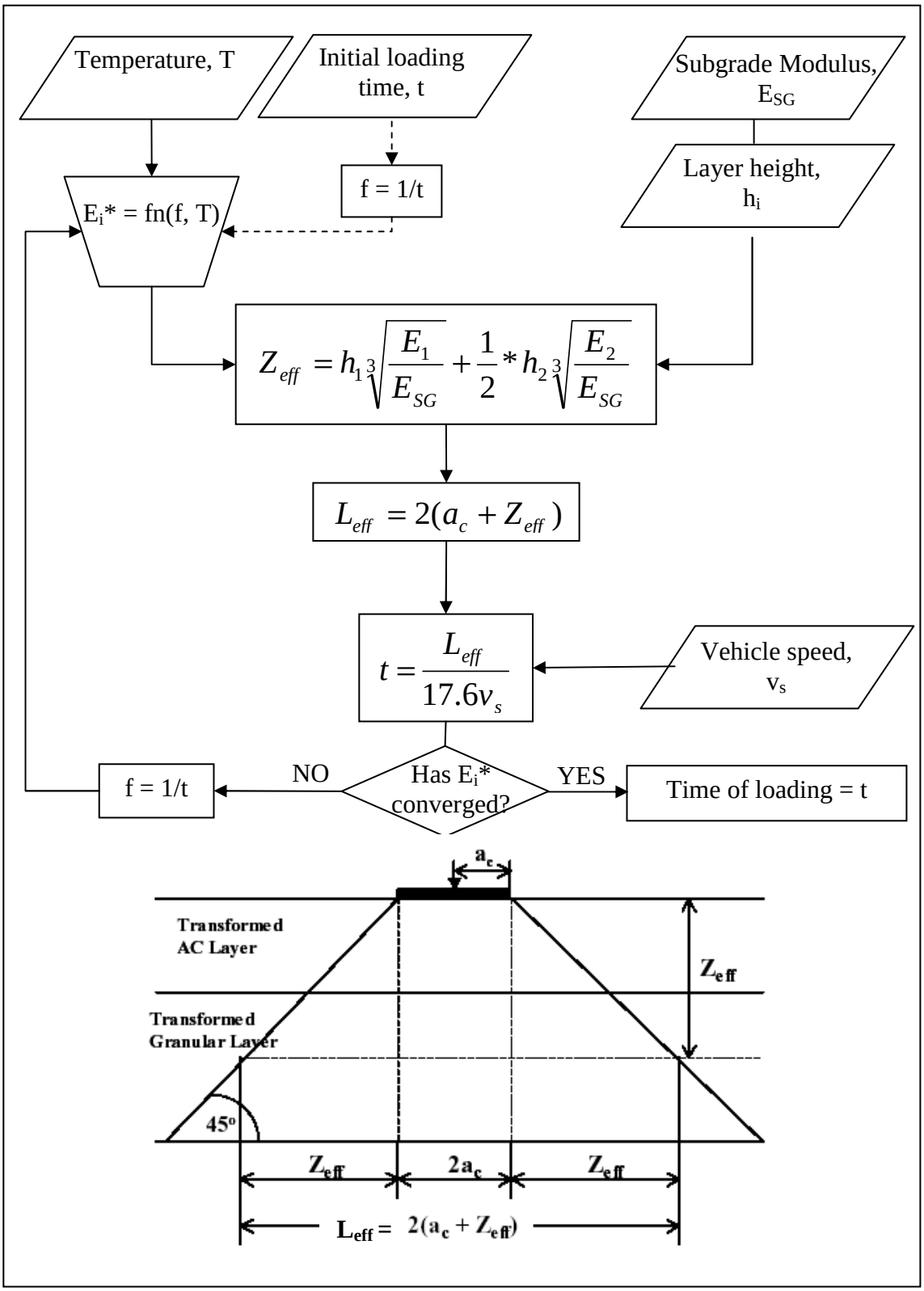

FIGURE 6.1 MEPDG Load Duration Procedure (Eres, 2003).

loading has yet to be computed, it must be assumed initially from which rate of loading is then computed.

In addition to the pavement structure, the time of loading is dependent on the axle configuration. Configurations are taken into account in the computation of the effective length of the stress pulse. Figure 6.1 illustrates the effective length for a single axle in which the effective length of the stress pulse is a function of the contact radius, a_c, and effective depth. This illustrates the assumption that the stress pulse is distributed throughout the pavement structure at a 45 degree angle from the edge of the contact at the surface (Eres, 2003). This assumption is held for all axle types. For tandem, tridem, and quad axles, the axle spacing must be known to determine the amount of overlap at the effective depth. Further discussion on axle types other than single axles are excluded because in the field, strain pulses under the tandem axles did not exhibit overlap at the deepest point measured (13.92 inches), and were therefore treated as two single axles.

Vehicle speed is taken into account in the determination of time of loading. Shown in Figure 6.1, load duration is inversely proportional to the vehicle speed and directly proportional to the effective length of the stress pulse. Given that this is an iterative process, and that E* is dependent on time of loading, the resulting load duration must be used in the time-frequency relationship to help compute E*. The entire procedure must be repeated several times until the HMA modulus of each layer has converged.

6.2.2 N9 E* Regression Analysis

In order to follow the MEPDG procedure, a means to estimate E* from temperature and loading frequency must first be established. It is prescribed in the

method that the frequency is inversely proportional to time, as described by Equation 6-1 (Eres, 2003).

$$f = \frac{1}{t} \tag{6-1}$$

where:

f = loading frequency (Hz)

t = time of loading (sec)

The MEPDG uses one of three methods to determine E* via the construction of a master curve, in which the method depends on the selected level of complexity in design. In two of the three methods an equation is utilized to compute E* from various volumetric properties and binder information. For the most complex level of design, the MEPDG requires E* laboratory test results to construct the master curve. E* laboratory testing was completed for the N9 section, at three temperature: 40, 70, and 100 ºF, and seven frequencies: 0.5, 1, 2, 5, 10, 20, and 25Hz. E* testing was discussed in more detail in Chapter Four. Given that the majority of the temperatures experienced in the field were within the range tested in the laboratory, a regression analysis was completed to develop a model to determine E* for each of the HMA layers in N9. The model, shown in Equation 6-2, was selected based on the very high coefficients of determination, and significance of each regression coefficient. Table 6.1 lists the coefficients for the regression equation by the HMA lift, as well as the coefficient of determination. Although the p-values are not listed, all coefficients were found to be significant with a p-value of less than 0.0001. It should be noted that the HMA lifts are numbered from the top down, with number one being the surface layer. Furthermore, the regression

coefficients for lifts three and four are the same because they were constructed of the same mix.

$$E^* = ab^T f^c \quad (6\text{-}2)$$

where:

E* = dynamic modulus of HMA (psi)

T = Temperature (ºF)

f = loading frequency (Hz)

a, b, c = regression coefficients

TABLE 6.1 E* Regression Coefficients by Lift

HMA Lift	Type	Thickness (in)	a	b	c	R^2
1	SMA	2.16	3,445,000	0.9719	0.1551	0.97
2	76-28	3.84	4,546,000	0.9712	0.1464	0.98
3	64-22	2.76	4,637,000	0.9740	0.1313	0.97
4	64-22	2.28	4,637,000	0.9740	0.1313	0.97
5	Rich Bottom	2.88	3,342,000	0.9692	0.1734	0.99

6.2.3 Load Duration Computation

To draw direct comparisons with the field measured load durations, the MEPDG method for computing was followed, utilizing the exact same conditions as experienced in the field. For each time of loading measured, the load duration was calculated for the same gage depth, pavement temperatures, and vehicle speed. To compute the E* of the necessary layers, in-situ pavement temperatures recorded by probes T7, T9, T11, T13 and T15 were employed. Probes in each layer were not consistently located at the mid-point of the layer, therefore, probes located closet to the gage depth were used, and hence the selection of the aforementioned probes. Table 6.2 lists the depth of the

embedded temperature probes used for this analysis, as well as the associated pavement layer.

TABLE 6.2 Location of Temperature Probes

Temperature Probe	Depth (in)	Lift
T7	2.02	1
T9	5.41	2
T11	8.38	3
T13	10.81	4
T15	14.08	5

To compute E*, an initial loading time was required to determine the loading frequency through Equation 6-1, for use in Equation 6-2. The seed value for time of loading was calculated following the equation developed by Brown (1973):

$$\log (t) = 0.5d - 0.2 - 0.94\log(v) \quad (6\text{-}3)$$

where:

d = depth (m)

v = vehicle speed (km/hr)

According to Brown, the loading time should be an average of the stress pulses in all three directions: vertical, radial, and tangential (Brown, 1973). As illustrated in Equation 6-3, Brown found that the time of loading was a function of the depth within the pavement and the vehicle speed. The vehicle speed calculated from the known axle spacing and time at which the axle passed a gage was utilized in the application of Equation 6-3. From this calculation an initial HMA modulus of each layer was determined. Due to the iterative process used in the MEPDG, any shortcomings of this equation are quickly resolved by successive iterations, and in reality any value could be used.

The calculated HMA modulus was then used to compute an effective depth of the stress pulse at the gage depth according to (Eres, 2003):

$$Z_{eff} = \sum_{i=1}^{n-1}\left(h_i \sqrt[3]{\frac{E_i}{E_{SG}}} \right) + h_n \sqrt[3]{\frac{E_n}{E_{SG}}} \quad (6\text{-}4)$$

where:

h_n = height of the bottom layer (at depth in question)

h_i = height of layer i (above the bottom layer)

E_i = Dynamic modulus of layer i (psi)

E_{SG} = Modulus of subgrade (psi)

E_n = Dynamic modulus of bottom layer (psi)

The average modulus of the underlying Track soil subgrade was utilized for use in Equation 6-4. As described in Chapter Three, the N9 structure consisted of 39.2 inches of soft Seale subgrade sandwiched between two layers of Track soil, an 8.4-inch base, and a deep subgrade. Backcalculation revealed very low moduli values for the Track soil as a base material, inconsistent with laboratory testing (Taylor, 2008). It was likely due to the soft Seale subgrade. Due to the fact that the Seale subgrade layer was thin relative to the deep underlying layer of the Track soil, it was elected to use the resilient modulus of the Track soil subgrade. To remain on the conservative side, the average resilient modulus value of 28,335 psi found in the laboratory (Taylor, 2008) was used rather than the larger resilient modulus found in the field through backcalculation.

Once the effective depth was computed, the effective length of the stress pulse was calculated for each time of loading measured. The effective load duration was calculated using Equation 6-5, given the desired depth within the pavement structure.

The contact radius was calculated for each tire, using the known axle weights for each truck (Table 3-4) and a tire pressure of 100 psi. The L_{eff} was calculated for only one of the tire loads on each axle, such that, for a single axle, the axle weight was considered to be equally distributed over 4 tires, resulting in four equal radii, of which only one was selected for the computation.

$$L_{eff} = 2(a_c + Z_{eff}) \quad (6\text{-}5)$$

where:

L_{eff} = effective length of load pulse (in.)

a_c = radius of tire contact area (in.)

Lastly, the time of loading was calculated following Equation 6-6, using the calculated vehicle speed. Once the load duration was calculated, it was used to compute frequency to begin the second iteration. The final load duration was taken once the HMA modulus of each layer converged. For this investigation a total of nine iterations were completed, although the moduli converged at iteration seven. An example of the convergence is shown in Figure 6.2.

$$t = \frac{L_{eff}}{17.6 v_s} \quad (6\text{-}6)$$

where:

t = duration of stress pulse (sec)

v_s = vehicle speed (mph)

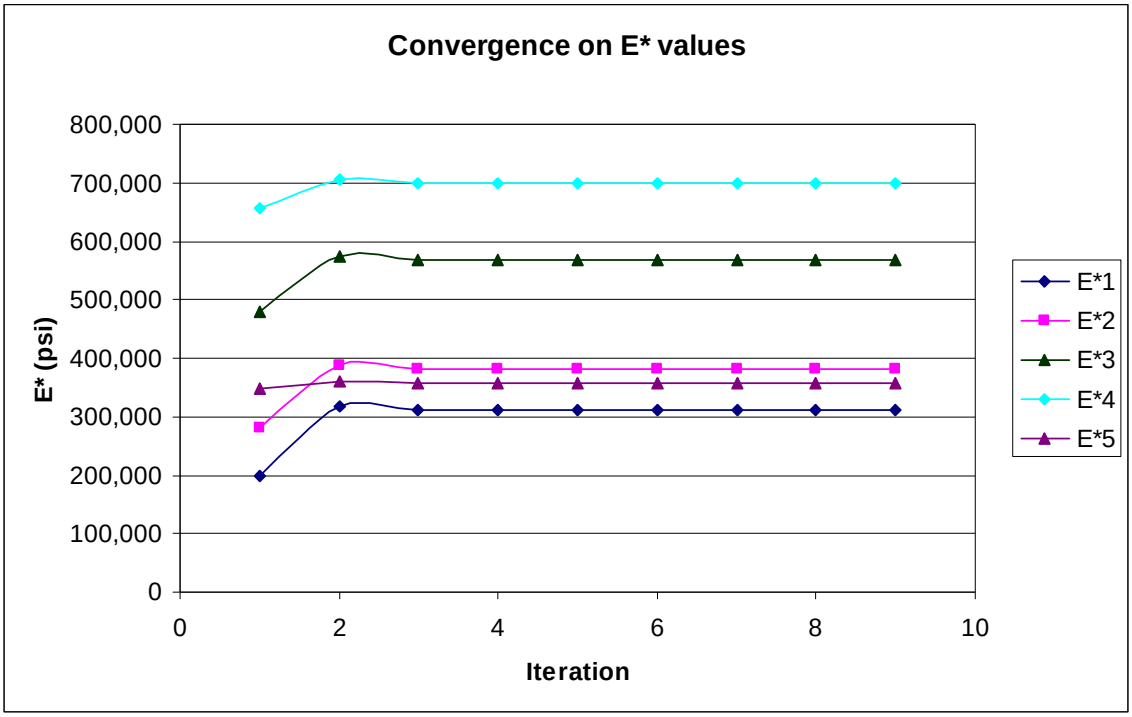

FIGURE 6.2 Example of E* Convergence.

6.2.4 Load Duration Comparisons

The load durations computed by the aforementioned MEPDG procedure were compared with the strain pulse durations measured during the field investigation. A direct comparison could be drawn because the field conditions (in-situ temperatures, calculated vehicle speed, and gage depth) for each measured time of loading were utilized to calculate a corresponding time of loading through the MEPDG procedure. Figure 6.3 illustrates the difference in the measured and calculated load durations for all gage depths, by plotting measured versus theoretical (MEPDG). It is evident that the MEPDG procedure consistently over-predicts the load durations as every data point on the plot is above the line of equality. Attaching a regression equation to the data, illustrates that this over-prediction is approximately 68% greater than the measured load durations. It should be noted that the measured load durations represent the tensile strain

pulse durations in the longitudinal direction, while the theoretical durations represent the duration of stress pulses in the longitudinal direction assumed to be at 45 degree angles to the horizontal. These differences may account in part for the over-prediction by the MEPDG procedure. However, it should be expected that better agreement exists regardless of strain or stress measurements.

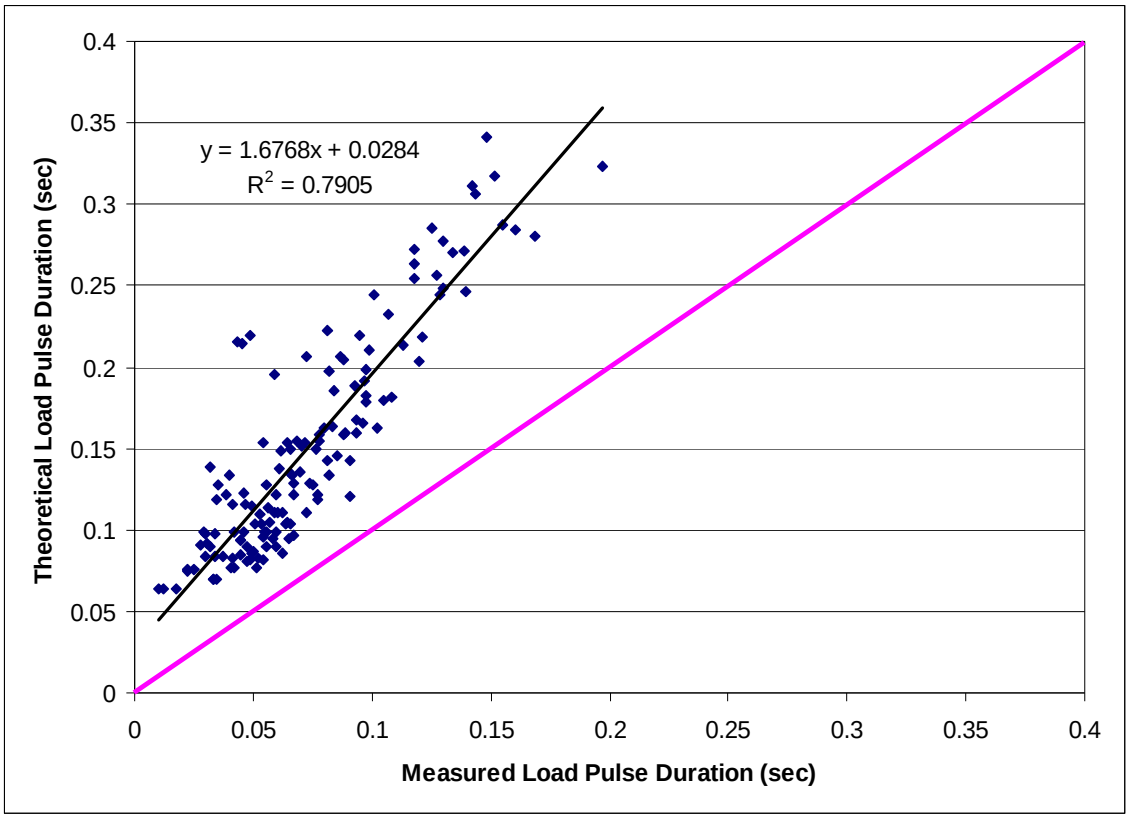

FIGURE 6.3 Measured Load Duration Versus Theoretical.

6.3 Effect of MEPDG Load Duration Calculations

It is imperative that the MEPDG be evaluated on its ability to characterize material properties because material properties directly influence pavement responses and ultimately pavement performance. As noted previously, one such property, E*, significantly influences tensile strain. Furthermore, tensile strain at the bottom of the

HMA is the controlling factor for the development of fatigue cracking. The MEPDG determines E* en route to computing load duration, both of which are dependent on each other. To assess the accuracy of the MEPDG, strain levels were predicted from these values using layered elastic analysis for comparison with strain values determined in the field, following Figure 6.4.

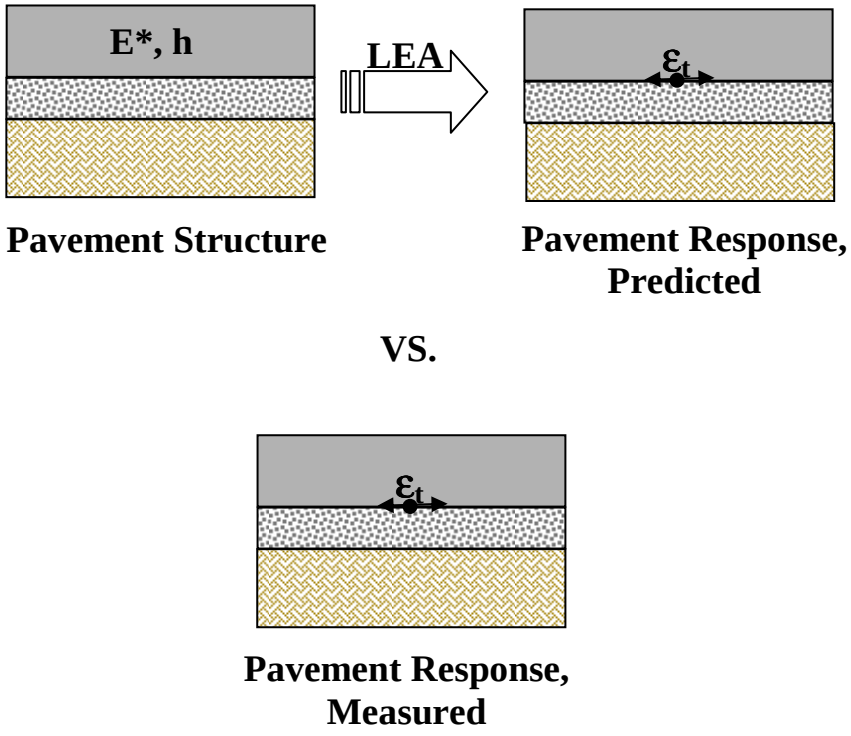

FIGURE 6.4 Evaluation of MEPDG by Pavement Response.

6.3.1 Strain Predictions Based on MEPDG Load Durations

The MEPDG neither outputs strains levels, nor is any process used to compute strain discussed in the associated appendices. Therefore, to assess the E* values computed through the method for determining load duration, strain values must be

predicted by another means. In this case, layered elastic analysis, specifically the software program WESLEA for Windows (version 3.0), was utilized.

WESLEA is capable of computing pavement responses provided a few material properties of each layer: modulus, Poisson's ratio, and layer height. The program is however limited to only three HMA layers atop a base layer and subgrade. Additionally, the program requires that axle configurations be defined, as well as tire load. Using layered elastic theory and the user defined inputs, pavement responses at critical locations are predicted.

To use WESLEA, the eight-layered pavement structure of N9 was converted to a five-layered structure. Doing so required that the heights and material properties of three layers of HMA be transformed into one, and the Track Soil base layer be combined with the Seale Subgrade layer. In order to do so, knowledge of the aforementioned properties of each of the eight layers were required. Thus, computation of the HMA modulus of each layer was necessary. First, a set of conditions was selected, listed in Table 6.3. To simplify the procedure, the in-situ pavement temperatures at all depths were considered equal. This eliminated the need to model the temperature gradient across the five HMA layers in the N9 structure. Using these conditions, the MEPDG's method for determination of time of loading was followed, as described previously, again using the E* regression equations listed in Equation 6-2 and Table 6.1.

TABLE 6.3 Conditions for Strain Predictions

Speed, mph	Temp, ºF
15	60
15	80
15	110
25	60
25	80
25	110
45	60
45	80
45	110

Because tensile strain at the bottom of the HMA is critical to fatigue cracking, only load durations at the bottom of the HMA (13.9 inches) were computed. To ensure accuracy, nine iterations were completed, from which the resulting E* values were used to describe each HMA layer, listed in Table 6.4. Although the exact calculated values are listed in this table, much less precision exists.

TABLE 6.4 Computed E* Values for N9 HMA Layers

Speed (mph)	Temp (ºF)	E_1* (psi)	E_2* (psi)	E_3* (psi)	E_4* (psi)	E_5* (psi)
15	60	968,585	1,058,003	1,169,592	1,129,741	614,110
15	80	554,358	601,895	705,472	681,703	337,579
15	110	239,461	257,795	330,112	319,260	137,448
25	60	1,046,470	1,136,962	1,247,353	1,204,823	668,494
25	80	599,042	646,893	752,429	727,048	367,496
25	110	258,830	277,125	352,129	340,529	149,646
45	60	1,143,832	1,235,113	1,343,234	1,297,401	737,049
45	80	654,912	702,834	810,331	782,961	405,212
45	110	283,055	301,160	379,280	366,757	165,026

Next, three HMA layers of the structure were transformed into one layer, illustrated by Figure 6.5. The first layer, a stone matrix-asphalt (SMA) mix, with PG 76-28 binder and the fifth, a rich bottom layer designed for 2% air voids and composed of PG 64-22 binder, were left as independent layers due to their uniqueness. The second, third and fourth HMA layers were combined into one. Given that the third and fourth layers were constructed of the same mix, combining these two was logical. The second

lift was also combined with this pair because the HMA moduli for the varying conditions were very similar to those in the third and fourth layers and because they were all standard mixes. The HMA modulus of the transformed second layer was calculated using a weighted average dependent on layer height, described by Equation 6-6. The resulting HMA moduli of the transformed structure are listed in Table 6.5; again much less precision in these values exists.

$$E_T^* = \frac{\sum\left(E_n^* h_n\right)}{\sum h_n} \qquad (6\text{-}6)$$

where:

E_T* = HMA Modulus of Transformed layer

E_n* = HMA Modulus of n^{th} layer

h_n = height of n^{th} layer

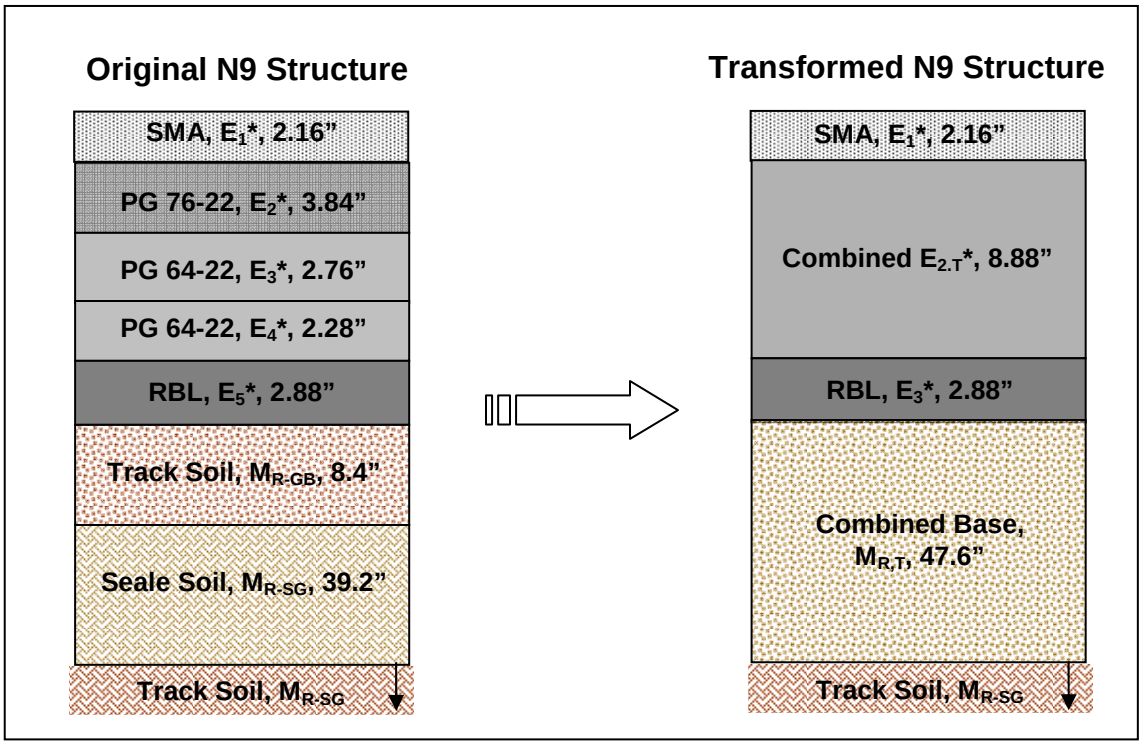

FIGURE 6.5 Transformation of Structure for Use in WESLEA.

TABLE 6.5 HMA Moduli for Transformed N9 Structure

Speed (mph)	Temp (ºF)	h_1 (in.)	E^*_1 (psi)	h_2 (in.)	E^*_{2T} (psi)	h_3 (in.)	E^*_3 (psi)
15	60	2.16	968,585	8.88	1,111,105	2.88	614,110
15	80	2.16	554,358	8.88	654,579	2.88	337,579
15	110	2.16	239,461	8.88	296,053	2.88	137,448
25	60	2.16	1,046,470	8.88	1,188,697	2.88	668,494
25	80	2.16	599,042	8.88	700,275	2.88	367,496
25	110	2.16	258,830	8.88	316,716	2.88	149,646
45	60	2.16	1,143,832	8.88	1,284,711	2.88	737,049
45	80	2.16	654,912	8.88	756,818	2.88	405,212
45	110	2.16	283,055	8.88	342,283	2.88	165,026

Next, the Track soil base layer was combined with the Seale soil subgrade layer, to create a transformed base layer 47.6 inches thick. These unbound materials were characterized in the laboratory through a previous investigation at the Test Track (Taylor, 2008). From this investigation the stress-sensitive resilient moduli were found to be described by Equation 6-7 (Taylor, 2008). The associated regression coefficients for each material are listed in Table 6.6.

$$M_R = k_1 p_a \left(\frac{\theta}{p_a} \right)^{k_2} \left(\frac{\sigma_d}{p_a} \right)^{k_3} \tag{6-7}$$

where:

M_R = resilient modulus of unbound material

p_a = atmospheric pressure = 14.696 psi

θ = bulk stress, psi

σ_d = deviatoric stress, psi

k_1, k_2, k_3 = regression coefficients

TABLE 6.6 Regression Coefficients for MR (Taylor, 2008)

Unbound Material	k_1	K_2	k_3
Seale Subgrade	225.09	0.3598	-0.7551
Track Soil	1095.43	0.5930	-0.4727

The resilient modulus is dependent on the states of stress within each layer. The state of stress within the base layer and subgrade layer are further dependent on the ability of the HMA layers above to disperse the applied load. Therefore, the properties of the transformed HMA layers, listed in Table 6.5 were used in WESLEA to determine the induced stresses in the transformed base layer and subgrade layer. Induced stresses, σ_x, σ_y, and σ_z, were used to determine the states of stress, bulk stress and deviatoric stress, for each layer independently. Through an iterative process the M_R of the transformed base layer and Track soil subgrade layer were determined.

To complete this iterative process, the bulk (θ) and deviatoric (σ_d) stresses were further defined by Equations 6-8 and 6-9.

$$\theta = \sigma_1 + \sigma_2 + \sigma_3 \quad (6\text{-}8)$$

$$\sigma_d = \sigma_1 - \sigma_3 \quad (6\text{-}9$$

where:

σ_1 = total axial stress, psi

σ_2, σ_3 = confining pressure, psi

The total axial stress, σ_1, is the sum of the principal stress, σ_{1p}, in the vertical direction and the induced stress in the vertical direction, σ_z, as determined from WESLEA. In this case, the principal vertical stress is due to the overburden stress of the overlying layers, computed by Equation 6-10.

$$\sigma_{1p} = (\gamma_1 h_1 + \gamma_2 h_2 + ... + \gamma_i h_i)/1728 \quad (6\text{-}10)$$

where:

σ_{1p} = principal vertical stress, psi

γ_i = unit weight of i^{th} layer, pcf

h_i = height of i^{th} layer, in.

The critical location where induced stresses were predicted in WESLEA for the determination of the base M_R was the mid-point of the base layer (37.7 inches deep) directly beneath the tire load. For the subgrade M_R, the critical location was the interface of the base and subgrade layers (61.5 inches deep), also directly beneath the tire load. To determine the principal vertical stress for either layer the unit weight of the base layer was required. Previous laboratory investigations for the 2006 Test Track reported a value of 126.9 pcf (Timm, 2008). The unit weight of each HMA layer was the product of the bulk specific gravity, G_{mb}, in the field and the unit weight of water. The percent compaction of the laboratory determined maximum specific gravity, G_{mm}, was recorded during construction. From this, the bulk specific gravity and unit weight of each HMA layer were computed using Equation 6-11 and the values listed in Table 6.7. To ensure accuracy, the properties of all five HMA layers in the original N9 pavement structure were used to compute the vertical principal stress for each the base and subgrade layer.

$$\gamma_{mb} = \gamma_w G_{mb} \quad (6\text{-}11)$$

where:

γ_{mb} = bulk unit weight of layer, pcf

γ_w = unit weight of water, pcf = 62.4

G_{mb} = bulk specific gravity = $\%G_{mm} * G_{mm}$

TABLE 6.7 Unit Weight by HMA Layer (Timm, 2008)

Lift	$\%G_{mm}$	G_{mm}	G_{mb}	γ_{mb} (pcf)
1	93	2.397	2.229	139.1
2	92.9	2.496	2.319	144.7
3	95.1	2.503	2.380	148.5
4	93.9	2.507	2.354	146.9
5	94.4	2.424	2.288	142.8

The confining pressures, σ_2 and σ_3, were equivalent due to the defined critical location, directly beneath the tire load, and the assumption that the materials were homogenous and isotropic. Confining pressure is further defined as the summation of the horizontal principal stress, σ_{3p}, and the induced horizontal stress, σ_x, determined in WESLEA. The horizontal principal stress is dependent on the at-rest lateral earth pressure, and was computed using Equation 6-12.

$$\sigma_{3p} = k_0 \sigma_{1p} \tag{6-12}$$

where:

σ_{3p} = horizontal principal stress, psi

k_0 = coefficient of at rest lateral earth pressure

σ_{1p} = vertical principal stress, psi (see Equation 6-10)

The coefficient of at rest lateral earth pressure, k_0, is dependent on the angle of internal friction of the soil. Using Equation 6-13 to compute k_0, the angle of internal friction was assumed to be 40º to be consistent with the previous investigation into the characteristics of these unbound materials (Taylor, 2008).

$$k_0 = 1 - \sin\phi \tag{6-13}$$

where:

ϕ = angle of internal friction, assumed to be 40º

To begin the iterative process of determining the resilient modulus of each base and subgrade layer, an initial M_R value of each was assumed. Again referring to prior research (Taylor, 2008) conducted on the unbound materials used at the Test Track, the initial values were selected based on representative states of stress. For a stress state with 25 psi of bulk stress and 7 psi of deviatoric stress, the resilient modulus of the transformed base layer was approximately 6,500 psi (Taylor, 2008). The transformed base layer was a combination of both the Track soil and Seale subgrade, therefore a slightly higher value of 10,000 psi was selected to account for the much stiffer Track soil. At the same state of stress used to select the base layer, the M_R value for the Track soil was approximated at 30,000 psi.

Once the initial values were selected, the M_R of the base layer was determined first. Using the HMA properties from the original N9 8-layer structure, the vertical and horizontal principal stresses were computed. Then using WESLEA, and the aforementioned seed values of the base and subgrade, the maximum stresses induced at the mid-point of the 47.6 inch deep transformed base layer were predicted. Table 6.8 lists the defined properties necessary to complete the analysis in WESLEA. It should be noted that to simplify the analysis, it was assumed that the pavement was under the load of a 20,000 lb single axle with single tires. Additionally the layer heights for each HMA layer are shown in Figure 6.5 for the original structure. The base layer height used was the height of the transformed base layer, 47.6 inches deep, also shown in Figure 6.5.

TABLE 6.8 Properties Defined for WESLEA

Property	Value
Poisson's Ratio – HMA	0.35
Poisson's Ratio – Transformed Base	0.45
Poisson's Ratio – Subgrade	0.45
Slip	1: Full adhesion
Axle	Steer
Tire Load	10,000 lb
Tire Pressure	100 psi

The resulting stresses, σ_x, σ_y, and σ_z, found at the mid-point of the base layer were then used to compute the bulk and deviatoric stresses. From these values, the resilient modulus of the transformed base layer was computed. Throughout the process, the resilient modulus of the subgrade was kept constant at 30,000 psi. The new base layer resilient modulus was then substituted into WESLEA to replace the initial seed value, starting the second iteration. This process was repeated until the resilient modulus of the transformed base layer converged (about 4 iterations). Following this process the resilient moduli of the transformed base layer was determined for the nine conditions listed in Table 6.3.

The same iterative process was also employed to determine the M_R values for the subgrade layer. The final M_R values for the base layer were kept constant in determining the resilient moduli values of the subgrade layer under the varying conditions. The final M_R values for the base and subgrade layers are listed in Table 6-9 for each condition.

TABLE 6.9 Final Resilient Moduli Values

Speed (mph)	Temp (ºF)	Base M_R (psi)	Subgrade M_R (psi)
15	60	9,253	25,301
15	80	8,825	25,615
15	110	8,154	26,082
25	60	9,282	25,254
25	80	8,869	25,569
25	110	8,223	25,993
45	60	9,349	25,227
45	80	8,947	25,498
45	110	8,294	25,969

Once, the moduli of each layer in the transformed structure (Tables 6.9 and 6.5) were established, WESLEA was again employed to estimate pavement responses. The properties defined in Table 6.8 were once again used; however, the analysis was completed for a 20,000 lb single axle with dual tires, which thereby reduced the tire load to 5,000 lbs. The maximum tensile strain was selected among two critical locations at the bottom of the HMA (13.9 inches deep). The first of the two critical locations was directly beneath the center of the outside tire load, and the second was located directly beneath the edge of the outside tire load, 6.75 inches from the center of the tire. The resulting maximum strain values are listed in Table 6.10 for the nine conditions investigated.

TABLE 6.10 Tensile Strain Based on MEPDG Load Durations

Speed (mph)	Temp (ºF)	ε_t (με)
15	60	50.95
15	80	77.8
15	110	158.01
25	60	47.82
25	80	76.23
25	110	149.07
45	60	44.41
45	80	70.94
45	110	139.35

6.3.2 Strain Predictions Based on Field-Modeled Load Duration

To assess the ability of the MEPDG to estimate those strain levels experienced in the field, two comparisons were drawn. The first was a comparison with the strain levels resulting from load durations modeled after field measurements. A procedure similar to

the procedure previously discussed for strain predictions from MEPDG load durations was used, with the only difference being the means to quantify load duration.

First, the load durations were calculated at the mid-depth of each of the five original HMA layers following Equation 5-6. This equation represents the load duration for tensile strain pulses at various points in the HMA layers of the N9 pavement structure. However, as was noted in Chapter Five, this equation results in negative values for pavement depths less than the depth to the neutral axis. This is an indication that the strain pulses are compressive in nature above the neutral axis. Depending on the conditions (speed and temperature), load durations were found to be negative as deep as the mid-point of the third HMA layer. The load durations at the mid-point of each HMA layer were necessary to compute the HMA modulus following the regression equation listed in Equation 6-2. Time of loading cannot be negative, and if only tensile strain durations were used, some HMA moduli values would be zero. Thus, in order to calculate the HMA moduli, some assumptions about the induced strain pulses were necessary.

It was assumed that above the neutral axis the critical response was compressive strain. At the surface the tensile strain can be assumed to be equal to zero, and it is assumed that the amount of tensile strain slowly increases with pavement depth. However, regardless of the amount of tensile strain, the pavement is still under loading and a strain pulse is still induced. Based on this, it was assumed that strain pulses were a function of the depth, vehicle speed and in-situ temperature regardless of the depth relative to the neutral axis. To further investigate the trends, Equation 5-6 was used to describe the load durations at the mid-point of all five HMA layers for a speed of 45

mph and in-situ temperatures equal to 60°F. The results were plotted in Figure 6.6. Although negative, the strain pulse durations near the surface of the pavement were found to be longer than the durations near the bottom. The strain pulse durations illustrated account for the time that the pavement was in its dominant strain mode only, either compressive or tensile. As discussed in Chapter Five, measuring the duration of an entire pulse, which included the strain reversal from compressive to tensile or vice versa, was nearly impossible. Thus, in measuring the duration of only the dominant strain mode (relative to the neutral axis), Equation 5-6 does so accurately. Thus, it was assumed that Equation 5-6 appropriately modeled strain pulse duration for either compressive or tensile strain as long as the absolute value of the duration is taken. Equation 5-6 is rewritten in Equation 6-14, taking into account these assumptions, allowing the strain pulse duration to be calculated regardless of the dominant strain mode.

$$t = \left|0.1131 \ln h + v^{-0.0807} + T^{-0.0628} - 1.7241\right| \quad (6\text{-}14)$$

The HMA moduli were calculated for the five layers of the original N9 pavement structure following Equation 6-2 from the regression analysis on the laboratory-determined E* values. The strain pulse durations were used to determine frequency following the assumption that they are inversely proportional, described by Equation 6-1. After the HMA moduli were determined, the resilient moduli of the transformed base and subgrade layers were determined following the same iterative procedure previously discussed. In following this iterative procedure, it was necessary to transform the original structure into a five-layered structure for evaluation in WESLEA. Equation 6-6

was again employed to transform the previously determined HMA moduli values for the transformed structure shown in Figure 6.5. The moduli of the transformed layers are listed in Table 6.11.

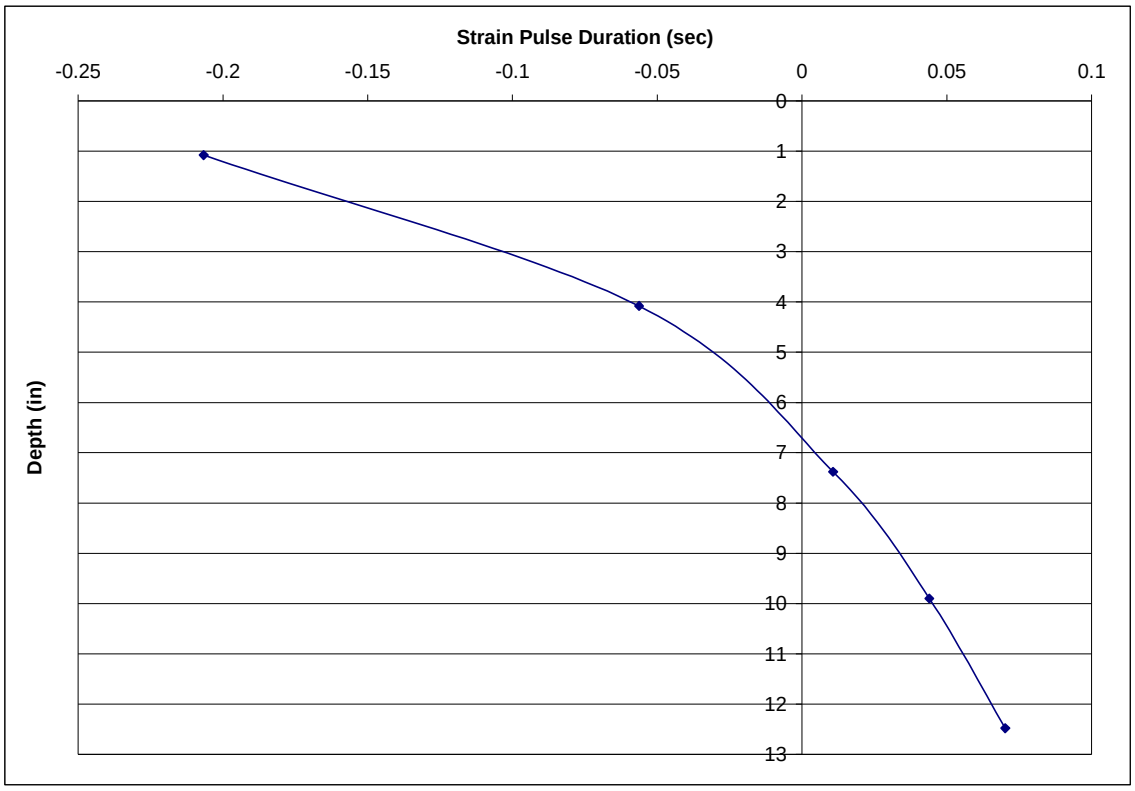

FIGURE 6.6 Field Modeled Strain Pulse Duration at 45 mph and 60 ºF.

TABLE 6.11 Moduli of Layers in Transformed Structure from Field Modeled Load Durations

Speed (mph)	Temp (ºF)	E^*_1 (psi)	E^*_{2T} (psi)	E^*_3 (psi)	Base M_R (psi)	Subgrade M_R (psi)
15	60	844,846	1,393,909	718,772	9,304	24,522
15	80	470,434	921,451	391,194	8,927	24,909
15	110	196,955	353,125	156,270	8,227	25,562
25	60	817,700	1,388,683	752,887	9,304	22,894
25	80	456,549	793,798	412,233	8,902	24,958
25	110	191,614	355,927	166,099	8,243	25,562
45	60	793,979	1,428,555	808,598	9,327	24,553
45	80	444,203	885,195	448,899	8,961	24,894
45	110	186,787	362,866	185,070	8,258	25,593

Next, the moduli values of the transformed structure were input in WESLEA to predict the tensile strain at the bottom of the pavement. The critical locations were

exactly as defined for the analysis of strain for MEPDG load durations. Just as was the case for the previous analysis, the values listed in Table 6.8 were defined in WESLEA, with the exception of the axle configuration and tire load. Rather then using a 20,000 lb steer axle, a 20,000 lb single axle was used to predict the strain values. The maximum tensile strains at the bottom of the HMA were predicted from WESLEA and are listed in Table 6.12.

TABLE 6.12 Tensile Strain Based on Field Modeled Load Durations

Speed (mph)	Temp (ºF)	ε_t (με)
15	60	45.15
15	80	69.05
15	110	145.44
25	60	44.78
25	80	72.31
25	110	142.92
45	60	43.24
45	80	67.61
45	110	137.82

6.3.3 Strain Predictions Based on Field Modeled Tensile Strain

The second comparison with the strain predictions due to the MEPDG load durations was drawn with the strain values predicted from measured tensile strain. In Chapter Five Equation 5-3 was developed to characterize the tensile strain at the bottom of the HMA layers for varying vehicle speed and in-situ pavement temperatures. For a single axle in the longitudinal direction, the developed equation is re-written in Equation 6-15. For the nine conditions listed in Table 6.3, the tensile strain at the bottom of the HMA was directly computed with results listed in Table 6.13.

$$\varepsilon_t = -40.57 \ln v + e^{0.053T} + 206.67 \qquad (6\text{-}15)$$

TABLE 6.13 Tensile Strain Based on Field Modeled Tensile Strain

Speed (mph)	Temp (ºF)	ε_t (με)
15	60	120.98
15	80	166.72
15	110	440.55
25	60	100.26
25	80	145.99
25	110	419.83
45	60	76.41
45	80	122.14
45	110	395.98

6.3.4 Comparison among Strain Predictions

Comparisons were drawn among the three aforementioned methods to predict strain for the evaluation of the MEPDG's method for determining load duration. The first comparison was drawn between the strain predicted from the MEPDG load duration method and the strain predicted from the field modeled strain pulse duration. Shown in Figure 6.7 are the strain predictions by temperature and speed.

The process to predict strain in both cases was identical, aside from the method to determine load duration, t. Both load duration computations produced strains that increased with temperature and decreased with speed, consistent with findings in the field investigation. Strain predictions as a result of the method prescribed by the MEPDG (labeled "MEPDG t" in Figure 6.7) were slightly higher than the predictions resulting from the load durations modeled after field measurements (labeled "Modeled t").

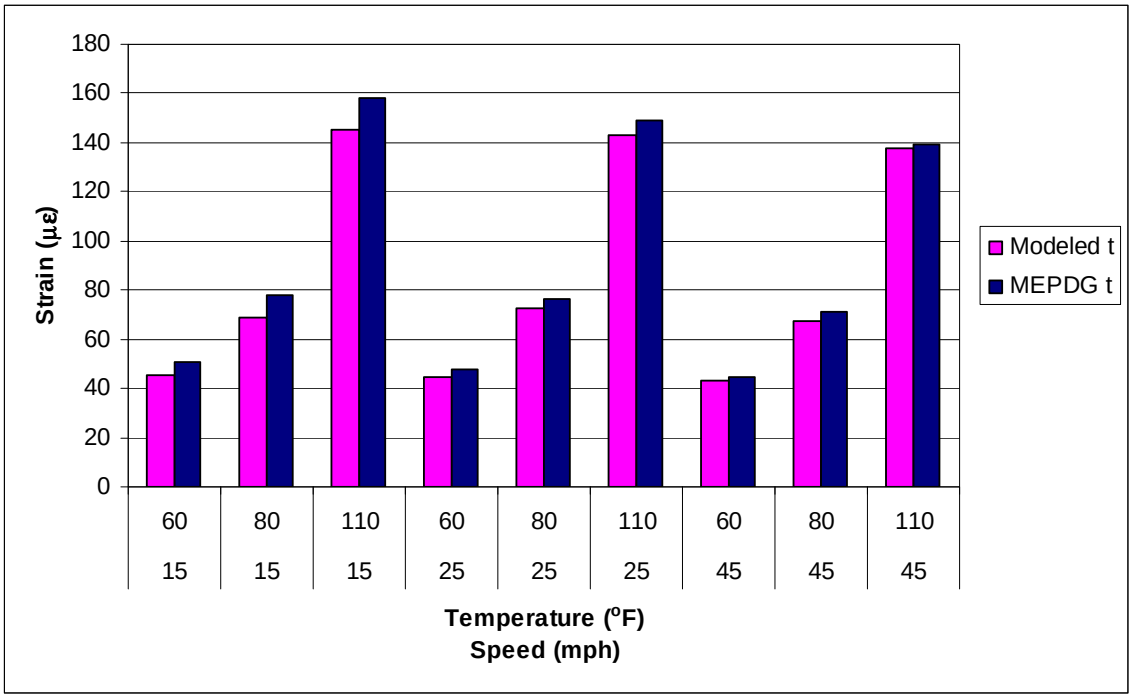

FIGURE 6.7 Predicted Strains by Temperature and Speed.

Over-prediction of load duration, as was found with the MEPDG method, would be expected to result in lower E* values, due to the inverse relationship with frequency and time, and the direct relationship between E* and frequency. This was found to be the case, in looking at Equation 6-2, and the resulting E* values in Tables 6.5 and 6.10, E* decreases with longer load durations. Illustrated in Tables 6.5 and 6.10, E* values were greater for surface mixes where the MEPDG estimated shorter load durations than Equation 5-6. Further down in the pavement structure, E* values were lower where load durations were over-predicted by the MEPDG. Although the MEPDG grossly over-predicted load duration deeper in the pavement relative to the model developed from field measurements, the E* values were not as greatly influenced. E* values in the bottom layer of the transformed structure differed by only 20,000-100,000 psi, approximately. The higher strain predictions for the MEPDG determination of load

durations could be attributed to the fact that E* values were overall found to be lower than those based on the field measured model for load duration.

Strain was also estimated utilizing the regression equation (6-15) developed in Chapter Five, characterizing tensile strain at the bottom of the HMA by speed and temperature. Figure 6.8 displays the strains simulated in WESLEA from both the MEPDG computed load durations, and the model from field measured load durations compared with the results from Equation 6-14. The modeled strains resulted from a regression analysis in which Equation 6-14 fit the measured strain values very well with a coefficient of determination of 0.983. The highest mid-depth pavement temperature recorded during the field investigation was 99.47^{o}F, at which a strain of 308 με was recorded at 15 mph, shown in Figure 5.6. Based on this, the strain predicted from the regression equation may be slightly higher than expected. This maybe an indication of the limits of the equation, as 110^{o}F is outside the range of measured mid-depth temperatures. But overall, the strain values in the field have been shown to be most accurately predicted by Equation 6-15.

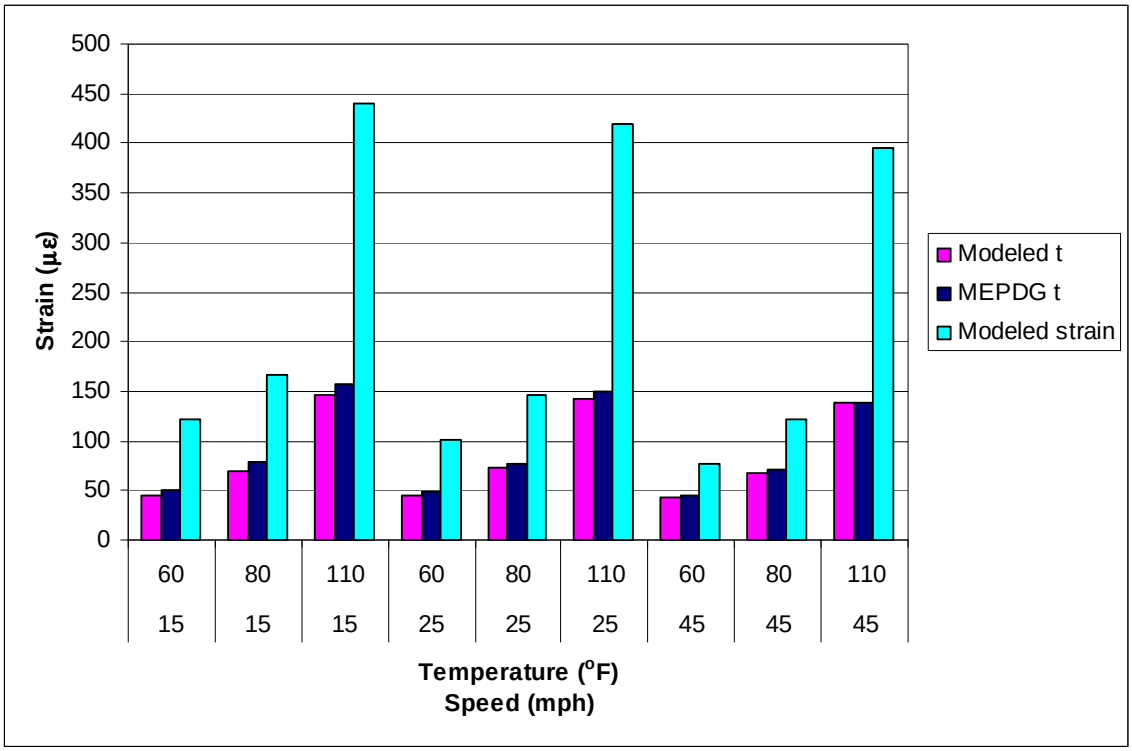

FIGURE 6.8 Simulated Strains Compared with Modeled Strains.

It is evident that the two strain simulations that were based on load durations underpredict the strain likely to be experienced at the conditions investigated. Looking at the results of all three strain predictions in Table 6.14, these simulations are nearly half of those predicted by the regression equation. The strain based on MEPDG load durations were closest to those from Equation 6-15, with percent differences ranging from 42% to 65%. Although these two simulations returned relatively close values, neither represented values likely to occur in the field under these conditions. Both simulations utilized the same procedure aside from the determination of load duration.

The large discrepancies in the strain predictions relative to Equation 6-14 may not be a result of the load duration calculations. The MEPDG overpredicted the load durations measured in the field. As discussed earlier, longer load durations lead to lower E* values and ultimately higher strain values. Although this was the case, the gross

overprediction of load duration only resulted in strain values that were at best 58% of those based on measured values. The other simulation was based on field measured load durations and still resulted in strain estimates that were a fraction of those modeled from field measured strain. Some of these errors may be a result of the assumption that the regression equation for load durations could be applied to pavement depths less than the neutral axis. However, following this assumption resulted in longer load durations at shallower depths which then produced higher strain values. Therefore, it is unlikely that either procedure to determine load duration was the major cause for the gross under-predictions of tensile strain levels.

TABLE 6.14 Resulting Strain Predictions

		Based on Load Durations		
Speed (mph)	Temp (ºF)	MEPDG t ε_t (με)	Modeled t ε_t (με)	Modeled ε_t (με)
15	60	50.95	45.15	120.98
15	80	77.8	69.05	166.72
15	110	158.01	145.44	440.55
25	60	47.82	44.78	100.26
25	80	76.23	72.31	145.99
25	110	149.07	142.92	419.83
45	60	44.41	43.24	76.41
45	80	70.94	67.61	122.14
45	110	139.35	137.82	395.98

Both simulations did however use the same E* regression analysis to predict HMA moduli from load durations. In computing E* for both load duration methods, the time-frequency relationship (f = 1/t) was utilized. Regardless of how load duration was computed, it was found that the resulting strain was nearly half of the strain determined from field measurements. Since the time-frequency relationship was consistent among strain predictions from load durations, it is possible that the large differences between measured strain and predicted strain are a result of this time-frequency relationship. In

order for the MEPDG to construct a master curve from E* laboratory results, both cold and warm temperatures are required. It is difficult to obtain accurate and reliable results at such extreme temperatures. Due to the lack of data at these extreme temperatures, the regression equation developed from the results that were obtained was used instead. The coefficients of determination for Equation 6-2 were very high (0.97-0.99) suggesting that it may be an acceptable alternative to a master curve. However, given that Equation 6-2 was used in both the simulations that returned poor correlation to modeled strains from field measurements, it is a possible source of error. Equation 6-2 was a product of the temperature in the layer in question. Although, in the simulations, it was assumed that a temperature gradient did not exist, and that all layers experienced the same temperature. The strain values modeled from field measurements however were dependent on mid-depth pavement temperature. Thus, the failure to account for a temperature gradient may have also contributed to the low strain values in both simulations. Also, the maximum temperature, 110ºF that was investigated was 10ºF beyond the highest temperature tested in the laboratory.

6.4 SUMMARY

The MEPDG's method for computing load duration was investigated relative to field measured load durations. Additionally, the effects of such computations were assessed based on strain predictions. The strain and load durations measured in the field investigation of test section N9 were used for comparison and evaluation of the MEPDG.

First, the method prescribed by the MEPDG for the computation of load duration was followed. The MEPDG method is an iterative procedure to determine the time of

loading modeled by a haversine stress pulse dependent on vehicle speed, depth in the pavement and HMA moduli. Although the MEPDG constructs a master curve to characterize E*, it was elected to use E* laboratory test results to develop a regression equation for each mix in the N9 test section. The resulting equations were a function of loading frequency and in-situ pavement temperature. The use of a regression equation seemed appropriate given the very high coefficients of determination (0.97-0.99) and the temperatures experienced in the field were almost all within the range tested in the laboratory. The procedure was completed for the exact same conditions at which measurements were made in the field enabling a direct comparison. The resulting load durations were found to over-predict measured strain pulse durations by approximately 68%. The difference in load duration definition was cited as a possible cause for the gross over-prediction. The durations measured in the field were of strain pulses in tensile strain only. However, regardless of whether stress or strain was measured, a better correlation should be expected.

A set of conditions were defined, representative of the conditions experienced in the field, to assess how the MEPDG load durations affected strain levels. The MEPDG itself does not output strain predictions directly. Therefore, strain levels at the bottom of the HMA were predicted using a separate layered elastic analysis program, WESLEA. To utilize WESLEA, the 8-layered structure of N9 was transformed into a 5-layer structure, in which the three middle HMA layers were combined into one, and the Track soil base layer was combined with the Seale subgrade layer. Using the regression equation developed for field measured strain pulse durations, strain predictions were also made through WESLEA for the same conditions and transformed structure. Both

simulations resulted in very similar tensile strain values, in which the maximum absolute difference was found to be 12.57 με. Further comparisons were made with strain calculated directly from vehicle speed and temperature using the regression equation developed from field measured tensile strain at the bottom of the HMA under a single axle. The strain simulated from the MEPDG load durations did display the expected trend of increased strain with an increase in load duration. However, the strain levels poorly replicated the strain calculated from the regression equation, with simulated levels at best 58% of the calculated levels. Overall, it was found that the over-prediction of the load durations by the MEPDG did not result in an over-prediction of strain levels. Contrary to theory, the elongated durations grossly under estimated the strain levels in the field. Such large differences in predicted strain and strain determined from field measurements could indicate that the time-frequency relationship utilized is inaccurate.

CHAPTER SEVEN

CONCLUSIONS AND RECOMMENDATIONS

7.1 SUMMARY

This thesis investigated the viscoelastic nature of HMA in an M-E pavement design framework, specifically the MEPDG, by means of E* predictive equations and measurable pavement responses under field conditions. To meet the objectives set forth in Chapter One of this thesis, a literature review was first completed on E* laboratory test procedures and results, E* predictive equations, load durations and tensile strain. An evaluation of three E* predictive equations, the Witczak 1-37A, the Witczak 1-40D, and the Hirsch, was completed for HMA mixes from the 2006 Test Track structural study. A field study was also conducted for one pavement section in the Test Track structural study, in which vehicle speeds were varied from 15-55 mph and varying pavement temperatures were recorded. During the field study, horizontal tensile strain pulses were recorded at multiple depths within the HMA layers, including the most critical point, the bottom of the HMA. The recorded strain pulses enabled an evaluation of tensile strain at the bottom of the HMA, as well as an evaluation of strain pulse durations at various depths. The MEPDG prescribed method for determining load duration was followed to offer comparisons with field measured strain pulse durations. Furthermore, field-measured and MEPDG load durations were utilized to predict E* and ultimately tensile strain at the bottom of the HMA using a layered-elastic analysis program. These

strains were then compared with measured strains, thus linking the time-element of E* to pavement response. Findings from these evaluations are further summarized in the following section.

7.2 CONCLUSIONS

7.2.1 Evaluation of E* Predictive Equations

To determine the most appropriate E* predictive model for HMA mixtures of the 2006 Test Track structural study, three equations were analyzed: the Witczak 1-37A, the Witczak 1-40D and the Hirsch E* predictive models. The dynamic moduli of these mixtures were determined in the laboratory at seven frequencies and three temperatures.

Following the Witczak 1-37A model, E* was estimated for three temperatures (40, 70, and 100°F) and seven frequencies (0.1, 1, 2, 5, 10, 20, and 25 Hz). E* was also estimated using the Witczak 1-40D and Hirsch E* predictive models for two temperatures (70, and 100°F) and three frequencies (1, 10, 25 Hz). In comparing the predicted dynamic moduli to measured dynamic moduli it was found that the Hirsch model predicted E* most accurately. The Witczak 1-37A model was the least precise for the mixtures tested, with large amounts of scatter on either side of the line of equality. The Witczak 1-40D model consistently grossly over estimated measured E* values by at most 5.6 times the measured values. When plotted against measured E* values, it was found that both the Witczak 1-40D and the Hirsch models flattened out at extreme values, rather than increasing with frequency as did the measured values. Therefore, neither model accurately captured the time-dependency of HMA at the extremes. However, this trend was more predominant in the Hirsch model at moduli values predicted at 70°F. Despite this flaw, the Hirsh model consistently hovered around the

line of equality, producing the highest coefficient of determination (0.707 in log scale) of the three models for its associated linear regression equation. Furthermore, the Hirsch model was very accurate for low moduli values (250,000-700,000 psi). Due to the large scatter resulting from the Witczak 1-37A predictions, and gross over predictions made by the Witczak 1-40D model, the Hirsch model is the most accurate and reliable predictive equation for the HMA mixtures evaluated.

The effect of mixture parameters on the accuracy of the models was investigated as well. Plots were developed comparing measured moduli to predicted moduli for each mixture type, binder type, grade, and NMAS included in the study. It was found that although these parameters influence the magnitude of measured and predicted moduli, none of these parameters were found to significantly affect the accuracy of the predictions made by these three models.

7.2.2 Evaluation of Field Measured Strain and Strain Pulse Durations

One pavement section at the Test Track was selected for a field study in which live traffic was applied to the N9 test section at a minimum of four different speeds (15, 25, 35, 45, and 55 mph) on four test dates. During the testing, embedded strain gages captured horizontal strain pulses at four depths while temperature probes recorded in-situ pavement temperatures. From these measurements tensile strain at the bottom of the HMA was characterized by mid-depth temperature and vehicle speed. Additionally, strain pulse durations were characterized by layer mid-depth temperature, vehicle speed, and pavement depth.

Tensile strains were found to vary by direction and axle type, with the highest strains recorded in the longitudinal direction and under single axles. In characterizing

tensile strain at the bottom of the HMA, it was found to be a function of the natural logarithm of vehicle speed and the exponent of the mid-depth temperature.

Strain pulse durations were defined by the time in which the pavement was in tensile strain when under dynamic loading. Strain pulse durations were characterized based on measurements at 8.76", 11.04" and 13.92" deep in the HMA structure. Increases in vehicle speed resulted in shortened strain pulse durations, while load durations elongated deeper in the pavement. As mid-depth pavement layer temperatures increased, the strain pulses were found to shorten in length.

7.2.3 Evaluation of the MEPDG's Method for Determining Load Duration

The MEPDG's method for computing load duration was investigated relative to field measured load durations. Additionally, the effects of such computations on strain predictions were assessed. The strain and load durations measured in the field for test section N9 were used for comparison and evaluation of the MEPDG.

The iterative procedure outlined in the MEPDG for the determination of load duration of a haversine stress pulse was followed for conditions identical to those in the field investigation. Comparing the load durations computed by the MEPDG and the measured strain pulse durations in the field, it was found that the MEPDG load durations were approximately 68% greater than those measured in the field.

For a set of given conditions, load durations were calculated by the MEPDG and by the model developed from field measured strain pulse durations, from which E* was calculated. Since the MEPDG does not output actual strain predictions, a separate layered elastic analysis program, WESLEA was employed to predict strain at the bottom

of the HMA for both load duration procedures. In comparing these strain predictions it was found that despite the 68% difference in load durations, there was little difference in strain levels. The maximum absolute difference between these strain predictions was only 12.57 με. Both procedures exhibited the expected trend of increased strain with an increase in load duration.

For the same set of conditions, tensile strain was computed by the regression equation developed from measured tensile strain from the field investigation. When compared with the strains simulated in WESLEA from MEPDG load durations and load durations based on field measurements, strains estimated from field measurements were nearly double the simulated strains. It should be noted that the strains simulated in WESLEA from either definition of load duration were dependent on the time-frequency relationship. It can be concluded from these findings that it is not the definition of load duration that is most influential in predicting strain from E*, but rather the relationship between load duration and frequency.

7.3 RECOMMENDATIONS

For the State DOTs from which the mixtures herein originated, the Hirsch E* model may be used to predict E* in the absence of E* laboratory testing. However, it should be used with caution given the discrepancies found at high frequencies and moderate temperatures. If the MEPDG is being utilized for design, Hirsch E* model estimates may be substituted in a Level One design for laboratory E* results, following extrapolation to colder temperatures. Furthermore, if the MEPDG is to be used in its current format it is recommended that calibration be completed both regionally and

nationally for the Witczak 1-40D model prior to implementation of the software program as the primary design tool.

Given the advancement in pavement design and global push towards mechanistic-empirical pavement design, characterizing the viscoelastic nature of HMA is imperative to successful designs. Therefore, based on the comparisons of load duration, it is recommended that further investigation in defining the load duration throughout the HMA be completed. Due to the under estimation of strain from either load duration definition, it is suggested that the time-frequency relationship is inaccurate and thus needs further refinement. Lastly, at the current state of the MEPDG, the output is in the form of pavement distresses which are predicted from estimated strain levels. Findings from this thesis identified the possible under estimation of strain based on procedures outlined within the MEPDG; therefore further investigation into the accuracy of the predicted distresses should be completed. Also, further refinement of the strain predictions, possibly by accurately characterizing the time-frequency relationship, should be completed before implementation of the program for design purposes.

REFERENCES

AASHTO TP 62-07. *Standard Test Method for Determining Dynamic Modulus of Hot-Mix Asphalt (HMA)*. AASHTO, 2007.

AASHTO T 315-06. *Standard Test Method for Determining the Rheological Properties of Asphalt Binder Using Dynamic Shear Rheometer (DSR)*. AASHTO, 2006.

ARA Inc., Eres Division. Part 2 Design Inputs: Chapter 2 Material Characterization. *Guide For Mechanistic-Empirical Pavement Design of New and Rehabilitated Pavement Structures*, Final Document, NCHRP 1-37A, 2004.

ASTM D3497-79 (2003). *Standard Test Method for Dynamic Modulus of Asphalt Mixtures*. ASTM International, West Conshohocken, PA. www.astm.org.

Andrei, D., M.W. Witczak, and W. Mirza. Appendix CC-4: Development of a Revised Predictive Model for the Dynamic (Complex) Modulus of Asphalt Mixtures. *Devlopment of the 2002 Guide for the Design of New and Rehabilitated Pavement Structures*, Final Document, NCHRP 1-37A, 1999.

Asphalt Institute. *Thickness Design, Asphalt Pavements for Highways and Streets. Report MS-1,* Asphalt Institute, 1982. (reprinted in 1999)

Azari, H., G. Al-Khateeb, A, Shenoy, and N. Gibson. Comparison of Measured SPT E* of ALF Mixtures with Predicted E* Using NCHRP 1-37A and Witczak's New Equations. In *Proceedings of the 86th Annual Meeting of the Transportation Research Board,* TRB, National Research Council, Washington, D.C., 2007.

Bari, J. and M.W. Witczak. Development of a New Revised Version of the Witczak E* Predictive Model for Hot Mix Asphalt Mixtures. *Journal of the Association of Asphalt Paving Technologists from the Proceedings of the Technical Sessions,* Vol. 75, pp 381-423, Savannah, Ga, 2006.

Barksdale, R.D. Compressive Stress Pulse Times in Flexible Pavements for Use in Dynamic Testing. In *Highway Research Record 345,* HRB, National Research Council, Washington, D.C., 1971, pp 32-44.

Bonnaure, F., G. Gest, A. Gravois, and P. Uge. A New Method of Predicting the Stiffness of Asphalt Paving Mixtures. *Proceedings of the Association of Asphalt Paving Technologists,* Vol. 46, 1977, pp64-104.

Brown, S.F. Determination of Young's Modulus for Bituminous Materials in Pavement Design. In *Highway Research Record 431*, HRB, National Research Council, Washington, D.C., 1973, pp 38-49.

Chatti, K., H.B. Kim, K.K. Yun, J.P. Mahoney, and C.L. Monismith. Field Investigations into Effects of Vehicle Speed and Tire Pressure on Asphalt Concrete Pavement Strains. In *Transportation Research Record: Journal of the Transportation Research Board, No. 1539*, TRB, National Research Council, Washington, D.C., 1996, pp 66-71.

Christensen, Jr., D.W., T. Pellinen, and R.F. Bonaquist. Hirsch Model for Estimating the Modulus of Asphalt Concrete. *Journal of the Association of Asphalt Paving Technologists from the Proceedings of the Technical Sessions*, Vol. 72, pp 97-121, Lexington, KY, 2003.

Dongre, R., L. Myers, J. D'Angelo, C. Paugh, and J. Gudimettla. Field Evaluation of Witczak and Hirsch Models for Predicting Dynamic Modulus of Hot-Mix Asphalt. *Journal of the Association of Asphalt Paving Technologists from the Proceedings of the Technical Sessions*, Vol. 74, 2005.

Eres Consultants Division. *Guide For Mechanistic-Empirical Pavement Design of New and Rehabilitated Pavement Structures; Appendix CC-3, Updated Traffic Frequency Calculation for Asphalt Layers*, Final Document, NCHRP 1-37A, 2003.

Federal Highway Administration (FHWA). Improving Pavement Performance with the Asphalt Mixture Pavement Tester. *Focus: Accelerating Infrastructure Innovations*. http://www.tfhrc.gov/focus/july08/01.htm, accessed March 30, 2009.

Flinstch, G.W., A. Loulizi, S.D. Diefenderfer, K.A. Galal, and B.K. Diefenderfer. *Asphalt Materials Characterization in Support of Implementation of the Proposed Mechanistic-Empirical Pavement Design Guide*. Virginia Department of Transportation Final Report. Report No. VTRC 07-CR10, 2007. http://www.virginiadot.org/vtrc/main/online_reports/pdf/07-cr10.pdf

Garcia, G., and M.R. Thompson. Strain and Pulse Duration Considerations for Extended Hot Mix Asphalt Pavement Design. *Proceedings of the 87th Annual Meeting of the Transportation Research Board*, Washington, D.C., 2008.

Huang, B., X. Shu, and J. Bass. Investigation of Simple Performance Characteristics of Plant-Produced Asphalt Mixtures in Tennessee. In *Transportation Research Record: Journal of the Transportation Research Board No. 2057*, TRB, National Research Council, Washington, D.C., 2008, pp 140-148.

Huang, Y.H. *Pavement Analysis and Design.* 1st Ed., Prentice Hall, Upper River Saddle, N.J., 1993.

Loulizi, A., I.L. Al-Qadi, S. Lahouar, and T.E. Freeman. Measurement of Vertical Compressive Stress Pulse in Flexible Pavements: Representation for Dynamic Loading Tests. In *Transportation Research Record: Journal of the Transportation Research Board No. 1816*, TRB, National Research Council, Washington D.C., 2002, pp 125-136.

Mateos, A. and M.B. Snyder. Validation of Flexible Pavement Structural Response Model with Data from the Minnesota Road Research Project. In *Transportation Research Record: Journal of the Transportation Research Board, No. 1806*, TRB, National Research Council, Washington, D.C., 2002, pp 19-29.

Mohammad, L.N., S. Saadeh, S. Obulareddy, and S. Cooper. Characterization of Louisiana Asphalt Mixtures Using Simple Performance Tests. In *Proceedings of the 86th Annual Meeting of the Transportation Research Board*, TRB, National Research Council, Washington, D.C., 2007.

Ping, W.V., and Y. Xiao. Evaluation of the Dynamic Complex Modulus Test and Indirect Diametral Test for Implementing the AASHTO 2002 Design Guide for Pavement Structures in Florida. *Final Report*, Florida Department of Transportation, BC-352-12, Tallahassee, FL, 2007.

Priest, A.L. and D.H. Timm. *Methodology and Calibration of Fatigue Transfer Functions for Mechanistic-Empirical Flexible Pavement Design*, Report No. 06-03, National Center for Asphalt Technology, Auburn University, 2006.

Tashman, L. and M. A. Elangovan. *Dynamic Modulus Test - Laboratory Investigation and Future Implementation in the State of Washington*. Washington State Department of Transportation Final Report. Final Research Report No. WA-RD 704.1, 2007. http://www.wsdot.wa.gov/research/reports/fullreports/704.1.pdf

Taylor, A. J. *Mechanistic Characterization of Resilient Moduli for Unbound Pavement Layer Materials*. M.S. Thesis, Auburn University, 2008.

Timm, D.H. *Design, Construction and Instrumentation of the 2006 Test Track Structural Study,* Draft Report, National Center for Asphalt Technology, Auburn University, 2008.

Timm, D.H. and A.L. Priest. Flexible Pavement Fatigue Cracking and Measured Strain Response at the NCAT Test Track. *Proceedings of the 87th Annual Meeting of the Transportation Research Board*, Washington, D.C., 2008.